CHAPTER V

ELASTIC AND INELASTIC SCATTERING

1. INTRODUCTION

Chapter IV is devoted to the study of reactions involving a relatively long interaction time as exemplified by compound nuclear resonances and by these reactions to which the statistical theory applies. The latter is appropriate when the excitation energy, U, of the residual nucleus is sufficiently large and the energy of the emitted particles are sufficiently small. The angular distribution is symmetrical about 90° and the energy variation of the cross section (assuming sufficiently good resolution) is rapid. In this chapter we consider the direct reaction, that is, prompt reactions (a term that we prefer to use if one could revise history!). In this case the interaction time is relatively short, on the order of the time it would take the projectile to traverse the nucleus. The angular distribution is asymmetric, thereby revealing the direction of the incident projectile. The variation of the cross section with energy is slow, as one would expect to follow from the short interaction time.

According to Chapter III, the governing description for prompt reactions is given by the multichannel optical model. The open channels are the ones usually included but on occasion, particularly near thresholds, it may be important to include closed channels as well. The phrase *optical model* refers to the fact the prompt reactions can be selected by considering the energy-averaged wave function, $\langle P\Psi \rangle$, which satisfies the equation

$$\left[E - H_{PP} - H_{PQ} \frac{1}{E - H_{QQ} + iI/2} H_{QP} \right] \Psi^{(\mathrm{opt})} = 0 \tag{1.1}$$

where

$$\Psi^{(\mathrm{opt})} = \langle P\Psi \rangle \tag{1.2}$$

In this equation, I is the energy interval over which the average is taken. It clearly has the function of smoothing the dependence of the propagator $(E - H_{QQ} + iI/2)^{-1}$ upon the energy. It is this term that takes into account the effect of the closed channels upon the optical model wave function. The function $\Psi^{(\mathrm{opt})}$ is a multicomponent wave function of dimension equal to the number of channels included in $\mathscr{P}$ space. If (1.1) is written in terms of the channel wave functions, it becomes a set of coupled Schrödinger equations.

In the approximate treatment of these coupled equations, the elastic channel plays a central role. We project it out by introducing the projection operator p and its orthogonal complement R. Defining $H^{(\mathrm{opt})}$ by

$$H^{(\mathrm{opt})} \equiv H_{PP} + H_{PQ} \frac{1}{E - H_{QQ} + iI/2} H_{QP} \tag{1.3}$$

(1.1) can be rewritten as follows:

$$\begin{aligned} (E - H_{pp}^{(\mathrm{opt})})\psi_{\mathrm{el}} &= H_{pR}^{(\mathrm{opt})}\psi_R \\ (E - H_{RR}^{(\mathrm{opt})})\psi_R &= H_{Rp}^{(\mathrm{opt})}\psi_{\mathrm{el}} \end{aligned} \tag{1.4}$$

using the notation

$$H_{pR}^{(\mathrm{opt})} = pH^{(\mathrm{opt})}R, \quad \text{etc.}$$

The wave function ψ_R is a multicomponent wave function containing all the reaction channels with the exception of the elastic channel, whose wave function is given by ψ_{el}. We can solve for ψ_R bearing in mind that the channels involved are open:

$$\psi_R = \frac{1}{E^{(+)} - H_{RR}^{(\mathrm{opt})}} H_{Rp}^{(\mathrm{opt})}\psi_{\mathrm{el}} \tag{1.5}$$

Therefore, ψ_{el} satisfies

$$\left[E - H_{pp}^{(\mathrm{opt})} - H_{pR}^{(\mathrm{opt})} \frac{1}{E^{(+)} - H_{RR}^{(\mathrm{opt})}} H_{Rp}^{(\mathrm{opt})} \right] \psi_{\mathrm{el}} = 0 \tag{1.6}$$

Note that

$$H_{pp}^{(\mathrm{opt})} = H_{pp} + H_{pQ} \frac{1}{E - H_{QQ} + iI/2} H_{Qp} \tag{1.7}$$

We see that the elastic channel wave function satisfies a Schrödinger equation with a complex and, therefore, absorptive interaction. The absorption has two sources. One is loss of flux from the incident channel, is produced by the prompt reactions that can occur. This is described by the third term, involving the subscript R, in brackets in (1.6). The other source stems from the fact that $\Psi^{(\mathrm{opt})}$, and therefore, ψ_{el}, are the results of an energy average of $P\Psi$. Following Friedman and Weisskopf (55), it can be argued that taking the energy average is equivalent to selecting the prompt component of $P\Psi$. In terms of the development under discussion here, this conclusion follows from the fact that $H^{(\mathrm{opt})}$ is a smooth function of E. The function $\Psi^{(\mathrm{opt})}$, and therefore ψ_{el}, will exhibit an absorption because they do not contain the delayed component of $P\Psi$. In more picturesque terms, the wave pocket formed by taking the energy average is attenuated on passing through the nucleus, because some of its flux is left behind to form the compound nucleus. This flux will be emitted later. It is this process that is described by the second term in brackets in (1.6). This effect is present even when only elastic scattering is possible, that is, for energies below the threshold for nonelastic reactions.

In principle, (1.6) can be used to determine the averaged elastic scattering amplitude. To determine the reaction amplitude leading to a particular channel c, we project out that channel with an operator c so that (1.4) becomes

$$(E - H_{pp}^{(\mathrm{opt})})\psi_{\mathrm{el}} = H_{pc}^{(\mathrm{opt})}\psi_c + H_{pr}^{(\mathrm{opt})}\psi_r \tag{1.8a}$$

$$(E - H_{cc}^{(\mathrm{opt})})\psi_c = H_{\mathrm{cp}}^{(\mathrm{opt})}\psi_{\mathrm{el}} + H_{\mathrm{cr}}^{(\mathrm{opt})}\psi_r \tag{1.8b}$$

$$(E - H_{rr}^{(\mathrm{opt})})\psi_r = H_{rp}^{(\mathrm{opt})}\psi_{\mathrm{el}} + H_{rc}^{(\mathrm{opt})}\psi_c \tag{1.8c}$$

where

$$R = c + r \qquad \text{and} \qquad cr = 0$$

Note that if ψ_r and ψ_c are eliminated, the resulting equation for ψ_{el} must be identical to (1.6). If ψ_r is eliminated, one obtains a pair of coupled equations for ψ_{el} and ψ_c. The inclusion of the effect of the other open channels

Problem. Show that these coupled equations for ψ_{el} and ψ_c are

$$\begin{aligned}(E - \mathscr{H}_{pp})\psi_{\mathrm{el}} &= \mathscr{H}_{pc}\psi_c \\ (E - \mathscr{H}_{cc})\psi_c &= \mathscr{H}_{cp}\psi_{\mathrm{el}}\end{aligned} \tag{1.9}$$

where

$$\mathscr{H} = H^{(\mathrm{opt})} + W$$

$$W_{ab} = H_{ar}^{(\mathrm{opt})} \frac{1}{E^{(+)} - H_{rr}^{(\mathrm{opt})}} H_{rb}^{(\mathrm{opt})} \tag{1.10}$$

Show that the transition matrix for the excitation of c is

$$\langle \mathscr{T}_{ci} \rangle = \langle \phi_c^{(-)} | \mathscr{H}_{cp} \psi_{el}^{(+)} \rangle \tag{1.11}$$

where

$$(E - \mathscr{H}_{cc})\phi_c^{(-)} = 0 \tag{1.12}$$

which are projected by r is required if multistep processes are important. If it is assumed that only a single-step process is important, the DWA (distorted wave approximation) is used. In this approximation [Lamarsh and Feshbach (65)] the exact equation for ψ_{el}, (1.6), is used and (1.8*b*) is replaced by

$$(E - H_{cc}^{(opt)})\psi_c \simeq H_{cp}^{(opt)} \psi_{el} \tag{1.13}$$

so that

$$\langle \mathscr{T}_{ci} \rangle = \mathscr{T}_{ci}^{(dir)} \simeq \langle \chi_c^{(-)} | H_{cp}^{(opt)} \psi_{el}^{(+)} \rangle \tag{1.14}$$

where

$$(E - H_{cc}^{(opt)})\chi_c^{(-)} = 0 \tag{1.15}$$

Comparing with the exact expression (1.11) we see that $\mathscr{H}_{pc}^{\dagger}\phi_c^{(-)}$ has been approximated by $H_{pc}^{\dagger}\chi_c^{(-)}$. The coupling of the channel c to the open channels r has been neglected in both $H_{pc}^{\dagger}$ and $\chi_c^{(-)}$. The waves $\chi_c^{(-)}$ and ψ_{el} are distorted (i.e., are not plane waves) because of the potential terms present in $H_{cc}^{(opt)}$ and in the effective Hamiltonian for the single-channel wave function ψ_{el} as given by (1.6). The approximate equation (1.14) for the transition amplitude is referred to as the *distorted wave born approximation* (DWA). Using the DWA requires the determination of the single-channel wave functions $\psi_{el}^{(+)}$ and $\chi_c^{(-)}$, as well as the coupling Hamiltonian H_{cp}. We discuss the first of these issues in the next section.

Note. In many applications of the DWA, the interaction Hamiltonian used in the calculation, (1.14), is empirically determined using parameter choices that produce best fits to the data. As a consequence, many of the effects of the omitted open channels are included to the extent that this is permitted by the forms used for the Hamiltonian. However, when these effects are too severe, it may be necessary to recognize their importance through the use of a system of coupled-channel Schrödinger equations, taking explicitly into account those channels that have the major impact.

2. THE SINGLE-CHANNEL OPTICAL MODEL

The empirical optical model is used to develop the single-channel wave functions required by the DWA. The model was developed originally to provide an

understanding of the low-energy neutron–neucleus interaction as observed by Barschall and his collaborators [Barschall (52)]. Although it was derived in the sense that it was shown that the model wave function and model scattering amplitude were energy averages of the exact wave function and exact scattering amplitude, the optical model has been used since semiempirically. An *a priori* form is chosen for the optical model potential, that is, for the Hamiltonian of (1.6). Its parameters are then adjusted so as to yield agreement with the data, such as the total cross section σ_T; the elastic angular distributions $d\sigma_{el}/d\Omega$; the polarization of the emergent particles, if available; and so on. Smooth behavior of the parameters with respect to changes in projectile energy and target are desired for physical significance. Substantial discontinuities may imply the presence of a phenomenon for which the single-channel optical model is inadequate, requiring, perhaps, the use of a multichannel optical model.

A. Average Cross Sections

Since in the optical model the scattering amplitude is energy averaged, the optical model cross section $\langle\sigma\rangle$ cannot, except for one situation, be compared directly with the energy-averaged cross sections, $\bar{\sigma}$, since cross sections are quadratic functions of the scattering amplitude. The one exception is the total cross section σ_T, since it is a linear function of the amplitude in virtue of the optical theorem:

$$\sigma_T = \frac{4\pi}{k} \operatorname{Im} f(0^\circ) \tag{2.1}$$

Energy averaging[‡] both sides then gives the result

$$\langle\sigma_T\rangle = \bar{\sigma}_T \tag{2.2}$$

that is, the optical model total cross section equals the energy-averaged total cross section. This is not the case for the angular distribution or other observables. In those cases we have from (IV.7.7)

$$|\mathscr{T}_{fi}|^2 = |\mathscr{T}_{fi}^{(\mathrm{opt})}|^2 + |\mathscr{T}_{fi}^{(\mathrm{FL})}|^2$$

Averaging, one obtains

$$\bar{\sigma}_{el} = \langle\sigma_{el}\rangle + \bar{\sigma}_{el}^{(\mathrm{FL})} \tag{2.3}$$

Before the optical model can be compared with experiment, the fluctuation cross section, $\bar{\sigma}^{(\mathrm{FL})}$, must be added to optical model cross section $\langle\sigma_{el}\rangle$.

[‡]Angular brackets are used to indicate model quantities and a bar indicates energy-averaged quantities.

The optical model also predicts an absorption cross section $\langle \sigma_r \rangle$, which is related to $\langle \sigma_T \rangle$ as follows:

$$\langle \sigma_r \rangle = \langle \sigma_T \rangle - \langle \sigma_{el} \rangle \tag{2.4}$$

A similar quantity can be defined for the energy-averaged cross sections

$$\bar{\sigma}_r = \bar{\sigma}_T - \bar{\sigma}_{el} \tag{2.5}$$

The relationship between $\bar{\sigma}_r$ and $\langle \sigma_r \rangle$ follows from (2.2) and (2.3):

$$\langle \sigma_r \rangle = \bar{\sigma}_r + \bar{\sigma}_{el}^{(FL)} \tag{2.6}$$

The first term, $\bar{\sigma}_r$, is a consequence of real inelastic processes, while $\bar{\sigma}_{el}^{FL}$ represents the contribution of the delayed processes. We have discussed the presence of these two contributions in Section 1 [see (1.6) and the ensuing discussion].

The cross section $\bar{\sigma}_{el}^{(FL)}$, is just the compound elastic scattering that was discussed in Chapter IV. Its calculation in terms of transmission factors is given there. One expects processes competitive with compound elastic scattering would become so significant as the projectile energy increases that $\bar{\sigma}_{el}^{(FL)}$ would tend to zero as that energy increases. In other words, the fraction of the flux that is delayed and reemitted into the elastic channel eventually decreases with energy. Most of the delayed flux will contribute to reactions. In the limit, then,

$$\begin{aligned} \langle \sigma_r \rangle &\to \bar{\sigma}_r \\ \langle \sigma_{el} \rangle &\to \bar{\sigma}_{el} \end{aligned} \tag{2.7}$$

The cross section $\langle \sigma_r \rangle$ is directly related to the transmission coefficients T_c [see (IV.7.28)]. From this last equation and for the single-channel case, each partial wave yields

$$T_c = 1 - |\langle S_{cc} \rangle|^2$$

The corresponding partial reaction cross section is

$$\langle \sigma_r^{(c)} \rangle = \pi \lambda^2 T_c$$

which must be multiplied by the appropriate weighting factor for each partial wave. For a spin-independent optical model potential the partial wave series is a series in the orbital angular momentum, l. In that case the weighting factor is $2l + 1$. Comparing with (IV.7.45), one finds that this cross section is identical with the $\sigma^{(c)}$, the cross section for the formation of the compound nucleus, so that

$$\langle \sigma_r \rangle = \sigma^{(c)} \tag{2.8}$$

B. Nonlocal Potentials

It is immediately obvious from the general expression (1.1) for the multichannel optical model, and *a fortiori* for the single-channel projection, (1.7), that the optical model Hamiltonian is energy dependent and nonlocal. The energy dependence is explicitly visible [see (1.1)] in the propagator $(E - H_{QQ} + iI/2)^{-1}$. The nonlocality originates in this term since it describes the process in which the system leaves the incident channel, going to $\mathcal{Q}$ space, propagates in $\mathcal{Q}$ space and then returns to the incident channel. In coordinate space this operator would be a function of two variables, the point at which the interaction, H_{QP}, induces the transition to $\mathcal{Q}$ space and the point at which the interaction, H_{PQ}, induces the return to $\mathcal{P}$ space.‡

Such a nonlocal energy-dependent operator can also be thought of as an energy- and momentum-dependent operator. To see this, let the nonlocal potential $\mathcal{V}$ (assumed spin independent, for simplicity) have the general form

$$\mathcal{V}\psi = \int v_E(\mathbf{r}, \mathbf{r}' - \mathbf{r})\psi(\mathbf{r}')\, d\mathbf{r}' \tag{2.9}$$

where the subscript E reminds us that v is energy dependent. This reduces to a local operator if

$$v_E(\mathbf{r}, \mathbf{r}' - \mathbf{r}) = \delta(\mathbf{r}' - \mathbf{r})v_E(\mathbf{r}) \tag{2.10}$$

since substituting in (2.9) yields

$$\mathcal{V}\psi = v_E(\mathbf{r})\psi(\mathbf{r})$$

Upon making the substitution

$$\mathbf{r}' - \mathbf{r} = \boldsymbol{\rho}$$

in (2.9), one obtains

$$\mathcal{V}\psi = \int v_E(\mathbf{r}, \boldsymbol{\rho})\psi(\mathbf{r} + \boldsymbol{\rho})\, d\boldsymbol{\rho}$$

or using the identity

$$e^{i/\hbar \boldsymbol{\rho}\cdot\mathbf{p}}\psi(\mathbf{r}) = \psi(\mathbf{r} + \boldsymbol{\rho})$$

‡One should combine this dynamic nonlocality, with the contribution of the nonlocality of the nucleon–nucleon forces, a consequence of the composite structure of the nucleon. From the existence of the excited state of the nucleon, the Δ at 1236 MeV, one estimates the size of the nucleon to be $\hbar/(m_\Delta - M_N)c \sim 0.7$ fm.

where

$$\mathbf{p} = \frac{\hbar}{i}\nabla_r \tag{2.11}$$

one obtains

$$\mathscr{V}\psi = \left(\int v_E(\mathbf{r}, \boldsymbol{\rho}) e^{i/\hbar \boldsymbol{\rho}\cdot\mathbf{p}} d\boldsymbol{\rho}\right)\psi(\mathbf{r})$$

Thus the nonlocal potential acting on ψ given by (2.9) can be written as an energy- and momentum-dependent potential

$$\mathscr{V} = V_E(\mathbf{r}, \mathbf{p}) \equiv \int v_E(\mathbf{r}, \boldsymbol{\rho}) e^{i/\hbar \boldsymbol{\rho}\cdot\mathbf{p}} d\boldsymbol{\rho} \tag{2.12}$$

Clearly, the $\mathbf{p}$ in the exponent operates on ψ and not on v_E.

For the most general operator $v_E(\mathbf{r}, \boldsymbol{\rho})V_E$ will contain all powers of the momentum operator $\mathbf{p}$. Two approximations that are commonly used are instructive. In the first, most appropriate at high energy [Perey and Saxon (64)] the momentum operator, $\mathbf{p}$, is replaced by the projectile momentum (in the center of mass) $\mathbf{p}_0$, so that

$$\mathscr{V} \simeq V_E(\mathbf{r}, \mathbf{p}_0) = \int v_E(\mathbf{r}, \boldsymbol{\rho}) e^{i/\hbar \boldsymbol{\rho}\cdot\mathbf{p}_0} d\boldsymbol{\rho} \tag{2.13}$$

With this approximation, $\mathscr{V}$ becomes just a function of E, the energy, and of $\mathbf{r}$. We note one important consequence of (2.13). Assuming that the dependence of v_E on $\boldsymbol{\rho}$ is smooth, that is, significant changes occurring over a range, a, then V_E will decrease with increasing momentum p_0, once $p_0 \geq \hbar/a$. Such a decrease would be modulated by the explicit energy dependence.‡ Indeed, as we shall discuss later, such a decrease does occur, the real part of the optical model potential going though a zero near a projectile energy of 200 MeV. In the present context, this could be considered to be the consequences of an averaging that occurs once the wave length $(\hbar/p_0)$ of the projectile is much smaller than the scale of the nonlocality.

The Perey–Saxon momentum approximation can be improved by using the momentum inside the interaction region [Frahn (65)] rather than that of the incident projectile. In this local momentum approximation one expands $V_E(\mathbf{r}, \mathbf{p})$

‡An empirical analysis omitting explicit E dependence yields ~ 1 fm, or a p_0 very close to the Fermi momentum p_F. As can be seen from the high-energy multiple scattering approximation for the optical potential (Chapter II), the nonlocal term is in part a consequence of correlations. The empirical scale, p_F, could be taken to indicate that the Pauli correlations generated by the exclusion principle is the one of significance.

about $p^2 = P^2$, that is,

$$V_E(\mathbf{r}, \mathbf{p}) \equiv \bar{V}_E(\mathbf{r}, p^2) \simeq \bar{V}_E(\mathbf{r}, P^2) + \left[\frac{\partial \bar{V}_E(\mathbf{r}, p^2)}{\partial p^2}\right]_{p^2 = P^2} (p^2 - P^2) \tag{2.14}$$

where we have made explicit use of the assumption that V_E depends only on p^2. Inserting (2.14), replacing $\mathbf{p}$ by $(\hbar/i)\nabla$, into the Schrödinger equation yields

$$\left\{E + \frac{\hbar^2}{2m}\nabla^2 - \bar{V}_E(\mathbf{r}, P^2) - V_L(\mathbf{r}) - 2m\left[\frac{\partial \bar{V}_E(\mathbf{r}, p^2)}{\partial p^2}\right]_{p^2 = P^2}\left[\left(\frac{\hbar^2}{2m}\nabla^2 + \frac{P^2}{2m}\right)\right]\right\}\psi = 0$$

where $V_L(\mathbf{r})$ is the local part of the optical model potential, H_{PP} of (1.1). If we now chose $P^2(\mathbf{r})$ to satisfy

$$\frac{1}{2m}P^2(r) = E - \bar{V}_E(\mathbf{r}, P^2(\mathbf{r})) - V_L(\mathbf{r}) \tag{2.15}$$

this Schrödinger equation reduces to

$$\left[\frac{\hbar^2}{2M}\nabla^2 + (E - \bar{V}_E(\mathbf{r}, P^2(\mathbf{r})) - V_L(r))\right]\psi = 0 \tag{2.16}$$

Equation (2.15) reduces to the choice $P = p_0$ when $V_L + \bar{V}_E \ll E$, that is, at high energies. It is otherwise an equation determining $P^2(r)$ and therefore the effective potential in (2.16).

Problem. Consider $v_E(\mathbf{r}, \boldsymbol{\rho}) = U(\mathbf{r})[1/(\pi^{1/2}a)^3]e^{-\rho^2/a^2}$. Solve (2.15) graphically, discussing the behavior of $\bar{V}_E(\mathbf{r},(P^2(r))$ as a function of E. Discuss the validity of the expansion equation (2.14). If a is on the order of 1 fm, beyond what energy can this nonlocal potential be treated as a small perturbation?

When the wave length of the incident projectile is long, an expansion of the exponential operator in (2.12) is appropriate:

$$V_E(\mathbf{r}, \mathbf{p}) = \int v_E(\mathbf{r}, \boldsymbol{\rho})\, d\boldsymbol{\rho} + \frac{1}{\hbar}\int v_E(\mathbf{r}, \boldsymbol{\rho})\boldsymbol{\rho}\cdot\mathbf{p}\, d\boldsymbol{\rho} + \frac{1}{2}\left(\frac{i}{\hbar}\right)^2 \int v_E(\mathbf{r}, \boldsymbol{\rho})(\boldsymbol{\rho}\cdot\mathbf{p})^2\, d\boldsymbol{\rho} + \cdots$$

The first term yields a local energy-dependent potential,

$$v_E(\mathbf{r}) \equiv \int v_E(\mathbf{r}, \boldsymbol{\rho})\, d\boldsymbol{\rho}$$

The second term vanishes if we assume that the dependence of $v_E(\mathbf{r}, \boldsymbol{\rho})$ on $\boldsymbol{\rho}$ is spherical, that is, depends only on ρ^2. (This may not be the case for deformed

nuclei or if the spin degree of freedom is taken into account). Under the same assumption the third term becomes

$$\frac{\partial V_E}{\partial p^2} = -\frac{p^2}{6\hbar^2}\int v_E(\mathbf{r},\boldsymbol{\rho})\rho^2\, d\boldsymbol{\rho}$$

so that with $k = p/\hbar$,

$$V_E(\mathbf{r},\mathbf{p}) \simeq v_E(\mathbf{r}) + \left(\frac{\partial V_E}{\partial k^2}\right)k^2 = v_E(\mathbf{r}) - \left(\frac{1}{2k}\frac{\partial V_E}{\partial k}\right)\nabla^2 \tag{2.17}$$

demonstrating explicitly the momentum dependence of the nonlocal $V_E(\mathbf{r},\mathbf{p})$. The partial derivatives are evaluated at $k=0$. This momentum- and energy-dependent potential can be written as an energy-dependent potential as follows. The optical model Schrödinger equation following from (2.17) is

$$\left[\frac{\hbar}{2m}\nabla^2 + E - V_L - v_E(r) + \frac{1}{2k}\frac{\partial V_E}{\partial k}\nabla^2\right]\psi = 0 \tag{2.18a}$$

or

$$\left\{\nabla^2 + \frac{2m}{\hbar^2}\left[E - V_L - v_E - \frac{(m/\hbar^2 k)(\partial V_E/\partial k)}{1+(m/\hbar^2 k)/(\partial V_E/\partial k)}(E - V_L - v_E)\right]\right\}\psi = 0 \tag{2.18b}$$

In discussing this equation one should bear in mind that v_E and $\partial V_E/\partial k$ may both be complex.

On the other hand, one could replace the energy dependence of the nonlocal potential by momentum dependence. Toward this end, expand v_E as follows:

$$v_E = v_0 + E\left(\frac{\partial v_E}{\partial E}\right)_0 + \cdots$$

In this equation we now replace E by

$$E \to -\frac{\hbar^2}{2m}\nabla^2 + V_L + v_0$$

where we have dropped the term in $\partial V/\partial k^2$ as being of higher order when multipled by $\partial v_E/\partial E$. The Schrödinger equation, (2.18*a*), becomes to this order

$$\left\{\left[\frac{\hbar^2}{2m} + \frac{1}{2k}\frac{\partial V_E}{\partial k} + \frac{\hbar^2}{2m}\left(\frac{\partial v_E}{\partial E}\right)_0\right]\nabla^2 + E - (V_L + v_0)\left(1 + \frac{\partial v_E}{\partial E}\right)_0\right\}\psi = 0 \tag{2.19}$$

The brackets multiplying ∇^2 can be related to a space-dependent complex effective mass, m_c^*

$$\frac{\hbar^2}{2m_c^*} = \frac{\hbar^2}{2m} + \frac{1}{2k}\frac{\partial V_E}{\partial k} + \frac{\hbar^2}{2m}\left(\frac{\partial v_E}{\partial E}\right)_0$$

or

$$\frac{m_c^*}{m} = \frac{1}{1 + (m/\hbar^2 k)(\partial V_E/\partial k) + (\partial v_E/\partial E)_0}$$

Define m_{Ec} and m_{kc} by

$$\frac{m_{Ec}}{m} \equiv 1 - \left(\frac{\partial v_E}{\partial E}\right)_0 \tag{2.20a}$$

$$\frac{m_{kc}}{m} \equiv \frac{1}{1 + (m/\hbar^2 k)(\partial V_E/\partial k)} \tag{2.20b}$$

where m_{Ec} depends on the change in mass arising from energy dependence and m_{kc} depends on the change due to momentum dependence. Then to first order,

$$\frac{m_c^*}{m} = \frac{m_{Ec}}{m}\frac{m_{kc}}{m} \tag{2.21}$$

This equation is satisfied exactly in the case of infinite nuclear matter [Migdal (61); Brown (72); the case m_{kc}/m is given in Feshbach (58b)]. No attempt has been made to separate out the imaginary components of m_c^*, m_{Ec}, and m_{kc}. If real values are desired, we define

$$\frac{m_E}{m} \equiv 1 - \mathrm{Re}\left(\frac{\partial v^{(0)}}{\partial E}\right)_0 \qquad \frac{m_k}{m} = \frac{1}{1 + (m/\hbar^2 k)\,\mathrm{Re}(\partial V_E/\partial k)} \tag{2.22a}$$

with

$$\frac{m^*}{m} = \frac{m_k}{m}\frac{m_E}{m} \tag{2.22b}$$

We note that for finite nuclei these quantities are functions of $\mathbf{r}$; in the case of infinite nuclear matter they are constants.

Evaluations of these quantities have been made for infinite nuclear matter using the Brueckner–Hartree–Fock approximation, similar to that described in Chapter VII of de Shalit and Feshbach (74) [Jeukenne, Lejeune, and Mahaux (76, 77); Mahaux (78)]. Brueckner–Hartree–Fock determinations of the optical potential have also been made by Brieva and Rook (77, 78) and Brieva, Geramb, and Rook (78). We shall not discuss these relatively complex calculations but

will use the results of the Liege group to illustrate the behavior of these effective masses with momentum in infinite nuclear matter. Usually the results obtained with a first-order calculation indicated by the subscript 1 will be presented. Higher-order calculations have been made. There are quantitative changes, but the qualitative picture is not modified. In Figs. 2.1 and 2.2 we show the behavior of m_{E1} as a function of k for two nucleon densities, $k_F = 1.35\,\mathrm{fm}^{-1}$ and $k_F = 1.10\,\mathrm{fm}^{-1}$. Two features should be noted. First, m_{E1}/m is greater than unity for $k < 1.5k_F$, and second, it has a sharp peak just above $k = k_F$. This last result depends critically on the choice of the reference spectrum (see Chapter VII of deShalit and Feshbach (74). If a sizable gap is introduced, the sharp energy dependence seen in Figs. 2.2 and 2.3 disappears. The calculated m_{k1}/m are shown in Fig. 2.3. This quantity increases smoothly as the momentum increases. Its value is less than unity, compensating to some extent for m_{E1}/m being greater than unity, in the calculation of the product, (2.23). The values for m_1^*/m are shown in Figs. 2.4 and 2.5.

The strong variation with k in m_{k1}/m persists in the values of m_1^*/m. From each of these sets of curves, Figs. 2.1 to 2.5, it is clear that in the momentum range $k \leqslant 2k_F$, the deviation of the effective mass from unity is substantial and

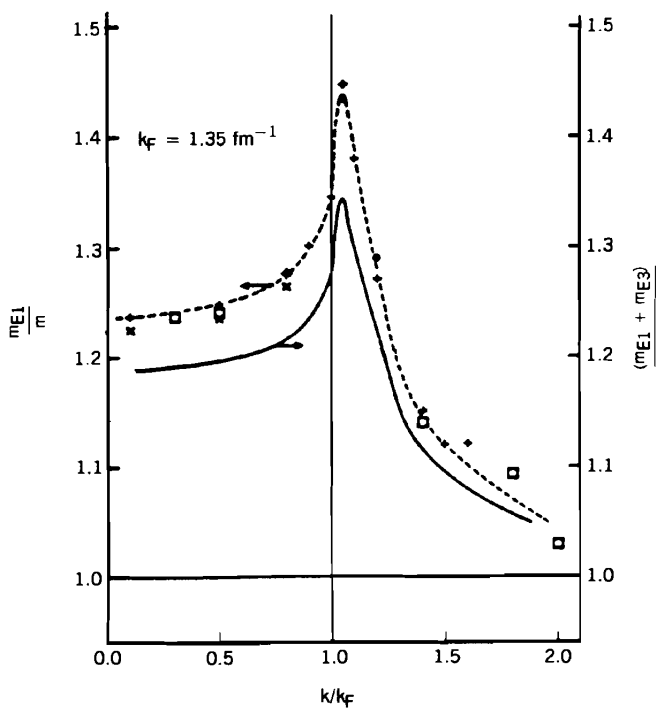

FIG. 2.1. Effective mass m_{E1}/m (dashed curve) and $(m_{E1} + m_{E3})/m$ (solid line) as a function of k for $k_F = 1.35\,\mathrm{fm}^{-1}$. [From Jeukenne, Lejeune, and Mahaux (76).]

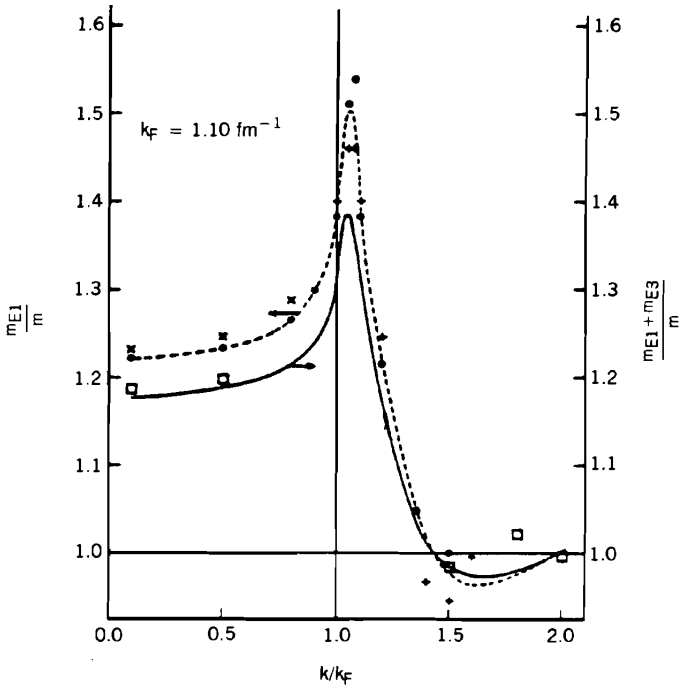

FIG. 2.2. Effective mass m_{E1}/m (dashed curve) and $(m_{E1} + m_{E3})/m$ (solid line) as a function of k for $k_F = 1.10\,\text{fm}^{-1}$. [From Jeukenne, Lejeune, and Mahaux (76).]

that there are appreciable effects arising from the nonlocal nature and energy dependence of the optical potential.

There are two consequences of nonlocality and energy dependence that are of special importance for applications. It follows directly from (2.9) (i.e., from nonlocality) that current conservation is not satisfied locally. This result holds also in the effective mass approximation. Using standard procedures (and taking m^* to be real in order to isolate the effect of interest; (current conservation is, of course, not valid in the presence of absorption), it follows from (2.19) that

$$\frac{\partial \rho}{\partial t} + \operatorname{div} \mathbf{j} = \left(1 - \frac{m}{m^*(r)}\right) \operatorname{div} \mathbf{j} \tag{2.23}$$

where $\mathbf{j}$, the current density, and ρ, the particle density, are given by

$$\mathbf{j} = \frac{\hbar}{2mi}[\psi^* \nabla \psi - \psi \nabla \psi^*] \qquad \rho = \psi^* \psi$$

From this current-conservation equation we see that in addition to the decrease in particle density because of current flow, there is a loss ($m^* < m$) because of

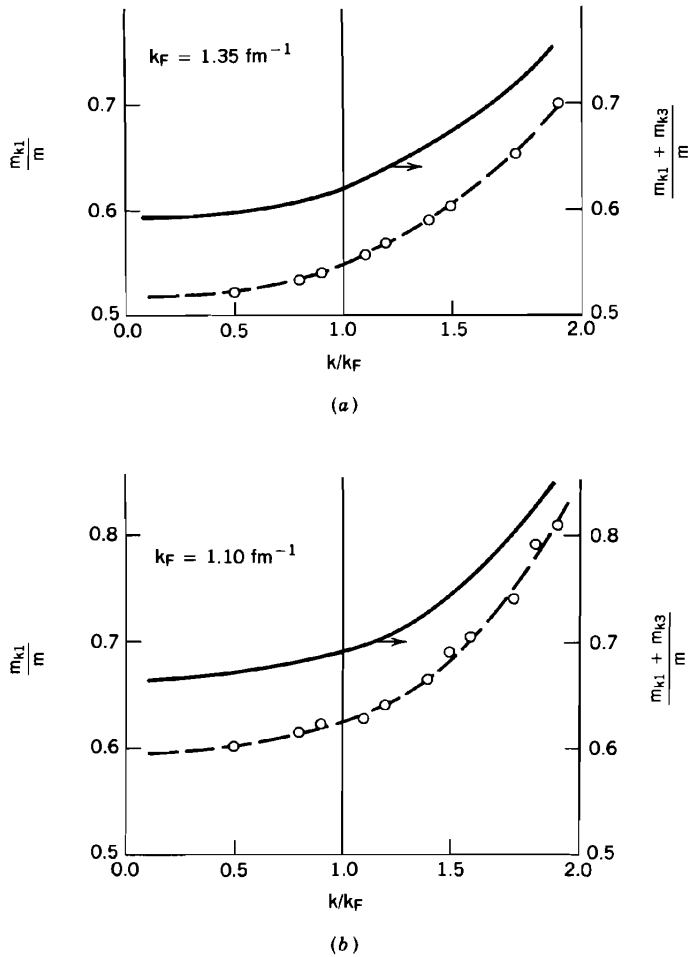

FIG. 2.3. Effective mass m_{k1}/m (dashed curve) and $(m_{k1} + m_{k3})/m$ (solid line) as a function of k_{for} (a) $k_F = 1.35\,\text{fm}^{-1}$ and (b) $k_F = 1.10\,\text{fm}^{-1}$. [From Jeukenne, Lejeune, and Mahaux (76).]

nonlocality and energy dependence. As a consequence, the actual value of ρ in the interaction region where $(m^* < m)$ will be less than that which would be computed using current conservation, as is done when a semiempirical optical model wave function is used. This is known as the *Perey effect* [Perey (63)]. When m^* is a constant independent of r, the empirical particle density should be multiplied by m^*/m, and the corresponding empirical wave function by $(m^*/m)^{1/2}$ in the interaction region.

The second consequence of energy dependence of the optical model potential is the nonorthogonality of wave functions corresponding to different energies. This is a real effect. The exact many-body wave functions are of course

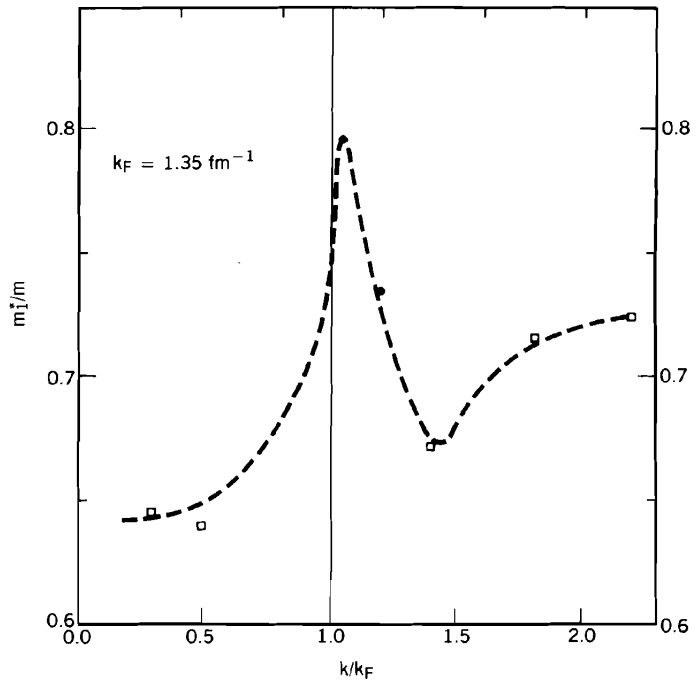

FIG. 2.4. Effective mass m_1^*/m as a function of k for $k_F = 1.35\,\mathrm{fm}^{-1}$. [From Jeukenne, Lejeune, and Mahaux (76).]

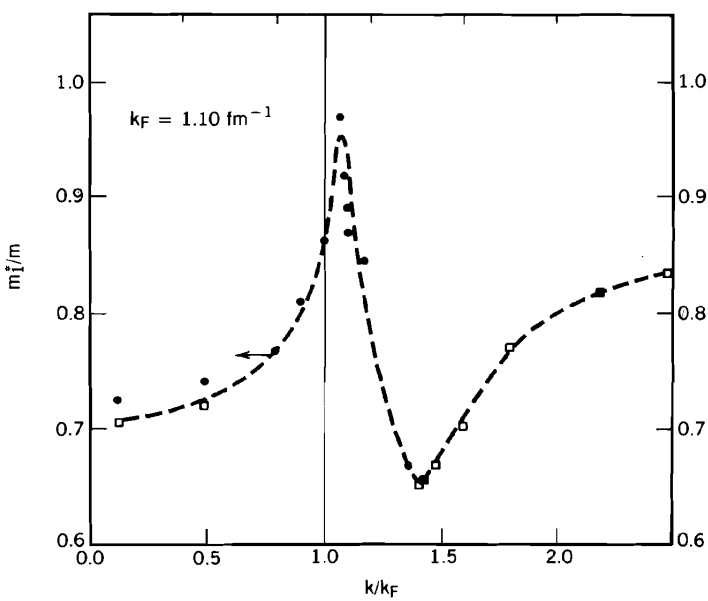

FIG. 2.5. Effective mass m_1^*/m as a function of k for $k_F = 1.10\,\mathrm{fm}^{-1}$ [From Jeukenne, Lejeune, and Mahaux (76).]

orthogonal. But their projections onto the open channels—in this case, to the elastic channel—are not. The physics lies in the fact that the coupling of the open channels to the closed ones (and to each other) is energy dependent, as is immediately obvious from (1.1). Even though the energy has been eliminated, the departure from orthogonality remains in the effective mass approximation, (2.19). The usual orthogonality there is replaced by the new condition

$$\int \tilde{\psi}_E^{(+)*} \psi_{E'}^{(+)} m^*(\mathbf{r}) d\mathbf{r} = 0 \qquad E \neq E' \tag{2.24}$$

where clearly the dependence of m^* on $\mathbf{r}$ is important.

C. The Infinite Medium

Before considering in some detail results obtained from semiempirical analysis, it is desirable to present a global qualitative view of features of the optical model potential for nucleons. Great theoretical simplifications occur if we limit the discussion to the infinite nuclear medium. In that case the nonlocal potential of (2.9) is constrained by the condition that translational invariance be maintained as follows:

$$v_E(\mathbf{r}, \mathbf{r} - \mathbf{r}') \to v_E(\mathbf{r} - \mathbf{r}')$$

Equation (2.12) becomes

$$\mathscr{V} = \int v_E(\boldsymbol{\rho}) e^{i\boldsymbol{\rho}\cdot\mathbf{k}} d\boldsymbol{\rho} = \mathscr{V}(E, \mathbf{k})$$

The local potential V_L must be constant but can depend upon E. Finally, we note that the solutions of the Schrödinger equation in the infinite medium are plane waves. For a wave of momentum $\hbar\mathbf{k}$, the Schrödinger equation reduces to

$$E = \frac{\hbar}{2m} k^2 + V(E, \mathbf{k})$$

$$V = V_L(E) + \mathscr{V}(E, \mathbf{k}) \tag{2.25}$$

an equation determining the relation $E(k)$ or $k(E)$. The nuclear medium is dispersive, the group velocity being given by $(1/\hbar)(dE/dk)$. From (2.25) one can write $V = V(E, k(E))$, where now the potential is local.

Problem. Prove that the group velocity is given by $\hbar k/m^*$.

We shall also make use of the dispersion relation connecting Re V and Im V. Such a relationship is given in (III.2.13). It is useful because even with modest

information on Im V obtained, both theoretically and experimentally, it permits calculating a component of Re V from Im V.

There are some penalties to be paid in going to the infinite nuclear matter. The spin-orbit potential no longer appears. We shall be concerned only with the central potential. The empirical values of the central potential are obtained through the analysis of collisions of nucleons with finite nuclei in which the surface plays a singificant role. Two extrapolations are used. In the first, the value of the local optical model potential (which has spatial and energy dependence, as we shall see in Section 2.E), $V_{\mathrm{OPT}}(E, r)$ at $r = 0$, $V_{\mathrm{OPT}}(E, 0)$, is used as the empirical value of $V(E, k(E))$. The thought is that the conditions which exist at the center of the nucleus approximate those of the infinite medium. As a function of mass number, there will be substantial fluctuations because of nuclear structure effects. There are also ambiguities, particularly with regard to Im $V(E, 0)$, because different models of the optical potential will weight the surface and volume differently. More recently, rather than using $V_{\mathrm{OPT}}(E, 0)$, the volume integral per nucleon of the potential

$$J = \frac{1}{A} \int V_{\mathrm{OPT}}(E, \mathbf{r})\, dv$$

is found to be less sensitive to these ambiguities.

It is also necessary to rephrase dispersion relation (III.2.13) since in the nuclear matter limit the sum over bound states is replaced by an integral as these states form a continuum below the Fermi energy ε_F. It is easy to "guess" the form of the answer, namely to extend the limits in the principal value integral to $-\infty$. The formal development proceeds by using the symmetric particle–hole representation of Chapter VII in deShalit and Feshbach (74, p. 554). Recalling that discussion, we define the creation operator $\alpha_k^\dagger$ as follows:

$$\alpha_k^\dagger = \begin{cases} a_k^\dagger & \varepsilon(k) > \varepsilon_F \\ -a_{-k} & \varepsilon(k) < \varepsilon_F \end{cases}$$

so that $\alpha_k^\dagger$ either creates a particle with energy $\varepsilon(k)$ greater than the Fermi energy or a hole if $\varepsilon(k) < \varepsilon_F$ in the Fermi sea. It is then possible to write

$$P\Psi = \int d\mathbf{k} \alpha_k^\dagger u_k |0\rangle$$

where $|0\rangle$ is the "vacuum", equal in this case to a Fermi sea filled to the Fermi energy ε_F, and u_k is the amplitude of the excitation $\alpha_k^\dagger|0\rangle$.

With this definition it is possible to carry out the derivation leading to

(III.2.13). One obtains

$$\text{Re } V_{\text{eff}}(E,k) = V_{PP} - \frac{1}{\pi}\mathscr{P}\int_{-\infty}^{\infty} \frac{\text{Im } V_{\text{eff}}(\mathscr{E},k)}{E-\mathscr{E}}\,d\mathscr{E} \tag{2.26}$$

One subtraction is performed.

$$\text{Re } V_{\text{eff}}(E,k) = \text{Re } V_{\text{eff}}(\varepsilon_F,k) + \frac{E-\varepsilon_F}{\pi}\mathscr{P}\int_{-\infty}^{\infty} \frac{\text{Im } V_{\text{eff}}(\mathscr{E},k)}{(\varepsilon_F-\mathscr{E})(E-\mathscr{E})}\,d\mathscr{E} \tag{2.27}$$

This relation agrees with that used by Mahaux and Ngô (81) if one replaces the E in their (10) by $E+i\varepsilon$, $\varepsilon\to 0^+$.

The momentum $\mathbf{k}$ appears as a parameter, that is, the dispersion relation must hold for each $\mathbf{k}$. The empirical results for V_{eff} are usually given as functions of the energy only. This reduction can be obtained in principle by replacing k by solving (2.25). In the high-energy limit, the Perey–Saxon result can be used. Or one can average both sides of (2.27) over a k domain. Or one can evaluate at a particular value of k. For example, $V_{\text{eff}}(E,k=0)$ gives the volume integral of $V_{\text{eff}}(E,\rho)$, which should be simply related to J. Mahaux and Ngô (81) assume that Im $V_{\text{eff}}(E,k)$ varies slowly with respect to k for $k<2.5\,\text{fm}^{-1}$. One cannot be that cavalier with Re $V_{\text{eff}}(E_F,k)$ since the nonlocalities arising from the Pauli principle must be taken into account. Mahaux and Ngô expand that term around k_F and use the effective mass approximation. Only m_k enters. The first term, Re $V_{\text{eff}}(\varepsilon_F,k_F)$, is given empirically by -53.3 MeV. With these approximations it is possible to proceed with the exploitation of dispersion relations (2.27).

However, we need an estimate of the magnitude of Im $V_{\text{eff}}(E)$. The method of Lane and Wandel (55) and Clementel and Villi (56), which makes explicit the role of the Pauli principle, provides a first look. The method used is that developed by Goldberger (48). It is based essentially on kinetic theory, from which we learn that the mean free path, L, for a nucleon traveling through a medium, in this case nuclear matter, composed in this case of nucleons, is given by

$$L = \frac{1}{\rho\sigma} \tag{2.28}$$

where ρ is the density of nuclear matter and σ is the nucleon–nucleon cross section. The mean free path L may be related to the imaginary part of the potential as follows. In an infinite medium, a plane wave, $e^{i(k_0+ik_I)Z}$, is a solution of the Schrödinger equation. It follows immediately that

$$L = \frac{1}{2k_I} \qquad k_I = \frac{\rho\sigma}{2} \tag{2.29}$$

Substituting in Schrödinger equation (2.25) gives for weak absorption

$$\begin{aligned} -\operatorname{Im} V &= \hbar v k_I \\ &= \frac{\hbar \rho v \sigma}{2} \end{aligned} \tag{2.30}$$

where v is the velocity, $\hbar k_0/m$.

The medium consists of a Fermi gas of nucleons with levels filled to an energy ε_F and momentum k_F. It is therefore necessary to average σv over the Fermi sea:

$$\langle \sigma \rangle \equiv \frac{\langle v\sigma \rangle}{v} = \frac{3}{4\pi p_F^3} \int \frac{|\mathbf{p}-\mathbf{k}|}{p} d\mathbf{k} \int \sigma(q, \mathbf{q}\cdot\mathbf{q}')\, d\Omega' \qquad q = q'$$

where $\sigma(q, \mathbf{q}\cdot\mathbf{q}')$ is the differential cross section, $\mathbf{p}$ is the incident nucleon momentum, $\mathbf{k}$ is the initial target nucleon momentum, and $\mathbf{q}$ and $\mathbf{q}'$ are the relative initial and final momenta [e.g., $\mathbf{q} = \frac{1}{2}(\mathbf{p}-\mathbf{k})$]. Assuming isotropy [no dependence on $(\mathbf{q}\cdot\mathbf{q})$, so that $\sigma(\mathbf{q}, \mathbf{q}\cdot\mathbf{q}')$ becomes $\sigma(q)/4\pi$, one obtains

$$\langle \sigma \rangle = \frac{3}{4\pi p_F^3 p} \int \frac{p^2 + k^2 - 2p_F^2}{|\mathbf{p}+\mathbf{k}|} \sigma(q)\, d\mathbf{k}$$

The integration over the Fermi sphere can be readily performed when $\sigma(q)$ is a constant σ_0. Then

$$\begin{aligned} \langle \sigma \rangle &= \sigma_0 \left(1 - \frac{7}{5} \left(\frac{p_F}{p} \right)^2 \right) \qquad p^2 > 2p_F^2 \\ &= \sigma_0 \left\{ 1 - \frac{7}{5} \left(\frac{p_F}{p} \right)^2 + \frac{2}{5} \left(\frac{p_F}{p} \right)^2 \left(2 - \left(\frac{p}{p_F} \right)^2 \right)^{5/2} \right\} \qquad p^2 \leqslant p_F^2 \\ &\to \frac{3}{4}\sigma_0 \left(1 - \frac{p_F^2}{p^2} \right)^2 \qquad p \to p_F \end{aligned} \tag{2.31}$$

The result is to be inserted into (2.30) to obtain an estimate of Im V.

We note that as p goes to p_F, Im V will go to zero. This is a consequence of the Pauli principle since it forbids all collisions in which either nucleon ends with an energy less that ε_F. As the incident nucleon energy approaches ε_F, the amount of phase space available for the collision goes to zero. The Pauli effect goes to zero and $\langle \sigma \rangle$ approaches σ_0 as p grows. Of course, the assumptions, such as a constant σ_0, are much too crude for comparison with experiment. Nevertheless, the correct order of magnitude of Im V is obtained with (2.30).

Passatore (67, 68) who pioneered the use of dispersion calculation of Re V_{eff},

showed that if Im V is constant at large energies, Re V at large energies decreases in magnitude, eventally becoming repulsive. As one can see when (2.31) is inserted into (2.27), initially the real part of the potential depends linearly on the energy but eventually develops a logarithmic dependence. Both of these results have been confirmed experimentally. See, for example, the results obtained by Nadasen et al. (81), described in Section V.2.

Mahaux and Ngô (81) quote results obtained using the results of nuclear matter calculations carried out by Mahaux and his collaborators, and compare them to the empirical results. This comparison is shown in Fig. 2.6. The values of $W = -\operatorname{Im} V$ for $E < \varepsilon_F$ are obtained from the spreading width of one-hole states $\Gamma^{\downarrow}/2 = W$. Up to $|E - \varepsilon_F| \sim 50$ MeV, the theoretical results are in reasonable agreement with experiment. There is, of course, a great deal of scatter in the empirical data, presumably a consequence of structure effects, which nuclear matter calculations cannot include explicitly. According to Mahaux and Ngô, the results for Re V are not sensitive to the values of W above $|E - \varepsilon_F| = 50$ MeV. Their results for the Re V are shown in Fig. 2.7 for $|E - \varepsilon_F| < 50$ MeV. The agreement with the empirical depths is good, as the

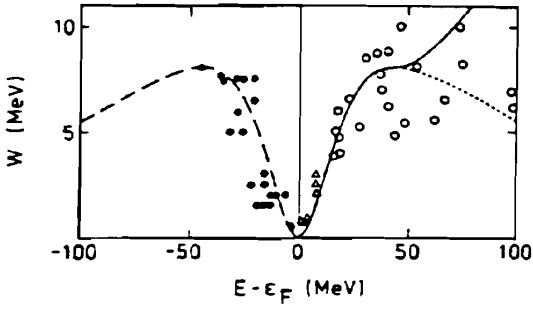

FIG. 2.6. Energy dependence of the imaginary part of the single-particle potential for medium-light nuclei. [From Mahaux and Ngó (81).]

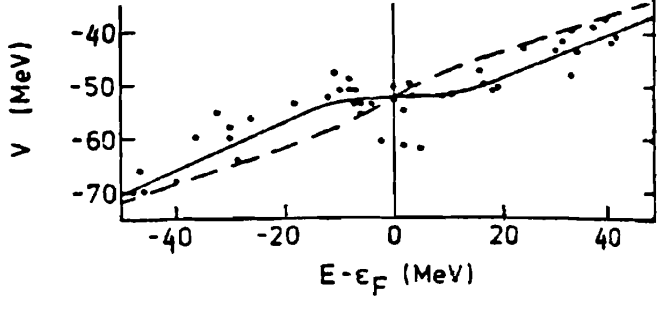

FIG. 2.7. Single-particle potential. The dashed curve gives the Hartree–Fock field and the solid curve the full shell model potential. The dots are the empirical depths. [From Mahaux and Ngô (81).]

theory describes correctly the magnitude, the overall energy dependence, and the plateau at $E = \varepsilon_F$. The plateau is a consequence of the peaking of m^*/m near ε_F.

We conclude this section with a description of the important influence of nonlocality on the imaginary part of the optical potential. To make the latter explicit, rewrite (2.25*a*) as follows:

$$E = \frac{\hbar^2}{2m} k^2 + V_R(E, \mathbf{k}) - iW(E, \mathbf{k}) \tag{2.32}$$

In the effective mass approximation, and assuming that W varies slowly with k, V can be expanded about a value of k, say k_0. Then

$$E \simeq \frac{\hbar^2 k^2}{2m} + V_R(E, k_0) - iW(E, k_0) + (k^2 - k_0^2)\frac{\partial V_R(E, k_0)}{\partial k_0^2} \tag{2.33}$$

If one now puts

$$k = k_R + ik_I \qquad L = \frac{1}{2k_I}$$

and chooses k_0 as the solution of

$$E = \frac{\hbar^2}{2m} k_0^2 + V_R(E, k_0) \tag{2.34}$$

one obtains from (2.32) to first order in k_I:

$$E = \frac{\hbar^2}{2m} k_R^2 + V_R(E, k_0) + (k_R^2 - k_0^2)\frac{\partial V_R}{\partial k_0^2}$$

$$0 = \frac{\hbar^2}{m} k_I k_R - W(E, k_0) + 2k_I k_R \frac{\partial V_R}{\partial k_0^2}$$

From the first of these equations and (2.34), $k_R = k_0$. From the second

$$k_I = \frac{mW(E, k_0)}{\hbar^2 k_0[1 + (m/\hbar^2 k_0)(\partial V/\partial k_0)]}$$

so that

$$k_I = \frac{m_k W(E, k_0)}{\hbar^2 k_0} \qquad L = \frac{\hbar^2 k_0}{2m_k W(E, k_0)} \tag{2.35}$$

This result has important implications. As noted earlier, k can be eliminated from the potential term in (2.32) so that only the potential energy terms depend only on E:

$$E = \frac{\hbar^2}{2m} k^2 + \bar{V}_R(E) - i\bar{W}(E) \tag{2.36}$$

where

$$\bar{V}_R(E) \equiv V_R(E, k(E)), \qquad \bar{W} \equiv W(E, k(E))$$

If one once more picks $k = k_0 + ik_I$ and uses (2.34) and (2.35), one finds that

$$\bar{W} = \frac{m_k}{m} W(E, k_0) \qquad L = \frac{\hbar^2 k_0}{2m_k \bar{W}(E)} \tag{2.37}$$

The last of these equations demonstrates the large effect of non-locality on the imaginary part of the optical potential [Negele and Yazaki (81); Fantoni, Frimen, and Pandhariponde (81); Bernard and Van Glai (78)]. When the nonlocal energy-dependent optical potential is approximated by a local energy-dependent potential through the Perey–Saxon approximation, $k \to k_0$, the imaginary part of the potential must be multiplid by m_k/m to take the effect of nonlocality into account. This effect must also be contained in the effective potential method of Frahn as outlined in the discussion following (2.14).

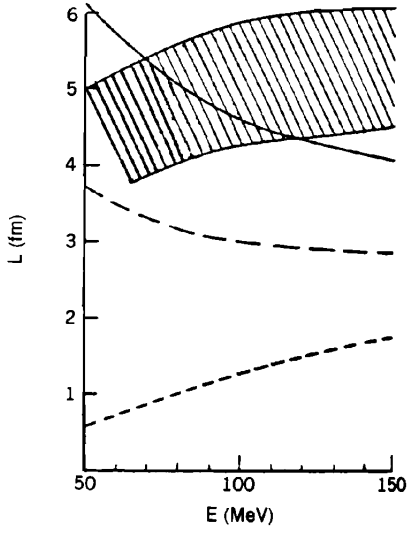

FIG. 2.8. Comparison of three approximations to the mean free path with the range of values compatible with the reaction cross sections for Ca, Zr, or Pb (shaded band). The short dashed curve is given by $(1/\sigma p)$; the long dashed curve is obtained from (2.37) neglecting the factor m_k/m. The solid line is the correct nonlocal expression in (2.37). [From Negele and Yazaki (81).]

An immediate application of these considerations is to the mean free path. Negele and Yazaki (81) calculated the mean free path using the results of Jeukenne Lejeune, and Mahaux (76) (see Fig. 2.8). Agreement with experiment, which provides only rough estimates, showed that the effective mass correction given by (2.37) is essential. It has the effect of increasing the mean free path by as much as 1.7. Negele and Yazaki make the point that the effect of nonlocality is important for an understanding of the large mean free path of a nucleon in nuclear matter, a result of importance for the understanding of the foundation of the mean field (shell model, optical model, etc.) approximation in nuclei.

D. Angular-Momentum-Dependent Potentials

Optical model potentials, which are functions of L^2 ($L = \mathbf{r} \times \mathbf{p}$), the square angular momentum operator, have been proposed by Kobos and MacIntosh (79). This particular kind of momentum dependence could be a consequence of a particular sort of nonlocality in which the kernel $v_E(\mathbf{r}, \mathbf{r}' - \mathbf{r})$ in (2.9) involves only those $\mathbf{r}'$ that can be obtained from $\mathbf{r}$ by a rotation. Such a special connection, $\mathbf{r}$ and $\mathbf{r}'$, could occur for interactions limited to the surface region of the nuclear system. The underlying physical mechanism could be surface waves propagating from $\mathbf{r}'$ to $\mathbf{r}$. If the system is deformed, these would correspond to excitation of rotational levels and their deexcitation. More generally, potentials that are L dependent can be obtained directly from (2.9) by expansion of v_E in a series of Legendre polynomials that are functions of $\mathbf{r}\cdot\mathbf{r}'$. Such an expansion is entirely equivalent to the Taylor series of (2.17).

E. Empirical Optical Model Potentials: Nucleon Projectile

In the empirical determination of the optical model potentials, one initially assumes the functional form of the potential involving a number of unspecified parameters. This is followed by a determination of these parameters which are chosen so as to obtain a best fit the experimental data. As the data have become more accurate and as more aspects of the nucleon–nucleus interaction have been studied, the forms used have become more elaborate. A commonly used form, the '*standard form*', is given by Perey (63), and Perey and Perey (74):

$$V_{\text{opt}} = \mathscr{V}_c + \boldsymbol{\sigma}\cdot\mathbf{L}\mathscr{V}_{so}$$

$$\mathscr{V}_c \equiv V_{\text{Coul}} - Vf(x_0) - i\left[Wf(x_W) - 4W_D\frac{d}{dx_D}f(x_D)\right] \tag{2.38a}$$

$$\mathscr{V}_{so} = \left(\frac{\hbar}{m_\pi c}\right)^2 V_{so}\frac{1}{r}\frac{d}{dr}f(x_{so}) \tag{2.38b}$$

and where $\hbar\mathbf{L}$ is the angular momentum operator and V, W, W_D, V_{so} are constants. V_{Coul} is the Coulomb interaction with a uniformly charged sphere of

radius R_c:

$$V_{\text{Coul}} = \begin{cases} \dfrac{zZe^2}{r} & r \geqslant R_c \\ \dfrac{zZe^2}{2R_c}\left(3 - \dfrac{r^2}{R_c^2}\right) & r \leqslant R_c \end{cases} \tag{2.39}$$

where ze is the charge of the projectile and Ze that of the target nucleus. The function $f(x)$ is usually taken to be in the Woods–Saxon (54) form:

$$f(x_i) = \frac{1}{1 + e^{x_i}} \qquad x_i = \frac{r - r_i A^{1/3}}{a_i} \qquad R_i = r_i A^{1/3} \tag{2.40}$$

The Woods–Saxon form (see Fig. 2.9) characteristically is roughly constant within the nucleus, decaying exponentially at large distances at a rate governed by the value of a_i. The radius parameters, R_i, is the value of r at which $f(x_i)$ is one-half of its value at $r = 0$. The function $-4f'(x)$ has its largest values in the surface region, $r = R \pm 1.5a$. Thus V_{opt} has a real term that has its largest value for $r < R_0$ and is therefore referred to as a volume term. The imaginary component has a volume term $f(x_W)$ and a surface term $(-4f'(x_D)$. In addition, there is a spin-orbit term that is concentrated at the surface. Qualitatively, these components are intuitively satisfactory. The real potential should be a reasonable continuation of the shell model potential into positive energies; the absorption should have a strong surface component, particularly at the lower energies, where the excitation of surface collective models should dominate; and the spin-orbit term should be surface dominated since it vanishes in the infinite nucleus limit.‡ However, it must not be forgotten that the Woods–Saxon form has no other validating support, and indeed many other forms have been used [see Marmier and Sheldon (70, p. 1102) and Feshbach (58)] that have similar properties. As we shall see at intermediate energies (see Section 2.F), it must be replaced by a nonmonotonic form with a repulsive central region and an attractive surface component.

The parameters, V, W, W_D, V_{so}, R_c, R_i, and a_i are adjusted to fit all the available data. Moreover, they are required to "track," that is, to vary smoothly with the nucleon energy and with atomic and mass number. By a fine tuning of the values of the parameters, one can generally obtain a nearly perfect fit of the data for each target nucleus and for each energy. Such precise fits are often necessary for the calculation of reaction processes. However, in this volume we

‡The comparison with the shell model potential is not straightforward. Both it and the optical model are single-channel potentials in which the effect of other channels or configurations are included approximately. It is not clear to what extent the approximations in the two cases are consistent. However, in the limit in which the mean field approximation (e.g., as obtained from the Brueckner–Hartree–Fock method) is accurate, the comparison is valid.

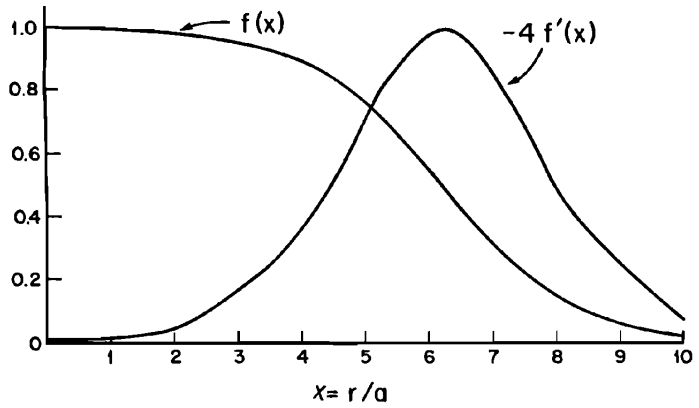

FIG. 2.9. Woods–Saxon potential and its derivative.

are concerned more with the global properties of these parameters to see the trends as a function of energy and target. Strong fluctuations away from the average for a given nucleus of class of nuclei could indicate the presence of nuclear structure effects. We shall discuss these in some detail later. For the present it will suffice to remark that strong fluctuations may be removed if the coupling of the elastic channel to other channels is explicitly considered through the use of the coupled-channel optical model in place of the single-channel description. Generally, this coupling gives rise to smooth behavior in the elastic channel, so that a single-channel optical model suffices. However, in the presence of special effects, as exemplified by coupling to vibrational or rotational states or generally to doorway state resonances, a single channel is inadequate and the results physically not meaningful.

Form equation (2.38) exhausts the possible spatial invariants only if the target nucleus has zero spin. If it has a spin I, with corresponding spin operator $\mathbf{I}$, many other invariants can be formed [Feshbach (58)]. A few of the many possibilities are

$$\boldsymbol{\sigma}\cdot\mathbf{I}, \quad \mathbf{L}\cdot\mathbf{I}, \quad (\boldsymbol{\sigma}\cdot\mathbf{r})(\mathbf{I}\cdot\mathbf{r}), \quad (\boldsymbol{\sigma}\cdot\mathbf{I})(\mathbf{L}\cdot\mathbf{I}), \quad \text{etc.} \tag{2.41}$$

The evidence for the presence of these terms is rather meager, indicating that they are relatively weak, on the order of a fraction of an MeV [see Hodgson (80); Batty (71)].

Phase-Shift Analysis: Elastic Scattering. Restricting our considerations to potential equation (2.38), that is, either to spin-zero target nuclei or neglecting terms dependent on the spin of the target I, such as those given in (2.41), the scattering amplitude can be written as follows (see Appendix B):

$$f = A(k,\theta) + B(k,\theta)\boldsymbol{\sigma}\cdot\mathbf{n} \tag{2.42}$$

where $\mathbf{n}$ is a unit vector perpendicular to the scattering place:

$$\mathbf{n} = \frac{\mathbf{k}_i \times \mathbf{k}_f}{|\mathbf{k}_i \times \mathbf{k}_f|} \tag{2.43}$$

where $\hbar\mathbf{k}_i$ is the incident momentum, $\hbar\mathbf{k}_f$ the final momentum, and θ is the angle between them:

$$\mathbf{k}_i \cdot \mathbf{k}_f = k^2 \cos\theta, \qquad |\mathbf{k}_i \times \mathbf{k}_f| = k^2 \sin\theta$$

The quantities A and B can be expanded in a partial wave series:

$$A(k,\theta) = \frac{1}{2ik} \sum_0^\infty [(l+1)(e^{2i\delta_l^{(+)}} - 1) + l(e^{2i\delta_l^{(-)}} - 1)] P_l(\cos\theta) \tag{2.44a}$$

$$B(k,\theta) = \frac{1}{2k} \sum_1^\infty (e^{2i\delta_l^{(+)}} - e^{2i\delta_l^{(-)}}) P_l^{(1)}(\cos\theta) \tag{2.44b}$$

where

$$P_l^{(1)} = \sin\theta \frac{d}{d(\cos\theta)} P_l(\cos\theta)$$

The phase shifts $\delta_l^{(\pm)}$ are obtained from the asymptotic form of the solutions to the radial Schrödinger equations

$$\frac{d^2\psi(j = l + \frac{1}{2}, r)}{dr^2} + \left[k^2 - \frac{l(l+1)}{r^2} - \mathscr{V}_c - l\mathscr{V}_{so} \right] \psi(j = l + \tfrac{1}{2}, r) = 0$$

$$\frac{d^2\psi(j = l - \frac{1}{2}, r)}{dr^2} + \left[k^2 - \frac{l(l+1)}{r^2} - \mathscr{V}_c + (l+1)\mathscr{V}_{so} \right] \psi(j = l - \tfrac{1}{2}, r) = 0$$

In obtaining these equations, we have made use of the results

$$(\boldsymbol{\sigma} \cdot \mathbf{L})\psi(j = l + \tfrac{1}{2}, r) = l\psi(j = l + \tfrac{1}{2}, r)$$

$$(\boldsymbol{\sigma} \cdot \mathbf{L})\psi(j = l - \tfrac{1}{2}, r) = -(l+1)\psi(j = l - \tfrac{1}{2}, r)$$

Asymptotically,

$$\psi(j = l \pm \tfrac{1}{2}, r) \to \sin\left(kr - \frac{l\pi}{2} + \delta_l^{(\pm)} \right) \tag{2.45}$$

The differential cross section for the elastic scattering of an unpolarized beam is

$$\left\langle \frac{d\sigma}{d\Omega} \right\rangle_{\text{unpol}} = |A|^2 + |B|^2 \tag{2.46}$$

while the total elastic cross section is

$$\langle\sigma_{\text{tot}}^{\text{el}}\rangle = \frac{\pi}{k^2}\sum_{l=0}\{|(l+1)(e^{2i\delta_l^{(+)}}-1)+l(e^{2i\delta_l^{(-)}}-1)|^2+[l(l+1)]|e^{2i\delta_l^{(+)}}-e^{2i\delta_l^{(-)}}|^2\}$$

or

$$\langle\sigma_{\text{tot}}^{(\text{el})}\rangle = \frac{\pi}{k^2}\sum_{l=0}^{\infty}[(l+1)|e^{2i\delta_l^{(+)}}-1|^2+l|e^{2i\delta_l^{(-)}}-1|^2] \tag{2.47}$$

The total cross section is given by the optical theorem:

$$\langle\sigma_{\text{tot}}\rangle = \frac{2\pi}{k^2}\sum_{l=0}^{\infty}[(l+1)(1-\text{Re}\,e^{2i\delta_l^{(+)}})+l(1-\text{Re}\,e^{2i\delta_l^{(-)}})] \tag{2.48}$$

The optical model reaction cross section is the difference, (2.4):

$$\langle\sigma_r\rangle = \langle\sigma_{\text{tot}}\rangle - \langle\sigma_{\text{tot}}^{(\text{el})}\rangle = \frac{\pi}{k^2}\sum_{l=0}^{\infty}[(2l+1)-(l+1)|e^{2i\delta_l^{(+)}}|^2-l|e^{2i\delta_l^{(-)}}|^2] \tag{2.49}$$

These expressions, (2.46), (2.47) (2.48), and (2.49), in the absence of the spin-orbit potential so that $\delta_l^{(+)}=\delta_l^{(-)}$, reduce to the spin-zero results. These are:

$$f(\theta) = \frac{1}{2ik}\sum_{0}^{\infty}(2l+1)(e^{2i\delta_l}-1)P_l(\cos\theta) \tag{2.44a'}$$

$$\langle\sigma_{\text{tot}}^{(\text{el})}\rangle = \frac{\pi}{k^2}\sum_{0}^{\infty}(2l+1)|e^{2i\delta_l}-1|^2 = \frac{4\pi}{k^2}\sum(2l+1)[\sin^2\xi_l e^{-2\eta_l}+\tfrac{1}{4}(1-e^{-2\eta_l})^2] \tag{2.47'}$$

inserting $\delta=\xi+i\eta$. Finally,

$$\langle\sigma_{\text{tot}}\rangle = \frac{4\pi}{k^2}\sum_{0}^{\infty}(2l+1)[\sin^2\xi_l e^{-2\eta_l}+\tfrac{1}{2}(1-e^{-2\eta_l})] \tag{2.48'}$$

$$\langle\sigma_r\rangle = \frac{\pi}{k^2}\sum(2l+1)(1-e^{-4\eta_l}) \tag{2.49'}$$

and the transmission factor [see (IV.3.2)

$$T_l = 1-e^{-4\eta_l} \tag{2.49''}$$

The polarization (= analyzing power if time-reversal invariance is satisfied) generated in the elastic scattering of an unpolarized beam is transverse to the

scattering plane:

$$\mathbf{P} = \frac{\operatorname{tr} f^{+} \boldsymbol{\sigma} f}{\operatorname{tr} f^{+} f} = 2 \frac{\operatorname{Re} AB^{*}}{|A|^{2} + |B|^{2}} \mathbf{n} = 2P\mathbf{n} \tag{2.50}$$

If the incident beam is polarized, the angular distribution becomes

$$\left\langle \frac{d\sigma}{d\Omega} \right\rangle_{\text{pol}} = \left\langle \frac{d\sigma}{d\Omega} \right\rangle_{\text{unpol}} (1 + P_p P \mathbf{n}_p \cdot \mathbf{n}) \tag{2.51}$$

where P_p gives the beam polarization and $\mathbf{n}_p$ its polarization direction. By measuring the asymmetry, that is, the difference in $d\sigma/d\Omega$ with respect to the scattering plane, one can determine P. Measurements of the angular distribution after a second scattering, that is, by analyzer, permit the determination of Im AB^{*} (and $|B|^{2}$) and finally, of A and B separately (to within a phase) if $\langle d\sigma/d\Omega \rangle_{\text{pol}}$ is measured as well.

The following parametrization for AB^{*} is often used:

$$\frac{2AB^{*}}{(|A|^{2} + |B|^{2})} = P(\theta) + iQ(\theta) \tag{2.52}$$

where Q is referred as the spin rotation function, so that

$$Q = \frac{2 \operatorname{Im} AB^{*}}{(|A|^{2} + |B|^{2})}$$

Q is related to the Wolfenstein parameters $R(\theta)$ and $A(\theta)$ (see Appendix B) by

$$Q = R(\theta) \sin\theta + A(\theta) \cos\theta \tag{2.53}$$

Note that if σ, P, and Q are measured, the amplitude f is determined to within a phase.

Low-Energy Scattering. At sufficiently low projectile energy only the $s, l = 0$ term in the partial wave analysis will be significant. The angular distribution is spherical,

$$A(k, \theta) \to \frac{1}{2ik} (e^{2i\delta} - 1) \tag{2.54}$$

$$B(k, \theta) \to 0$$

At these low energies only neutral projectiles, in particular neutrons, are useful. Writing

$$\delta_0 = \xi_0 + i\eta_0 \qquad \eta_0 \geq 0 \tag{2.55}$$

since the potentials involved are complex and absorptive, we obtain for the scattering amplitude equation (2.42):

$$\langle f \rangle = \frac{i}{2k}(1 - e^{-2\eta_0} e^{2i\xi_0}) \tag{2.56}$$

The various cross sections are

$$\langle \sigma_{\text{tot}}^{(\text{el})} \rangle = \frac{4\pi}{k^2}\left[e^{-2\eta_0} \sin^2 \xi_0 + \left(\frac{1 - e^{-2\eta_0}}{2} \right)^2 \right] \tag{2.57a}$$

$$\langle \sigma_{\text{tot}} \rangle = \frac{4\pi}{k^2}\left[\left(e^{-2\eta_0} \sin^2 \xi_0 + \frac{1 - e^{-2\eta_0}}{2} \right] \right) \tag{2.57b}$$

$$\langle \sigma_r \rangle = \frac{\pi}{k^2}(1 - e^{-4\eta_0}) \tag{2.57c}$$

Note that according to (2.49″), the optical model transmission factor $1 - |e^{2i\delta_0}|^2$ equals

$$\langle T_0 \rangle = 1 - e^{-4\eta_0} \tag{2.57d}$$

At zero energy both ξ_0 and η_0 approach zero. Define these limits by

$$\xi_0 \to -ka \qquad \eta_0 \to kb \tag{2.58}$$

so that

$$kA \to \delta_0 \to -k(a - ib) \tag{2.59}$$

where a—ib is a *complex scattering length.* The total elastic cross section is

$$\begin{aligned} \langle \sigma_{\text{tot}}^{(\text{el})} \rangle &\to 4\pi(a^2 + b^2) \\ \langle \sigma_r \rangle &\to 4\pi\left(\frac{b}{k} - 2b^2 \right) \end{aligned} \tag{2.60}$$

so that

$$\langle \sigma_{\text{tot}} \rangle \to 4\pi\left(a^2 - b^2 + \frac{b}{k} \right) \tag{2.61}$$

where the assumption that follows from the effective range relation has been made:

$$\eta_0 \to kb + O(k^3)$$

The reaction and total cross section both grow like $1/k$ as k approaches zero. This is the familiar $(1/v)$ absorption law. The elastic cross section $\langle \sigma_{\text{tot}}^{(\text{el})} \rangle$ is used to define an effective radius, $\bar{R}$:

$$\langle \sigma_{\text{tot}}^{(\text{el})} \rangle = 4\pi \bar{R}^2$$

where

$$\bar{R}^2 = a^2 + b^2 \tag{2.62}$$

For reference we give the low-energy limit for the case of a target nucleus with spin I. The two possible values for the total J are $I \pm \frac{1}{2}$. Since the weighting factor for each value of J is

$$g = \frac{2J+1}{2(2I+1)}$$

(2.47) is replaced by

$$\langle \sigma_{\text{tot}} \rangle \to 4\pi \left[g_+ (a_+^2 - b_+^2) + \frac{b_+}{k} \right] + 4\pi \left[g_- (a_-^2 - b_-^2) + \frac{b_-}{k} \right] \tag{2.63}$$

where $a_+ - ib_+$ is the scattering length for $J = I + \frac{1}{2}$, $a_- - ib_-$ for $J = I - \frac{1}{2}$. The weights g_+ and g_- are given by

$$\begin{aligned} g_+ &= \frac{I+1}{2I+1} \\ g_- &= \frac{I}{2I+1} \end{aligned} \tag{2.64}$$

Finally, we shall relate the parameter b with the strength function $\langle \Gamma/D \rangle$. To that end we write the exact elastic amplitude as the sum of a potential scattering term plus a sum of resonance terms. Moreover, at these very low energies, the width for inelastic processes (radiative capture) can be neglected compared to the elastic width. Hence [see (IV.2.18)]

$$f = \frac{1}{k} \left[e^{i\delta} \sin \delta - e^{2i\delta} \sum_\lambda \frac{\Gamma_\lambda/2}{E - E_\lambda + (i/2)\Gamma_\lambda} \right]$$

where δ, the potential scattering phase shift, is real. This formula assumes that the resonances in the sum over λ are not overlapping. Using the "box" averaging (it is assumed that δ, k, Γ_λ, or E_λ do not vary appreciably over ΔE),

$$\langle f \rangle = \frac{1}{k} \left[e^{i\delta} \sin \delta - e^{2i\delta} \sum_\lambda \frac{1}{\Delta E} \int_{E_\lambda - \Delta E/2}^{E_\lambda + \Delta E/2} \frac{(\Gamma_\lambda/2) dE}{E - E_\lambda + i(\Gamma_\lambda/2)} \right]$$

The integral is easily evaluated. Assuming that $\Delta E/\Gamma_\lambda \gg 1$, one obtains

$$\langle f \rangle = \frac{1}{k}\left(e^{i\delta}\sin\delta + \frac{i\pi e^{2i\delta}}{2}\sum_\lambda \frac{\Gamma_\lambda}{\Delta E}\right)$$

Noting that

$$\frac{\sum \Gamma_\lambda}{\Delta E} = \frac{\langle \Gamma \rangle}{D}$$

where D is the average distance between levels λ, we rewrite $\langle f \rangle$ in a form that makes comparisons with (2.56) easy:

$$\langle f \rangle = \frac{i}{2k}\left(1 - e^{2i\delta} + \frac{\pi\langle \Gamma \rangle}{D} e^{2i\delta}\right)$$

This yields

$$e^{-2\eta_0 + 2i\xi_0} = e^{2i\delta}\left(1 - \frac{\pi\langle \Gamma \rangle}{D}\right)$$

For $\langle \Gamma \rangle / D < 1$, it follows that

$$\xi_0 = \delta$$

$$e^{-2\eta_0} = 1 - \pi\frac{\langle \Gamma \rangle}{D} \tag{2.65a}$$

so that

$$\langle \sigma_r \rangle = \frac{4\pi}{k^2}\frac{\pi\langle \Gamma \rangle}{2D}\left(1 - \frac{\pi\langle \Gamma \rangle}{2D}\right) = \frac{\pi}{k^2}\langle T_0 \rangle \tag{2.65b}$$

$$\langle \sigma_{\text{tot}} \rangle = \frac{4\pi}{k^2}\left[\left(1 - \frac{\pi\langle \Gamma \rangle}{D}\right)\sin^2\xi_0 + \frac{\pi}{2}\frac{\langle \Gamma \rangle}{D}\right] \tag{2.65c}$$

Comparing (2.65a) with (2.60), we find that

$$b = \frac{1}{k}\frac{\pi\langle \Gamma \rangle}{2D}\left(1 + \frac{\pi\langle \Gamma \rangle}{2D}\right) \tag{2.66}$$

The relevant experimental data are generally summarized in two figures. In one the strength function S_0 (the subscript refers to the l value)

$$S_0 = \frac{\langle \Gamma \rangle}{D}\left(\frac{E_0}{E}\right)^{1/2}$$

where E_0 is an arbitrary energy, usually taken to be 1 eV, is plotted. In the other, the length

$$R' \equiv \left(1 - \frac{\pi\langle\Gamma\rangle}{D}\right)^{1/2} a$$

Figure 2.10 gives the strength function $(E_0/E)^{1/2}S_0$ with $E_0 = 1$ eV. The experimental points are obtained by direct measurement of the width of individual neutron s-wave resonances, summing the widths in an interval ΔE and dividing the sum by ΔE. The solid line gives the results of an optical model calculation which includes the effect of deformation, while the dashed line is obtained from a spherical optical model. The peaks represent values of A, or more precisely, values of the nuclear radius R for which the overlap of the square magnitude of the wave function inside the nucleus $|\chi_0|^2$ [see (2.68)] with the imaginary potential is a maximum. Using the rough formula

$$\sqrt{\frac{2mV_0}{\hbar^2}}\, R = (n + \tfrac{1}{2})\pi$$

which gives the values of n for which the s radial wave function has a maximum at R, one can readily show that the maxima Fig 2.10 are due to the $3s(n = 2)$ and $4s(n = 3)$ resonances. Deformations split the large peak at $A \sim 152$ into two peaks with maxima near $A \sim 148$ and $A \sim 185$, in substantial agreement with

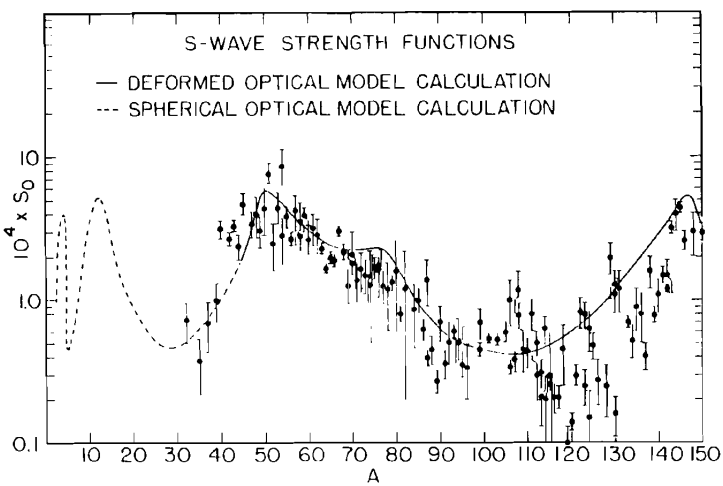

FIG. 2.10. Comparison of theoretical with experimental values of the s-wave neutron strength function. The solid curve represents deformed optical model calculations, and the dashed curve is based on spherical optical model calculations [Mughabghab, Divadeenam, and Holden (84)].

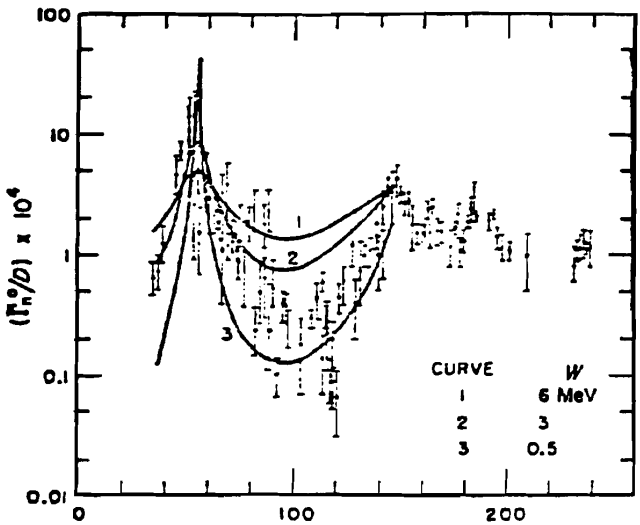

FIG. 2.11. S-wave strength function comparison of experiment with three strengths for the volume absorption potential. [From Moldauer (63).]

much of the data. A splitting that is much less pronounced occurs near the $A \sim 60$ peak. However, anomalies remain. The most pronounced is the large group of very low values of S_0 in the region extending from $A \sim 80$ to $A \sim 130$. This can be summarized by stating that the value of the imaginary potential W is anomolously low in this region (Fig. 2.11).

One physical explanation has been suggested by Block and Feshbach (63), in which it is proposed that the density of the two particle–one hole doorway states, through which the formation of the compound nucleus proceeds, is low in this region. The comparison between experiment and theory is shown in Fig. 2.12. More recently, Kirouac (75) has considered, on essentially this basis, the strength function $\langle S_0 \rangle$ for $143 < A < 158$, where, as he has shown, there is a strong odd–even effect, as illustrated in Fig. 2.13. The theoretical results are in good agreement with the data (Fig. 2.14). The Block mechanism, based on nuclear structure considerations, thus provides an explanation for the fluctuations as well as the average behavior.

On the other hand, a fit to the average behavior has been obtained by Moldauer (63) by using "surface" absorption optical potential concentrated somewhat outside the surface region. The maximum of this potential is 0.5 fm greater than the radius parameters of the Woods–Saxon form used for the volume potentials, $Vf(x_0)$ of (2.26) (see Fig. 2.15).

These two approaches exemplify one of the tactical problems that arise in making optical model fits. Should one adjust the parameters of the potential to obtain a fit, or should one search for the explanation of an anomoly in nuclear structure properties? The first procedure is of importance for

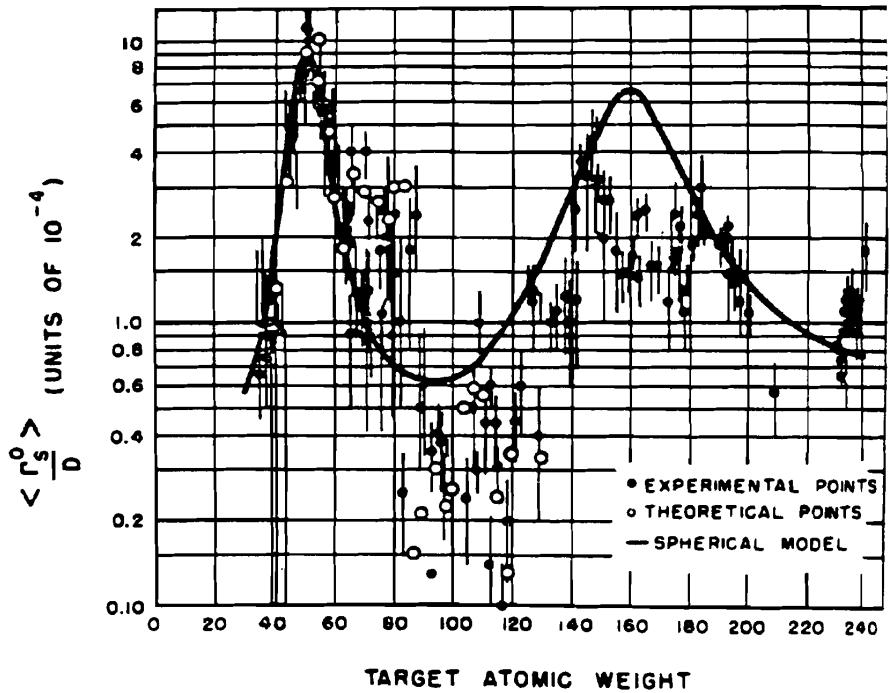

FIG. 2.12. *S*-wave strength function. [From Block and Feshbach (63).]

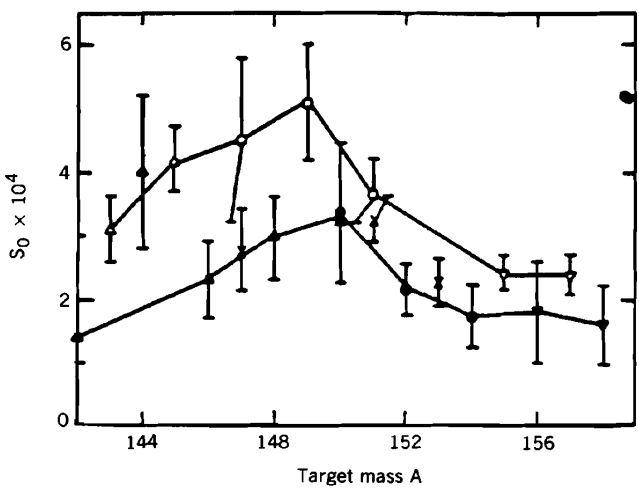

FIG. 2.13. *S*-wave neutron strength functions of even *Z*-odd *N* nuclei (open symbols) and even *Z*-even *N* nuclei (closed symbols) in the first peak of the 4*S* resonance. Three odd-*Z* isotopes (×) are also shown. [From Kirouac (75).]

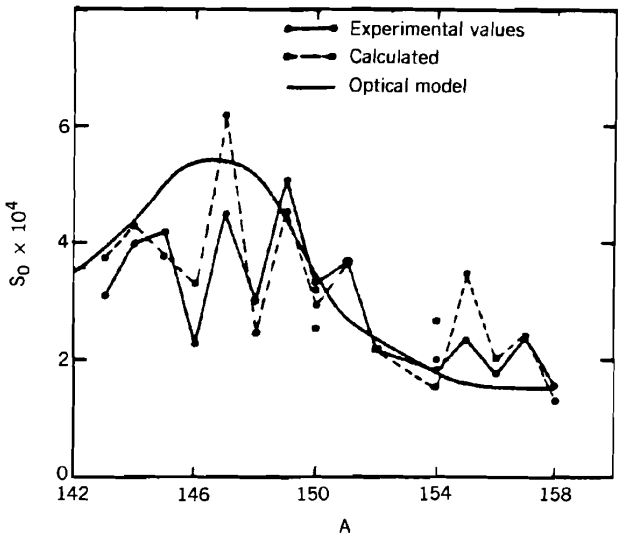

FIG. 2.14. Calculated fluctuations in s-wave neutron strength functions $143 < A < 158$. [From Kirouac (75).]

applications. But differences in the various potentials will be difficult to interpret, being sensitive to the choice of the forms used for the optical model potential. The second is, in the long run, more fundamental, but its meaning will be clarified completely only with the development of a quantitative understanding of the optical model potential.

Problem. Starting with the equation

$$\frac{1}{r^2}\frac{d}{dr}r^2\frac{d\chi_l}{dr}+\left[k^2-\frac{l(l+1)}{r^2}-\frac{2\mu}{\hbar^2}(V+iW)\right]\chi_l=0$$

derive (IV.3.3)

$$\langle T_l\rangle = 4k\int\chi_l^*\left(-\frac{2\mu}{\hbar^2}W\right)\chi_l r^2\,dr$$

Using the approximate relation [see (2.65b) and (2.57d)], valid for $\Gamma_0/D \ll 1$,

$$\langle T_0\rangle = 2\pi\frac{\langle\Gamma_0\rangle}{D} \tag{2.67}$$

show that

$$\frac{\langle\Gamma_0\rangle}{D}=\frac{2k}{\pi}\int\chi_0^*\left(-\frac{2\mu}{\hbar^2}W\right)\chi_0 r^2\,dr \tag{2.68}$$

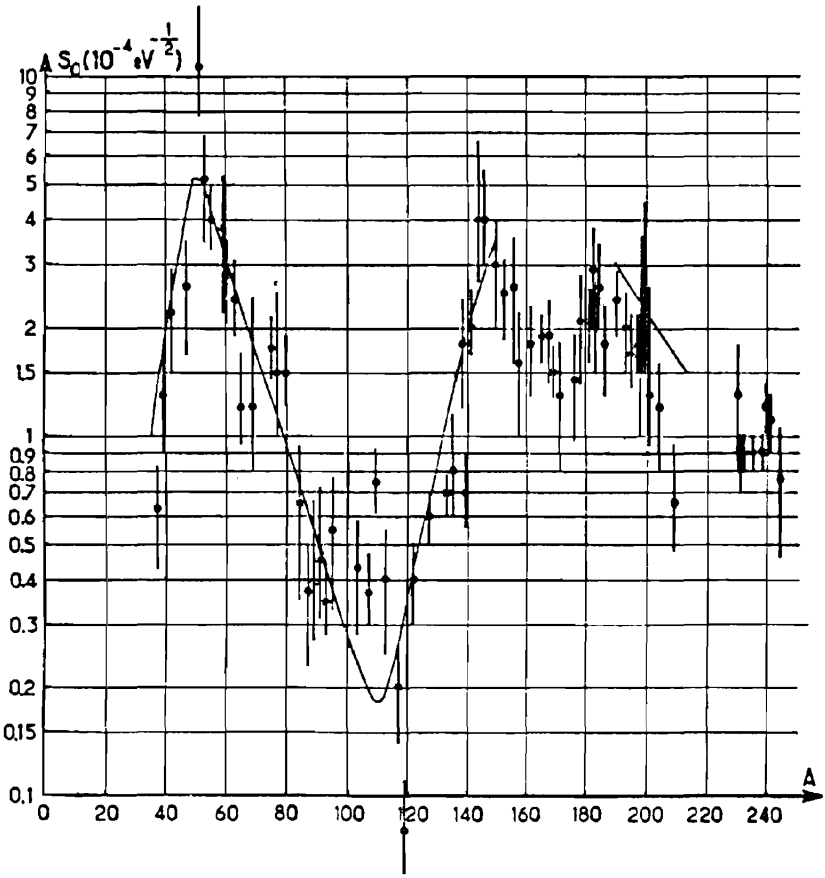

FIG. 2.15. Strength-function S_0 calculated using the potential of Moldauer (63), a Woods–Saxon potential with surface absorption:

$$V(r) = U_0\left[1 + \exp\left(\frac{r-R}{d}\right)\right]^{-1} + iW_0 \exp\left(-\frac{r-R-c}{f}\right)^2$$
$$+ U_{so}\left(\frac{\hbar}{m_\pi c}\right)^2 \boldsymbol{\sigma}\cdot\mathbf{l}\frac{1}{r}\frac{d}{dr}\left[1 + \exp\left(\frac{r-R}{d}\right)\right]^{-1}$$

where $R = r_0 A^{1/3} + r_1$; $U_0 = -46$ MeV; $W_0 = -14$ MeV; $U_{s0} = 7$ MeV; $r_0 = 1.16$ fm; $r_1 = 0.6$ fm; $d = 0.62$ fm; $f = 0.5$ fm; $c = 0.5$ fm. [From Morgenstern, Alves, Julien, and Samour (69).]

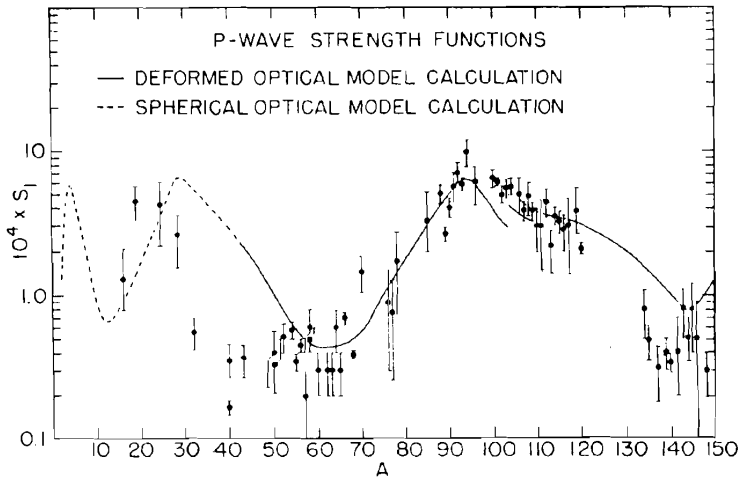

FIG. 2.16. Comparison of theoretical with experimental values of the p-wave neutron strength function. The solid curve represents deformed optical model calculations, and the dashed curve is based on spherical optical model calculations of Mughabghab, Divadeenam, and Holden (84).

Discuss the sensitivity of the calculated $\langle\Gamma\rangle/D$ to χ_0 when W is sharply peaked at the surface. Note particularly the effect of a node of χ_0 at the nuclear surface. Relate to the Moldauer potential.

It is considerably more difficult to measure the strength function for $l=1$ and $l=2$ neutrons. The measured values are given in Figs. 2.16 and 2.17. These strength functions S_1 and S_2 are defined by

$$\frac{\langle\Gamma_l\rangle}{D} \equiv s_l(kR)S_l \tag{2.69}$$

where an average over the possible spins $j=l\pm\frac{1}{2}$ with the weights $(2j+1/2)$ has been performed in obtaining Γ_l/D. The functions s_l are given in (IV.3.15). Obviously, in any study of S_l one should ascertain the value of R and E_0 that were used in extracting S_l. Quite good agreement with optical model calculations is obtained once the effects of deformation are included. However, there are substantial deviations from the optical model predictions, indicating the presence of structure effects.

The values of a are given in Fig. 2.18 together with the calculations of Perey and Buck (62). Substantial agreement has been obtained. The s-wave strength functions for protons should be similar to those of neutrons at energies at which the protons are moving with nearly zero energy, that is,

$$E_p \rightarrow E_n + \text{C.B.}$$

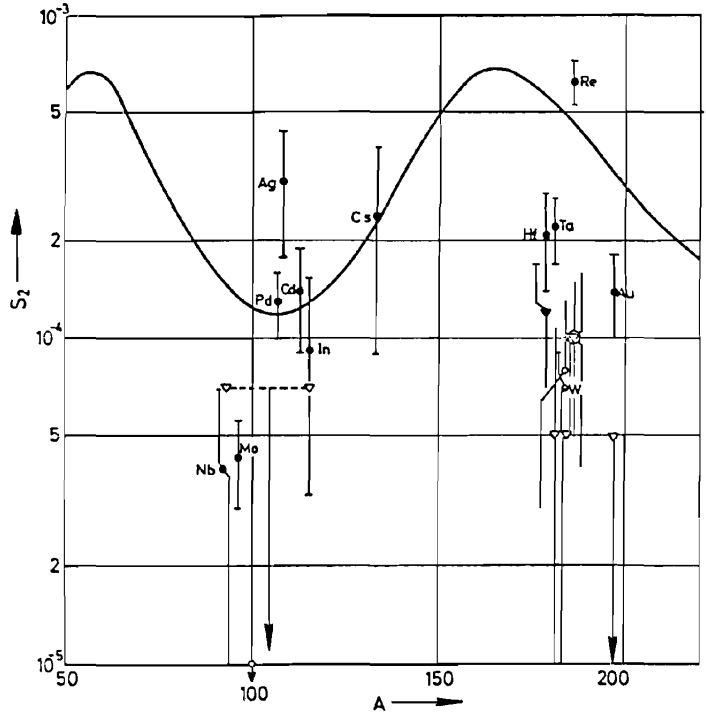

FIG. 2.17. *D*-wave strength function. [From Wilmore and Hodgson (1975).]

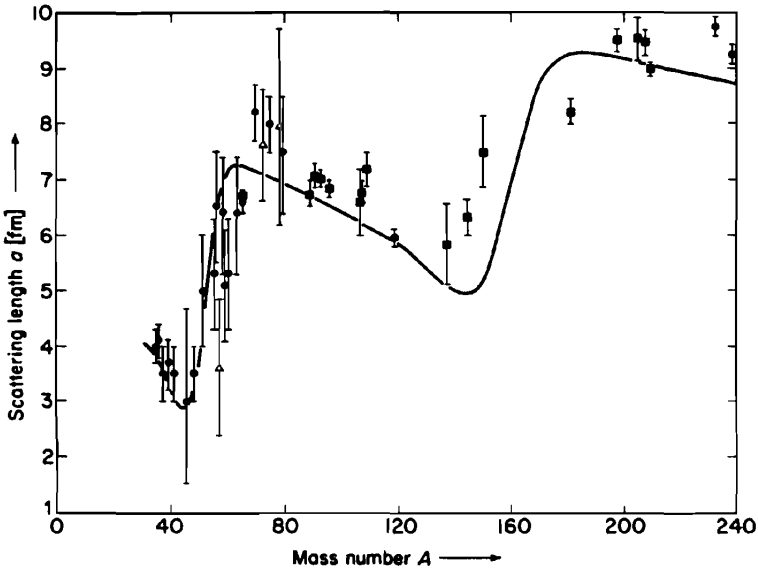

FIG. 2.18. Comparison of measured values (■:BNL; ●:Duke; △:ORNL) of the scattering length a for a range of nuclei with the predictions of the Perey–Buck nonlocal optical potential. [From Marmier and Sheldon (70)].

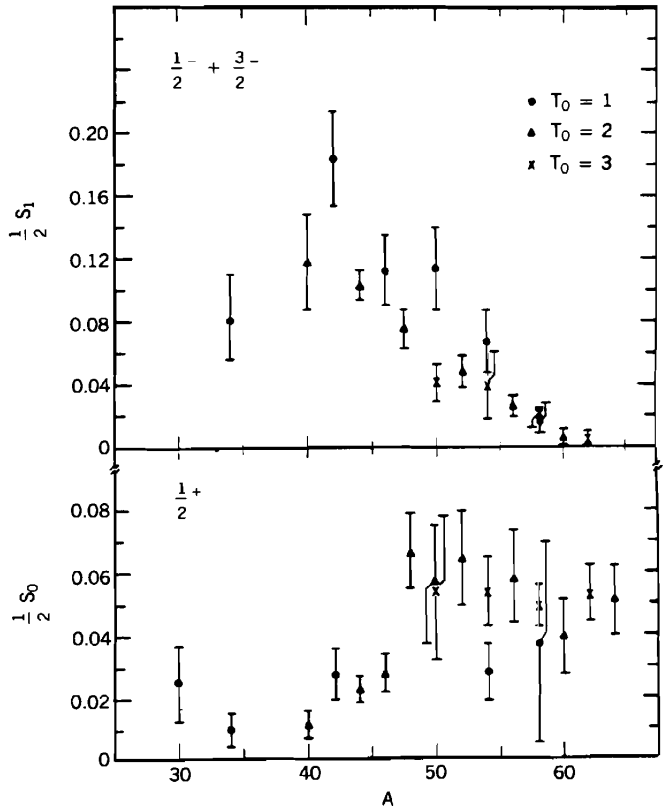

FIG. 2.19. Proton strength function for P- and S-wave resonances. [From Mitchell (80).]

where C.B. is the Coulomb barrier energy [Margolis and Weisskopf (57); Johnson, Galonsky, and Ulrich (58)]. For experimental examples, see Schiffer and Lee (57, 58); Johnson, Galonsky, and Ulrich, Schiffer (64); Elwyn, Marinov, and Schiffer (66); Johnson and Kernell (69, 70). These are for the most part based on the (p, n) reaction.

Developments in experimental methods, particularly by the Duke group, have made it possible to measure the widths of isolated resonances in proton resonance reactions [Bilpuch, Lane, Mitchell, and Moses (76)]. The resulting strength functions are shown in Fig. 2.19, where the Coulomb penetrabilities have been factored out; that is, in (2.69) the Coulomb wave functions have been to evaluate s_l. For the case of the $l = 1$ strength function, a maximum corresponding to a $2p$ resonance at about $A = 40$ is observed.

***Intermediate Energies* ($E < 100$ MeV).** The form (2.38) for the optical model potential contains parameters: the radius parameters r_c, r_0, r_W, r_D, and r_{so}; the surface parameters a_0, a_W, a_D, and a_{so}; and the parameters giving the strength

of the potential, V, W, W_D, and V_{so}. Perey and Perey (74) tabulate a list of values of these parameters for individual target nuclei and various projectiles. For our purposes the global parameters they give are of more interest. These are given in Table 2.1 together with those obtained by Rosen, Beery, Goldhaber, and Auerbach (65) after a full study of polarization. The Wilmore–Hodgson potential is the local equivalent of the Perey–Buck potential (62):

$$V\psi = -\left(\frac{\hbar}{m_\pi c}\right)^2 \frac{1}{ar} \frac{e^{(r-R_{so})/a_{so}}}{(1+e^{(r-R_{so})/a_{so}})^2} V_{so}\left(\frac{\boldsymbol{\sigma}}{2}\cdot\mathbf{L}\right)\psi + \int V(\mathbf{r},\mathbf{r}')\psi(\mathbf{r}')\,d\mathbf{r}' \quad (2.70)$$

where

$$V(\mathbf{r},\mathbf{r}') = U(\tfrac{1}{2}|\mathbf{r}+\mathbf{r}'|)T\left(\frac{|\mathbf{r}-\mathbf{r}'|}{\rho}\right) \quad (2.71)$$

Nonlocality follows when T deviates from a delta function; the quantity ρ parameterizes the range of the nonlocality. Perey and Buck take

$$T(r) = \left(\frac{1}{\sqrt{\pi}\rho}\right)^3 e^{-r^2/\rho^2} \quad (2.72)$$

and

$$U(r) = V_0 f(x_0) + 4iW_D \frac{d}{dx_d} f(x_D) \quad (2.73)$$

Their fit to neutron data yields $V_0 = 71$ MeV, $W_D = 15$ MeV, $r_{so} = r_0 = r_D = 1.22$ fm, $a_{so} = a_0 = 0.65$ fm, $a_D = 0.47$ fm, $\rho = 0.85$ fm, and $V_{so} = 7.2$ MeV.

Turning to Table 2.1, we note that the leading term of the central potential, V, as well as the radius parameter, r_0, which are independent of energy, N and Z dependence are in agreement, reflecting the diffraction structure of the differential cross section. The imaginary term is dominated by the surface term W_D, the value of W_D, a_D, and r_D being sensitive to the reaction cross section. Some volume absorption improves the fit. Including it results in a value of r_D that is considerably larger than the real potential, in qualitative agreement with Moldauer's (63) suggestion. The spin-orbit terms, needed to explain the polarization data [Rosen, Beery, Goldhaber, and Auerbach (65)], are in reasonable agreement with each other. The energy dependence in several of the parameters reflects the nonlocality and energy dependence of the nonlocal potential (e.g., that of Perey and Buck). The term $0.4Z/A^{1/3}$ is an estimate of the change of the Coulomb potential because of the nonlocality using the effective mass approximation. It needs to be identified before the symmetry term in $(N-Z)/A$ can be extracted empirically. Unfortunately, it is not easy to separate the $(N-Z)/A$ term from the $Z/A^{1/3}$ term. Some removal of this ambiguity can be obtained by including the charge exchange (p,n) interaction. This is discussed in Section 3.

TABLE 2.1

	V (MeV)	r_0 (fm)	a_0 (fm)	W (MeV)	r_W (fm)	a_W (fm)	W_D (MeV)	r_D (fm)	a_D (fm)	V_{so} (MeV)	r_{so} (fm)	a_{so} (fm)	r_c
						Protons							
Becchetti and Greenless (69); $A>40$, $E<50$ MeV	$54.0-0.32E$ $+24\frac{N-Z}{A}$ $+0.4Z/A^{1/3}$	1.17	0.75	$0.22E-2.7$ if >0 0 otherwise	1.32	$0.51+0.7\times\frac{N-Z}{A}$	$11.8-0.25E$ $+12\frac{N-Z}{A}$ if >0 0 otherwise	1.32	$0.51+0.7\frac{N-Z}{A}$	6.2	1.01	0.75	1.149 $+1.788A^{-2/3}$ $-1.163A^{-4/3}$
Menet et al. (71); $E<60$ MeV	$49.9-0.22E$ $+26.4\frac{N-Z}{A}$ $+0.4Z/A^{1/3}$	1.16	0.75	$1.2+0.09E$	1.37	$0.74-0.008E$ $+1.0\frac{N-Z}{A}$	$4.2-0.05E$ $+15.5\frac{N-Z}{A}$	1.37	$0.74-0.008E$ $+1.0\frac{N-Z}{A}$	6.04	1.064	0.78	1.25
Rosen et al. (65)	$53.8-0.33E$	1.25	0.65				7.5	1.25	0.7	5.5	1.25	0.65	
						Neutrons							
Becchetti and Greenlees (69); $A>70$, $5<E<24$ MeV	$56.3-0.32E$ $-24\frac{N-Z}{A}$	1.17	0.75	$0.22E-1.56$ if >0 0 otherwise	1.26	0.58	$13-0.25E$ $-12\frac{N-Z}{A}$ if >0 0 otherwise	1.26	0.58	6.2	1.1	0.75	
Wilmore and Hodgson (64)	$47.01-0.267E$ $-0.018E^2$	$1.32-0.76\times(10^{-3}A)$ $+4(10^{-3}A)^2$ $-8(10^{-3}A)^3$	0.66				$9.42-0.053E$	$1.266-0.37(10^{-3}A)$ $+2(10^{-3}A)^2$ $-4(10^{-3}A)^3$	0.48				
Rosen et al. (65)	$49.3-0.33E$	1.25	0.65				5.75	1.25	0.7	5.5	1.25	0.65	

The optical model potential should be a reasonable continuation, into the positive energy domain, of the single-particle shell model potential (see footnote, p. 356). To make such a comparison, it is necessary to know, for example, the energies of the single-particle shell model states. However, in most cases these states are fragmented by the action of the residual potential. Determination of the centroid of the single-particle strength, to be calculated as the mean energy of the fragmented states weighted by the fraction of each state that is single-particle strength (i.e., spectroscopic factor), is difficult, as it is rare that the single-particle strength has been completely ascertained. This also has the consequence that it will be difficult to describe the continuation of the imaginary part of the optical model potential into the bound-state domain. In principle, this could be calculated from the fragmentation of a single-particle shell model

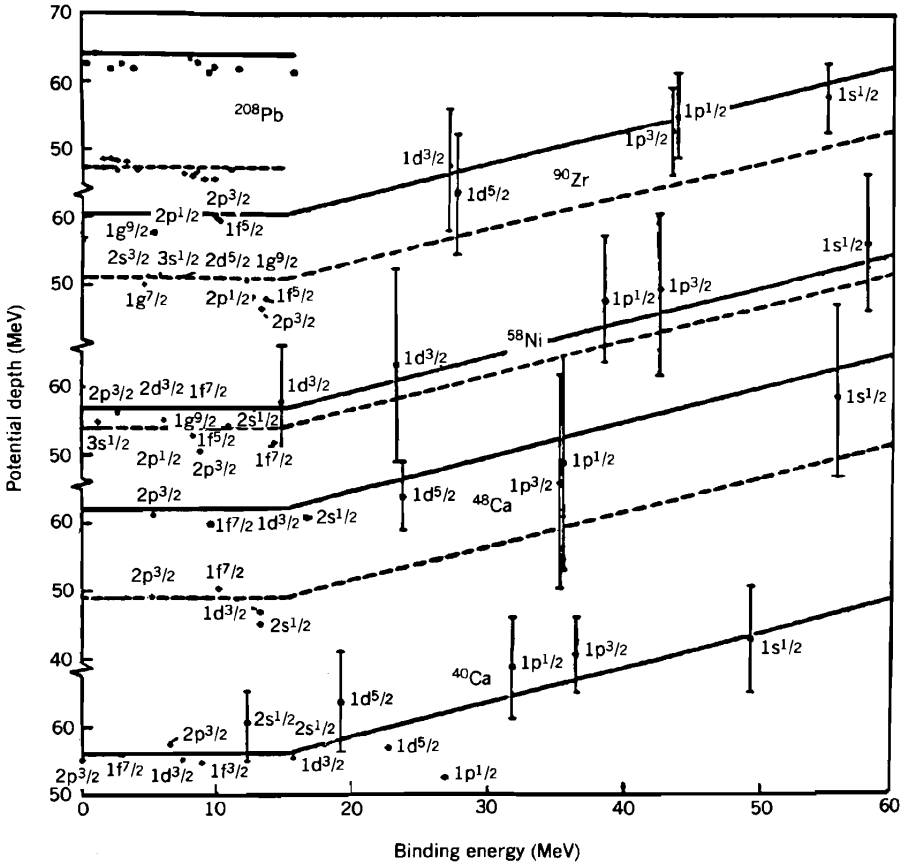

FIG. 2.20. Nuclear potential depths for single-particle states of ^{40}Ca, ^{48}Ca, ^{58}NI, ^{90}Z, and ^{208}Pb compared with average best-fit lines. ○, ——, proton; +, ------, neutron. [From Bear and Hodgson (78).]

level, which is analogous to the fragmentation of a single-particle resonance into fine structure resonances as described in Chapter III [see (III.4.49)].

Bear and Hodgson (78) have therefore restricted their study to the single-particle energies of nuclei nearly closed shells, where level fragmentation is minimal. The form of the potential they use is that given by (2.38) with $W = W_D = 0$. They take $r_0 = 1.236$ fm, $a = 0.62$ fm, and $a_{so} = 0.65$ for the spin-orbit case. Moreover, V_{so} is chosen to be 7 MeV, leaving only V to be determined. The results are shown in Fig. 2.20 and can be fitted as indicated by

$$V = \begin{cases} V_0 \pm V_1 \dfrac{N-Z}{A} & \text{for } E > -15 \text{ MeV} \\ V_0 \pm V_1 \dfrac{N-Z}{A} + \beta(E+15) & \text{for } E < -15 \text{ MeV} \end{cases} \tag{2.74}$$

where E is measured from the Fermi energy E_F. The empirical values of V_0, V_1, and β are given in Table 2.2.

Folding Model: Empirical. Satchler (67), Slanina and McManus (68), and Greenless, Pyle, and Tang (68) have suggested an alternative form for the optical model potential, to be used in place of that given by (2.38). This development is suggested by the high-energy multiple scattering theory, which in first order yields the potential of the form

$$V(\mathbf{r}) = \int \rho(\mathbf{r}_1) t(\mathbf{r} - \mathbf{r}_1)\, d\mathbf{r}_1$$

where t is the two-nucleon free-space transition matrix. This expression is not correct as the nucleon energy is lowered. There are already substantial errors, presumably arising because of the influence of the medium in which the two interacting nucleons find themselves at proton energies of 500 MeV [Ray (83)].

A similar result is obtained if one drops the second term in the effective

TABLE 2.2

Nucleus	V_0 (MeV)	V_1 (MeV)	β
^{12}C	56.7		
^{16}O	56.0		
^{40}Ca	56.0		
^{48}Ca	54.9	38.1	0.32
^{58}Ni	57.4	40.0	0.64
^{90}Zr	54.4	42.8	0.47
^{208}Pb	54.5	36.2	

Hamiltonian of Chapter III:

$$H_{\text{eff}} = H_{PP} + H_{PQ}\frac{1}{E^{(+)} - H_{QQ}}H_{QP} \tag{2.75}$$

keeping only H_{PP}. Recall that when P projects only on the elastic channel,

$$P\Psi = \mathscr{A}u_0\phi_0$$

where ϕ_0 is the ground-state wave function of the target nucleus. As a consequence,

$$V_{PP}(P\Psi) = \left\langle \phi_0 \middle| \sum_i v_{0i} \middle| \mathscr{A}u_0\phi_0 \right\rangle$$

where v_{oi} is the interaction between the ith target nucleon and the incident projectile. Evaluating the matrix element on the right (the integrations are only over the target nucleon coordinates), one obtains

$$V_{PP}(P\Psi) = \left[\int \rho(\mathbf{r}_1)v_{01}(\mathbf{r}_0, \mathbf{r}_1)\,d\mathbf{r}_1\right]u_0(\mathbf{r}_0) - \int \rho(\mathbf{r}_1, \mathbf{r}_0)v_{01}(\mathbf{r}_0, \mathbf{r}_1)u_0(\mathbf{r}_1)\,d\mathbf{r}_1 \tag{2.76}$$

The errors in this approach come mainly from the neglect of the second term in (2.75), which contains the effects that can be described as involving excitation of the target nucleus, such as core polarization and correlations.

The empirical folding potential takes account of these limitations by replacing the two-nucleon interaction v_{01} by an effective two-body potential, so that (2.76) is replaced by

$$V\chi_{\text{opt}} = \left[\int \rho(\mathbf{r}_1)g_{pt}(\mathbf{r}_p, \mathbf{r}_1)\,d\mathbf{r}_1\right]\chi_{\text{opt}}(\mathbf{r}_p) - \int \rho(\mathbf{r}_1, \mathbf{r}_p)g_{pt}(\mathbf{r}_p, \mathbf{r}_1)\chi_{\text{opt}}(\mathbf{r}_1)\,d\mathbf{r}_1 \tag{2.77}$$

The quantity $g_{pt}(\mathbf{r}_p, \mathbf{r}_1)$ is the effective two-body interaction in the nucleus, where $\mathbf{r}_p$ represents all the projectile coordinates (spatial, spin, isospin) and $\mathbf{r}_1$ those of a target nucleon. The subscripts p and t refer to projectile and target, respectively. Note that the single-channel wave function u_0 of (2.76) has been replaced by the optical model wave function χ_{opt}. This can be justified using the partition proposed by Kawai, Kerman, and McVoy (75) given by (III.8.5). Note that this form reduces to that developed by first-order multiple scattering (which neglects the effects of the Pauli principle) theory as noted above, with g_{pt} replacing the two-body transition matrix $t(\mathbf{r}_p - \mathbf{r}_1)$.

The linear dependence of V_{opt} on the density is illusory, as the effective interaction g_{pt} depends on the nuclear medium, and thus on the density and other parameters describing the nuclear system. The hope is that g_{pt} will depend

slowly on these variables and thus can be replaced by an average value over a substantial range of target nuclei and energy.

Note. A microscopic theory of the effective interaction can be developed. Clearly, the Bethe–Goldstone equation (now with one nucleon in the continuum) will yield information. The papers of Mahaux and his school and of Brieva and Rook discussed earlier employ the Bruecker–Hartree–Fock method to calculate the effective single-body potential in nuclear matter. In the course of this calculation the effective two-body interaction in nuclear matter is obtained. One can then apply a local density approximation to obtain an effective two-body interaction appropriate for two nucleons in a finite nucleus. This procedure is a generalization of the G-matrix method described in Chapter VII of deShalit and Feshbach (74). The g_{pt} obtained in this manner is density dependent. Moreover, if such a calculation were to be done directly for a finite nucleus rather than by applying the local density approximation, g_{pt} would show nuclear structure effects arising from core polarization and correlation effects.

Returning to (2.77), let us define and/or describe $\rho(\mathbf{r}_1)$, $\rho(\mathbf{r}_1, \mathbf{r}_p)$ more completely. The quantity $\rho(\mathbf{r}_1)$ is the one-particle target ground state density *normalized to A*:

$$\rho(\mathbf{r}_1) = A \int |\Psi_0(\mathbf{r}_1, \mathbf{r}_2, \mathbf{r}_3, \ldots)|^2 \, d\mathbf{r}_2 \cdots \tag{2.78}$$

The quantity $\rho(\mathbf{r}, \mathbf{r}')$ is the ground-state density matrix discussed in Chapter II of deShalit and Feshbach (74). It is defined by

$$\rho(\mathbf{r}, \mathbf{r}') = A \int \Psi_0^*(\mathbf{r}, \mathbf{r}_2, \ldots)\Psi_0(\mathbf{r}', \mathbf{r}_2, \ldots) \, d\mathbf{r}_2 \cdots \tag{2.79}$$

Note that the density $\rho(\mathbf{r})$ is just the diagonal element of $\rho(\mathbf{r}, \mathbf{r}')$:

$$\rho(\mathbf{r}) = \rho(\mathbf{r}, \mathbf{r}) \tag{2.80}$$

Problem. Prove

$$\rho(\mathbf{r}) = \left\langle \Psi_0 \middle| \sum_i \delta(\mathbf{r} - \mathbf{r}_i) \middle| \Psi_0 \right\rangle \tag{2.81}$$

and

$$\rho(\mathbf{r}, \mathbf{r}') = \frac{1}{A-1} \left\langle \Psi_0(\mathbf{r}_1, \mathbf{r}_2, \ldots) \middle| \sum_{i \neq j} \delta(\mathbf{r} - \mathbf{r}_i)\delta(\mathbf{r}' - \mathbf{r}_j') \middle| \Psi_0(\mathbf{r}_1', \mathbf{r}_2', \ldots) \right\rangle \tag{2.82}$$

Note in (2.82) that the factor $\delta(\mathbf{r}-\mathbf{r}_i)\delta(\mathbf{r}'-\mathbf{r}'_j)$ is understood to be multiplied by the unit operator in the other coordinates, $\delta(\mathbf{r}_1-\mathbf{r}'_1)\delta(\mathbf{r}_2-\mathbf{r}'_2)\cdots$.

The factor $g_{pt}(\mathbf{r}_p, \mathbf{r}_1)$ is the effective projectile nucleon–target nucleon interaction inside the target nucleus. It depends not only on $\mathbf{r}_p$ and $\mathbf{r}_1$ but on the spin and isospin variables (i.e., on $\boldsymbol{\sigma}_1$, $\boldsymbol{\sigma}_p$, $\mathbf{r}_1$, and $\mathbf{r}_p$) as well.

Note. For reasons of simplicity in presentation, the spin/isospin dependence of g_{pt}, $\rho(\mathbf{r})$ and $\rho(\mathbf{r}, \mathbf{r}')$ have been suppressed. The effective interaction g_{pt} can be written as a linear combination

$$g_{pt} = \sum_{S,T} g_{pt}^{ST} P^{ST} \tag{2.83}$$

where P^{ST} are projection operators in spin and isospin space:

$$P^{ST} = P^S P^T \tag{2.84}$$

where S and T can have the values zero (singlet) or 1 (triplet). The corresponding operators are

$$P^{(0)} = \frac{1-\boldsymbol{\sigma}_p\cdot\boldsymbol{\sigma}_1}{4} \qquad P^{(1)} = \frac{3+\sigma_p\cdot\sigma_1}{4}$$

Note that expansion (2.83) is valid in the presence of spin-orbit $(\boldsymbol{\sigma}_p+\boldsymbol{\sigma}_1)\cdot\mathbf{l}_{p1}$, and tensor $(3\boldsymbol{\sigma}_p\cdot\hat{\mathbf{r}}_p\boldsymbol{\sigma}_1\cdot\hat{\mathbf{r}}_1-\boldsymbol{\sigma}_p\cdot\boldsymbol{\sigma}_1)$ interaction terms, since these vanish in the singlet spin state.

Under these circumstances $\rho(\mathbf{r}_1)g_{pt}$ of (2.77) becomes

$$\rho(\mathbf{r}_0)g_{pt} \to \sum_{S,T} \rho^{ST}(\mathbf{r}_0)g_{pt}^{ST}$$

where, for example,

$$\rho^{10}(\mathbf{r}_0) = \left\langle \Psi_0 \middle| \sum_i \delta(\mathbf{r}_0-\mathbf{r}_i)\left(\frac{3+\boldsymbol{\sigma}_0\cdot\boldsymbol{\sigma}_i}{4}\right)\left(\frac{1-\boldsymbol{\tau}_0\cdot\boldsymbol{\tau}_i}{4}\right)\middle|\Psi_0\right\rangle$$

In an empirical analysis the form of g_{pt} is assumed. Its parameters are then adjusted to fit the data under investigation.

The first term in (2.66) for the folded potential V_{opt} is referred to as the *direct term*, $V_{\text{opt}}^{(D)}$:

$$V_{\text{opt}}^{(D)} \equiv \int \rho(\mathbf{r}_1)g_{pt}(\mathbf{r}_p, \mathbf{r}_1)\,d\mathbf{r}_1 \tag{2.85}$$

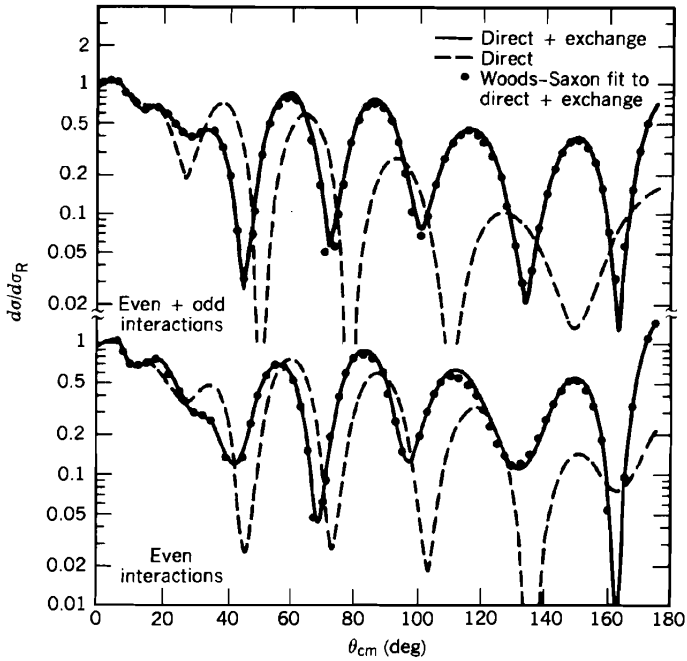

FIG. 2.21. Differential cross sections for 30-MeV protons on ^{120}Sn. [From Owen and Satchler (70).]

and the second is referred to as the *exchange term.* In the earliest formulations of the folding potential model this term was omitted. However, as Owen and Satchler (70) soon demonstrated, this exchange contribution cannot be neglected (see Fig. 2.21). The exchange term is nonlocal. Because of its origin, one can expect it to have a range of the order of $1/k_F$. In calculations it is often replaced by a local equivalent potential using one of the methods described earlier in this section (see Sec. 2B this chapter).

The effective nucleon–nucleon potential to be inserted for g_{pt} in (2.77) has the general form [Greenlees, Pyle, and Tang (68); Petrovitch and Love (80)]

$$\mathscr{V}_{\text{eff}} = v_{00}^C + v_{01}^C \boldsymbol{\tau}_0 \cdot \boldsymbol{\tau}_i + v_{10}^C \boldsymbol{\sigma}_0 \cdot \boldsymbol{\sigma}_i + v_{11}^C \boldsymbol{\sigma}_0 \cdot \boldsymbol{\sigma}_i \boldsymbol{\tau}_0 \cdot \boldsymbol{\tau}_i + [v_0^T + v_1^T \boldsymbol{\tau}_0 \cdot \boldsymbol{\tau}_i] S_{0i} + [v_0^{LS} + v_1^{LS} \boldsymbol{\tau}_0 \cdot \boldsymbol{\tau}_i] \mathbf{L}_{0i} \cdot (\boldsymbol{\sigma}_0 + \boldsymbol{\sigma}_i) \tag{2.86}$$

In this expression, the coefficients v_{ab}, v_a^T, and v_a^{LS} are functions of the distance, $|\mathbf{r}_0 - \mathbf{r}_i|$, between the incident projectile $\mathbf{r}_0$ and the target nucleus nucleon $\mathbf{r}_i$. The subscripts a and b refer to the spin and isospin character of the interaction. The superscripts C for central, T for tensor, and LS for spin-orbit refer to the spatial symmetry. The tensor operator S_{0i} is defined by

$$S_{0i} = 3\boldsymbol{\sigma}_0 \cdot \hat{\mathbf{r}}_0 \boldsymbol{\sigma}_i \cdot \hat{\mathbf{r}}_i - \boldsymbol{\sigma}_0 \cdot \boldsymbol{\sigma}_i \tag{2.87}$$

where $\hat{\mathbf{r}}_0$ is the unit vector in the $\mathbf{r}_0$ direction, while

$$\mathbf{L}_{0i} = \frac{1}{\hbar}(\mathbf{r}_0 - \mathbf{r}_i) \times (\mathbf{p}_0 - \mathbf{p}_i) \tag{2.88}$$

It is useful to break up the interaction, (2.86), according to the spin and isospin of the interacting pair, using the projection operators P^{ST} of (2.84).

Noting that both the tensor and spin-orbit potentials vanish when operating as a single spin state ($\boldsymbol{\sigma}_0 = -\boldsymbol{\sigma}_i$), we obtain

$$g_{pi} \equiv v_{\text{eff}} \equiv P^{(11)}V_i^{(11)} + P^{(01)}V_i^{(01)} + P^{(10)}V_i^{(10)} + P^{(00)}V_i^{(00)} \tag{2.89}$$

where

$$V_i^{(11)} = v_{00}^C + v_{01}^C + v_{10}^C + v_{11}^C + (v_0^T + v_1^{(T)})S_{0i} + (v_0^{LS} + v_1^{LS})\mathbf{L}_{0i}\cdot(\boldsymbol{\sigma}_0 + \boldsymbol{\sigma}_i)$$
$$V_i^{(01)} = v_{00}^C + v_{01}^C - 3v_{10}^C - 3v_{11}^C$$

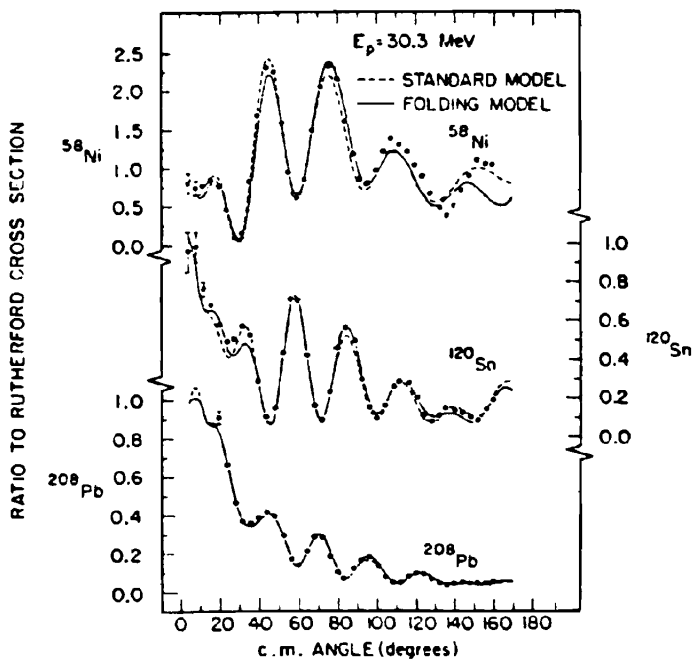

FIG. 2.22. Experimental differential cross-section data points, with errors, for the elastic scattering of 30.3-MeV protons together with predictions. (From Greenlees, Hnizdo, et al. (70).]

$$V_i^{(10)} = v_{00}^C - 3v_{01}^C + v_{10}^C - 3v_{11}^C + (v_0^T - 3v_1^T)S_{0i} + (v_0^{LS} - 3v_1^{LS})\mathbf{L}_{0i}\cdot(\boldsymbol{\sigma}_0 + \boldsymbol{\sigma}_i)$$
$$V_i^{(00)} = v_{00}^C - 3v_{01}^C - 3v_{10}^C + 9v_{11}^C \tag{2.90}$$

The Pauli principle requires that $V_i^{(11)}$ and $V_i^{(00)}$ act only when the relative orbital angular momenta of the two interacting nucleons are odd. The often-used Serber force puts both of these equal to zero so that v_{eff} acts only on even relative orbital states. Applications of interaction equation (2.89) to elastic scattering of protons (energies extending up to 40 MeV) have been made by Greenless and his collaborators [Greenlees, Pyle, and Tang (68); Greenlees, Makofake, and Pyle (70)]. Only the first term in (2.77), the direct term, was used. The exchange term containing effects of the Pauli principle was neglected. Presumably some of its effects are included in the empirical $g(\mathbf{r}_1, \mathbf{r}_p)$. The targets were all even–even nuclei, with the consequence that only v_{00}^C, v_{01}^C and $(v_0^{LS} + v_1^{LS})$ contribute to V_{opt}. These interactions were taken to be real. It was, therefore, necessary to add imaginary potentials of the surface and volume variety, familiar from (2.38), to the V_{opt} of (2.77). The reader is referred to the original papers for the details of the calculation. Comparison of the calculation (eight empirical parameters) with data is shown in Figs 2.22 and 2.23. This subject is discussed further in Section 5.

Intermediate Energies **100 *MeV*** $< E <$ **200 *MeV*** [Nadasen, Schwandt, et al. (81); Schwandt (83)]. The analysis based on the standard model, (2.38), has been continued to higher energies as these have become available. The overall situation has been reviewed by Schwandt (83). We shall make use of that review as well as the paper by Nadasen, Schwandt, et al. (81). In that paper, an optical model analysis using the standard model is developed for the observed angular distribution and polarization for protons with energies ranging up to about 180 MeV elastically scattered from a wide variety of nuclei. The results are given in Table 2.3. The symbols used are those of (2.38). E_p is the proton energy in MeV. $E_p^>$ in the expression for W signifies that the expression $(E_p^> - 135)$ differs from zero only for $E_p > 135$ MeV.

Note that the linear energy dependence of the depth of real part of the central potential as given in Table 2.1, valid at lower energies, is replaced by a logarithmic energy dependence, in agreement with Passatore's earlier prediction. Second, the imaginary term has no surface term and grows rapidly with energy above 135 MeV, presumably as a consequence of pion production. Note, again in contrast with Table 2.1, that the geometrical factors r_0, a_0, r_W, and a_W are energy dependent. Finally, we see that the spin-orbit depth is complex.

The experimental reason for the latter lies in the dominance of the contributions of the spin channel component $\sigma^{(+)}$ corresponding to $\boldsymbol{\sigma}\cdot\mathbf{n} = 1(\mathbf{n} = \hat{k}_{\text{in}} \times \hat{k}_{\text{out}})$ over the contribution from the $\boldsymbol{\sigma}\cdot\mathbf{n} = -1(\sigma^{(-)})$ component, as demonstrated in Fig. 2.24. From the point of view of the optical model this result is a consequence of the complex spin-orbit potential, which enhances the $j = l + \frac{1}{2}$ partial wave with respect to the $j = l - \frac{1}{2}$ component.

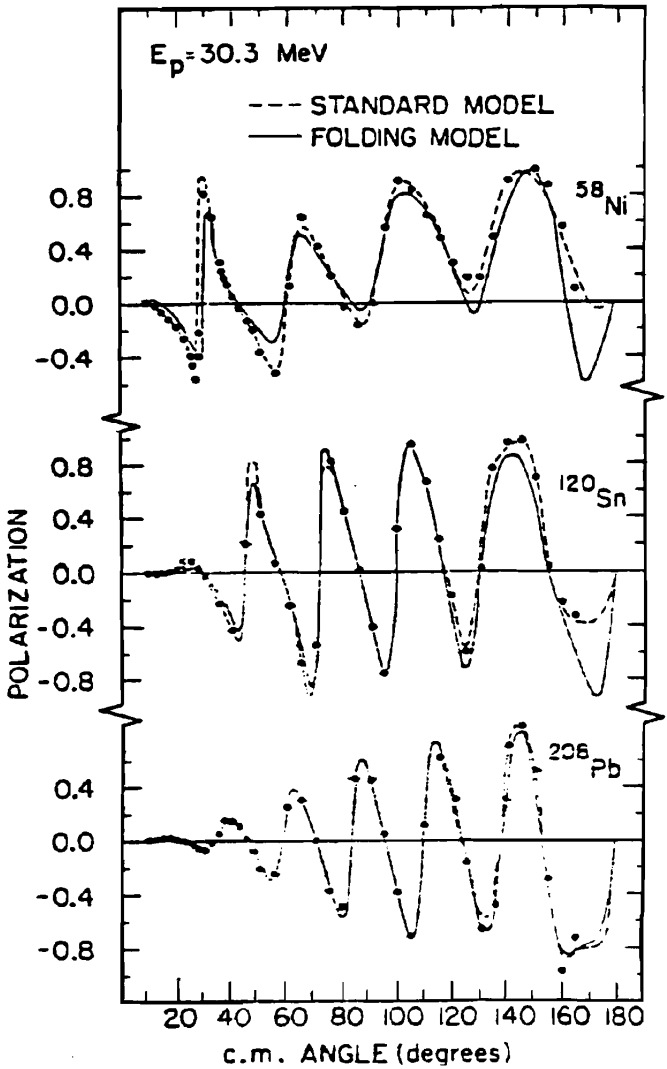

FIG. 2.23. Experimental polarization data points for the elastic scattering 30.3-MeV polarized protons, together with predictions. [From Greenlees, Hnizdo, et al. (70).]

An indication of the energy and isospin dependence of the parameters in Table 2.3 can be obtained from Fig. 2.25. The energy dependence of these optical model parameters seems to indicate the need for modification of the standard equation (2.38) model.

***Intermediate Energies* > 200 MeV.** The difficulties that are suggested by the comparatively rapid energy dependence of the optical model parameters become

TABLE 2.3

$$V = \left(92.5 + 64\frac{N-Z}{A}\right)(1 - 0.155 \ln E_p) \quad \text{MeV}$$

$$r_0 = 1.18 + \left(0.34 + \frac{6.5}{A}\right)10^{-3}E_p \quad \text{fm}$$

$$a_0 = 0.77 - (1.2 \times 10^{-4})A^{0.4}(180 - E_p)$$

$$W = 3.8 + 3\frac{N}{Z} + (1.23 \times 10^{-3})(E_p^> - 135)^2 \quad \text{MeV}, \qquad W_D = 0$$

$$r_W = 1.16 + \beta \ln(185 - E_p), \qquad \beta = \begin{cases} 0.065 \text{ Ca} \\ 0.053 \text{ Zr} \\ 0.058 \text{ Pb} \end{cases} \quad \text{fm}$$

$$a_W = 0.37 + (1.8 \times 10^{-3})E_p \quad \text{fm}$$

The V_{so} of (2.38b) is replaced by $V_{so} + iW_{so}$.

$$V_{so} = 16.5(1 - \eta \ln E_p) \quad \text{MeV}, \qquad \eta = 0.160 + 0.06\frac{N-Z}{A}$$

$$W_{so} \simeq 5.2(1 - 0.262 \ln E_p) \quad \text{MeV}$$

$$r_{so} \simeq 1.015 + 5 \times 10^{-4}A \quad \text{fm}$$

$$a_{so} \simeq 0.60 \quad \text{fm}$$

explicit in this energy region. For example, the standard Woods–Saxon model fails to provide a good fit to the angular distribution and analyzing power observed in the elastic scattering of 400-MeV protons by ^{40}Ca (see Fig. 2.26). As Meyer, Schwandt et al. (81) have shown, this failure is a consequence of the restriction of the radial behavior of the components of the potential to the Woods–Saxon form. If, for example, the real central potential $-Vf_{WS}(x_0)$ is modified by the addition of a repulsive term:

$$-Vf_{WS}(x_0) \rightarrow -V[f_{WS}(x_0) + \eta f_{WS}^2(x_0)] \tag{2.91}$$

and similarly for other terms, agreement with experiment is vastly improved (see Fig. 2.27). The corresponding central potentials, real and imaginary, are shown in Fig. 2.28. We see the presence of a repulsive central region in the real part of the central potential, together with a substantial increase in the absorptive term. The need for a repulsive central region together with an attractive potential at large r was first suggested by Elton (66).

A qualitative explanation of this important result is provided by the local density approximation using the infinite matter calculation of the real potential, V. As can be seen from Fig. 2.29, the variation of V with energy depends strongly on the density. It decreases more rapidly with energy with the larger density ρ_0 than for the density $\rho_0/2$. The first, in fact, becomes repulsive at roughly 250 MeV, while close to 200 MeV the second already exceeds the first. In the local density approximation one can thus expect a nonmonotonic form for the

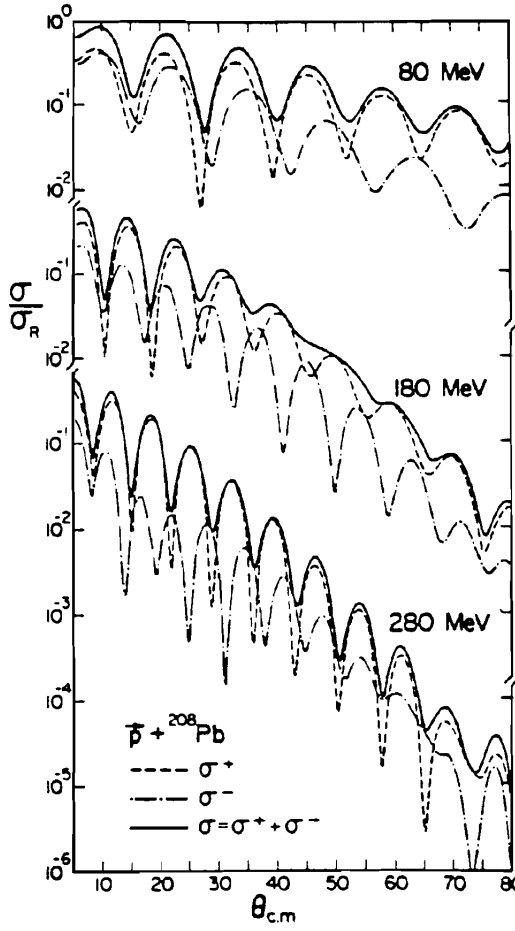

FIG. 2.24. Calculated differential cross-section angular distributions (solid curves) plotted as ratio-to-Rutherford for 80-, 180-, and 280-MeV proton elastic scattering from ^{208}Pb. The partial spin-channel decompositon of the cross sections ("spin up" dashed curves; "spin-down" dot–dashed curves) is also plotted, illustrating the origin of the damping of the oscillatory structure observed around 180 MeV. [From Nadasen, Schwandt, et al (81).]

central potential. In the small r region the potential will become repulsive, while for larger r in the surface region where the density is reduced, the potential will remain attractive, although eventually it, too, will become repulsive at sufficiently large energies in agreement with high-energy (~ 1 GeV) analysis.

Quantitatively good agreement with the 400-MeV data is obtained using the local density approximation and the infinite nuclear matter real potential obtained by Geramb and Nakano (83) based on the Paris nucleon–nucleon potential. A direct comparison is shown in Fig. 2.30 for 400-MeV proton

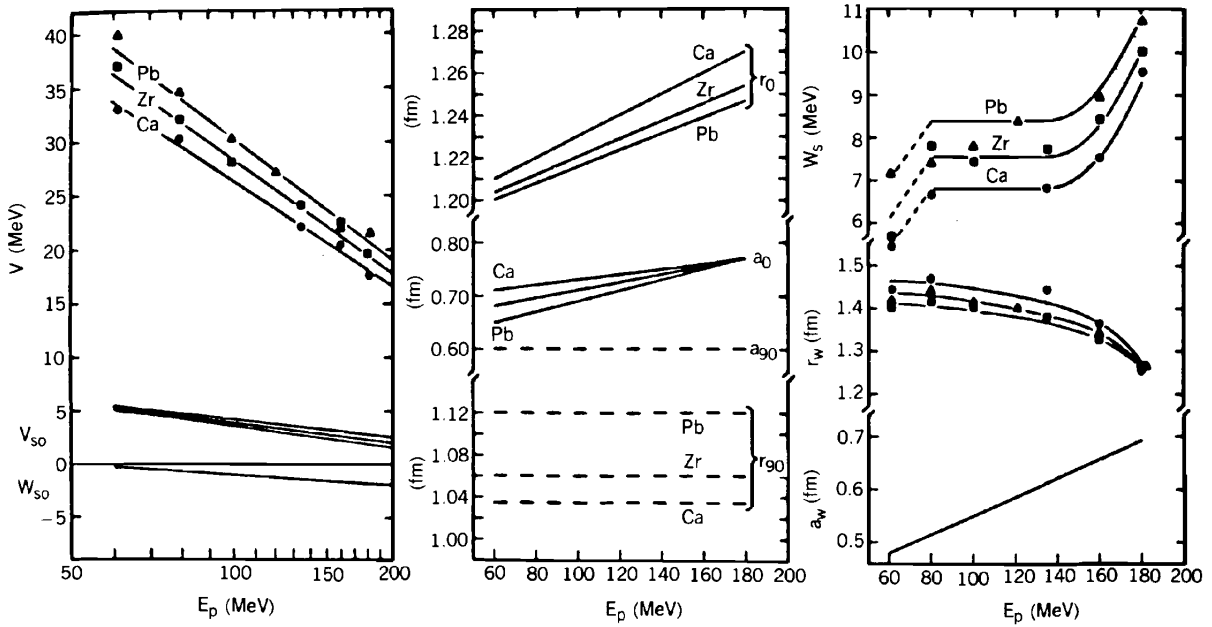

FIG. 2.25. Energy dependence of the complex central and spin-orbit potential parameters obtained in the fixed-spin-orbit fits to the cross-section data. Note the logarithmic energy scale in the left-hand panel. [From Nadasen, Schwandt, et al. (81).]

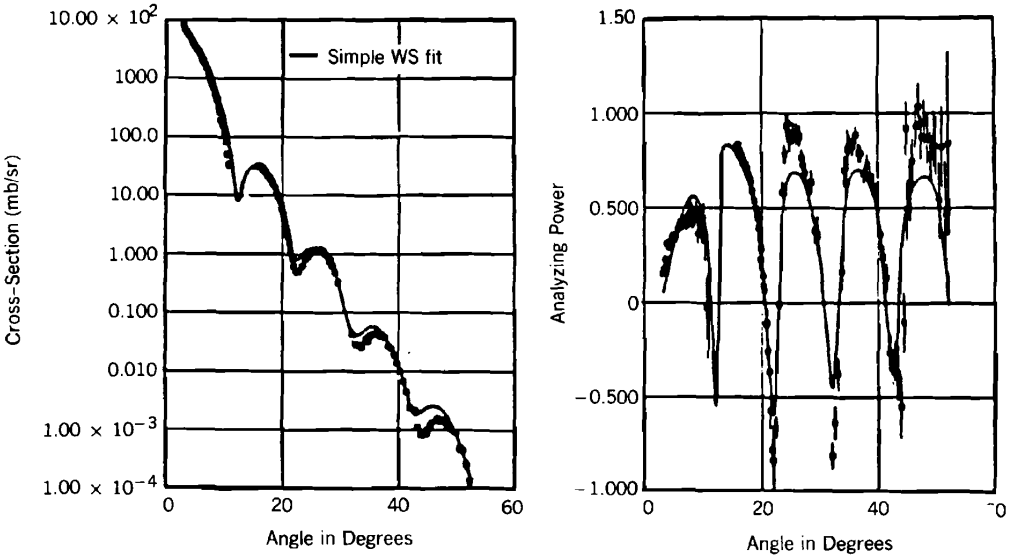

FIG. 2.26. Angular distribution (*a*) and analyzing power (*b*) compared to the Woods–Saxon fit. [From Schwandt (8.3).]

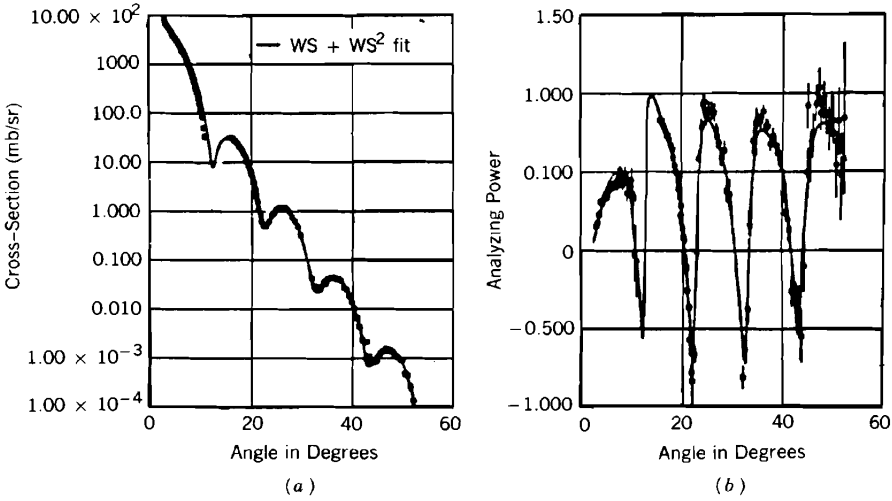

FIG. 2.27. Angular distribution (*a*) and analyzing power (*b*) compared to a Woods–Saxon plus (Woods–Saxon)^2 fit. [From Schwandt (83).]

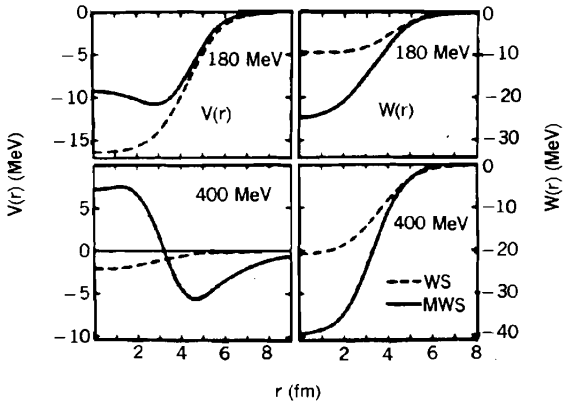

FIG. 2.28. Radial dependence of the real and imaginary parts of the central potential at 180 and 400- MeV. The solid lines give the modified Woods–Saxon fit (see Fig.2.27). [From Schwandt (83).]

scattering by ^{208}Pb. These microscopic calculations remain viable below 200 MeV, as Fig. 2.31 indicates from a comparison of the cross section for 135-MeV protons scattered by ^{16}O with theory. Of course, in this energy region the standard model provides a good fit, as discussed earlier.

The Relativistic Optical Model: Dirac Phenomenology [Clark, Hama, and Mercer (83)]. In this analysis the Schrödinger wave equation is replaced by

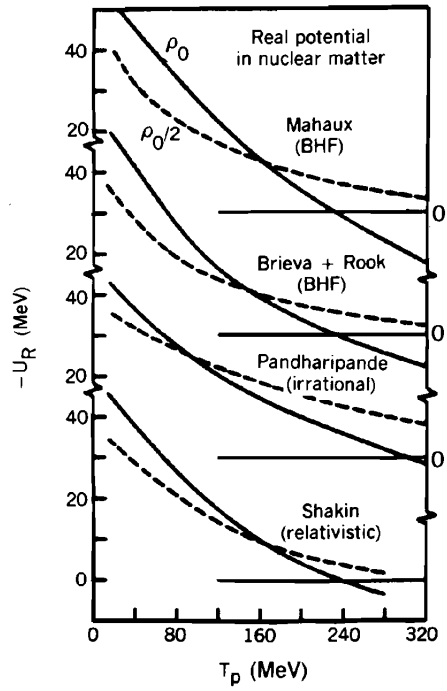

FIG. 2.29. Dependence of the real potential in nuclear matter for normal nuclean density ρ_0 and for $\rho_0/2$ for several models. [From Schwandt (83).]

the Dirac equation as if the incident nucleon were a relativistic spin-$\frac{1}{2}$ particle moving in the field of an infinite mass nucleus. This single-channel formulation omits any explicit calculation of recoil associated with the target. The results are in surprisingly good agreement with experiment. When the Dirac equation is reduced to an equivalent Schrödinger equation, the repulsive addition [see. (2.91)], energy dependence, and correct spin-order coupling are obtained. Inasmuch as the physical origins of, for example, the energy dependence in the relativistic model differ so sharply from the physics of the nonrelativistic model of, say, Jeukenne, Lejeune, and Mahaux (76), one remains tentative in evaluating the success of the relativistic model.

The Dirac equation in Hamiltonian form‡ is

$$[c\boldsymbol{\alpha}\cdot\mathbf{p} + \beta(mc^2 + U_s) + U_0]\psi = E\psi \tag{2.92}$$

‡For notation, see appendix to ChIX, deShalit and Feshbach (1974) and ChIX.

FIG. 2.30. Angular distribution (*a*) and analyzing power (*b*) for 400-MeV protons scattered by ^{208}Pb compared with the calculations using the effective interactions derived by von Geramb and Nakano (83) and with the second-order multiple scattering using a modified Hartree–Fock nucleon density. [From Ray (83).]

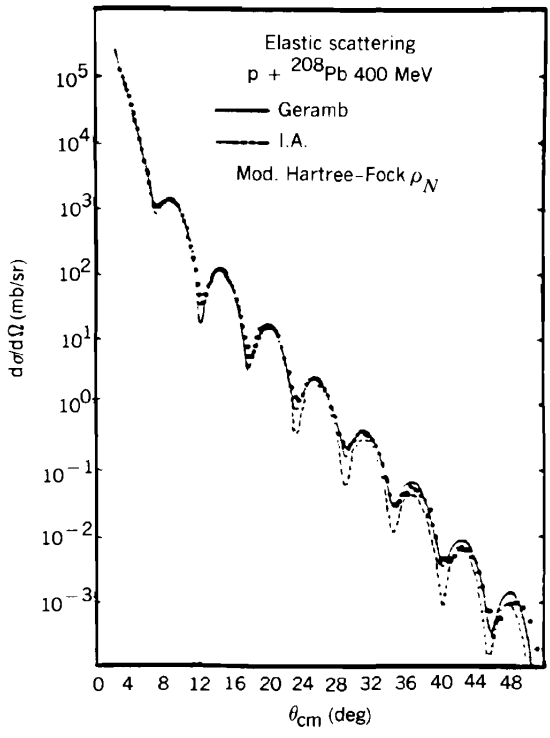
Elastic scattering
p + 208Pb 400 MeV
Geramb
I.A.
Mod. Hartree-Fock ρ_N
dσ/dΩ (mb/sr)
10^5
10^4
10^3
10^2
10^1
10^0
10^{-1}
10^{-2}
10^{-3}
0 4 8 12 16 20 24 28 32 36 40 44 48
θ_{cm} (deg)

(*a*)

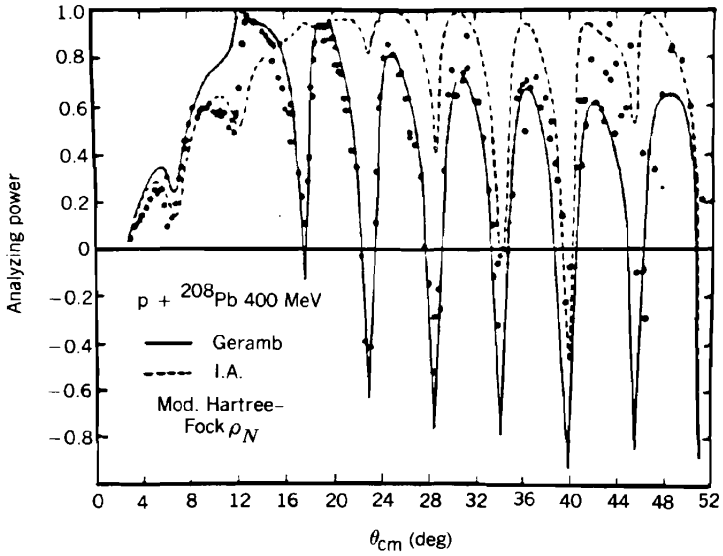
Analyzing power
1.0
0.8
0.6
0.4
0.2
0
−0.2
−0.4
−0.6
−0.8
p + 208Pb 400 MeV
Geramb
I.A.
Mod. Hartree-Fock ρ_N
0 4 8 12 16 20 24 28 32 36 40 44 48 52
θ_{cm} (deg)

(*b*)

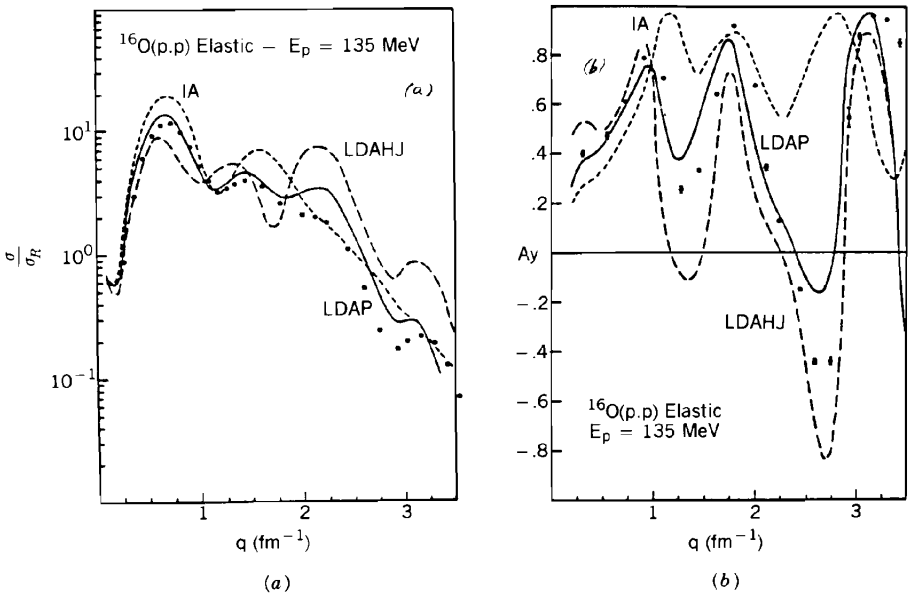

FIG. 2.31. Angular distribution (*a*) and asymmetry (*b*) for 135-MeV protons scattered by ^{16}O compared with the impulse approximation (IA), with the local density approximation using the Paris potential (LDAP) or using the Hamada–Johnston potential (LDAHJ). The quantity q is the momentum transfer. [From Kelly (83).]

Other invariants can be added to the β term, but it has sufficed for the empirical treatment to employ only the combination of a scalar potential U_s and the fourth component of a four-vector, U_0. To obtain a comparison with the Schrödinger optical model equation, one first introduces

$$\psi = \begin{pmatrix} \psi_L \\ \psi_S \end{pmatrix} \tag{2.93}$$

and obtains

$$(\boldsymbol{\sigma}\cdot\mathbf{p})\psi_S = [(E - U_0) - (mc^2 + U_s)]\psi_L \tag{2.94a}$$

$$(\boldsymbol{\sigma}\cdot\mathbf{p})\psi_L = [(E - U_0) + (mc^2 + U_s]\psi_S \tag{2.94b}$$

Solving the second of these equations for ψ_s and introducing the result into (2.94*a*) yields

$$[(E-U_0)^2-(mc^2+U_s)^2]\psi_L$$
$$=\left[(E-U_0)+(mc^2+U_s)c\boldsymbol{\sigma}\cdot\mathbf{p}\frac{1}{E-U_0+mc^2+U_S}c\boldsymbol{\sigma}\cdot\mathbf{p}\right]\psi_L$$

Evaluating the quantity on the right under the assumption that U_0 and U_s are functions of r yields only

$$[(E-U_0)^2-(mc^2+U_S)^2]\psi_L=c^2p^2\psi_L+\left[i\frac{c^2}{rA}\frac{\partial A}{\partial r}\boldsymbol{\sigma}\cdot\mathbf{L}-c^2\frac{1}{rA}\frac{\partial A}{\partial r}(\mathbf{r}\cdot\mathbf{p})\right]\psi_L$$

where

$$A\equiv\frac{(E-U_0)+(mc^2+U_S)}{E+mc^2} \tag{2.95}$$

To remove the linear term in $\mathbf{p}$ we replace ψ_L by

$$\psi_L=A^{1/2}\phi \tag{2.96}$$

with the result

$$\left[\frac{1}{c^2}(E-U_0)^2-\frac{1}{c^2}(mc^2+U_S)^2-p^2\right]\phi$$
$$+\left[-\frac{3}{4}\frac{1}{A^2}\left(\frac{\partial A}{\partial r}\right)^2+\frac{1}{2r^2A}\frac{\partial}{\partial r}\left(r^2\frac{\partial A}{\partial r}\right)+\frac{1}{rA}\frac{\partial A}{\partial r}\boldsymbol{\sigma}\cdot\mathbf{L}\right]\phi=0$$

or placing

$$E^2-m^2c^4\equiv c^2k^2$$

one obtains the Schrödinger equation:

$$\left(\frac{k^2}{2m}-\frac{p^2}{2m}-V_{\text{eff}}\right)\phi=0 \tag{2.97}$$

$$V_{\text{eff}}\equiv\frac{E}{mc^2}U_0+U_S+\frac{1}{2mc^2}(U_S^2-U_0^2)+\frac{3}{8m}\frac{1}{A^2}\left(\frac{\partial A}{\partial r}\right)^2$$
$$-\frac{1}{4mr^2A}\frac{\partial}{\partial r}r^2\frac{\partial A}{\partial r}-\frac{1}{2mrA}\frac{\partial A}{\partial r}\boldsymbol{\sigma}\cdot\mathbf{L} \tag{2.98}$$

In V_{eff}, note the energy dependence of the U_0 term as well as the presence of the square terms, which by suitable choice of U_s and U_0 can produce a repulsive

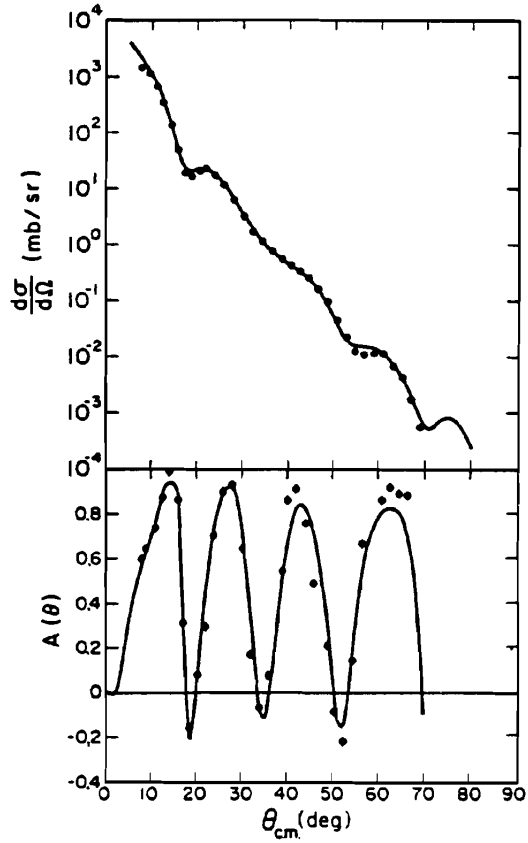

FIG. 2.32. Elastic p–^{40}Ca cross sections and analyzing powers at 181 MeV. The smooth curves are the results of the relativistic optical model analysis described in the text. [From Arnold, Clark, Mercer, and Schwandt (81).]

term as required by (2.91). These three terms would appear naturally in any single-body relativistic formulation, as they originate from $[(E - U_0)^2 - (mc^2 + U_S)^2]$. In the above, the Coulomb term is included in U_0. The spin-orbit term and the preceding two terms (also making repulsion contribution) are consequences of the special character of the Dirac equation. To obtain the energy dependence observed, $\mathrm{Re}\, U_0$ must be repulsive (positive) and $\mathrm{Re}\, U_S$ attractive (negative). Note that U_0 and U_S are complex. The effect of an attractive U_S is to reduce the nucleon mass inside the interaction region considerably (~ 0.5 m), thereby, amplifying the relativistic effects.

In using the Dirac optical model, (2.92), to fit experimental data [see Clark, Hama, and Mercer (83) for a summary], U_S and U_0 are chosen as follows:

$$U_0 = V_0 f_0(r) + iW_0 g_0(r)$$

$$U_s = V_s f_s(r) + iW_s g_s(r)$$

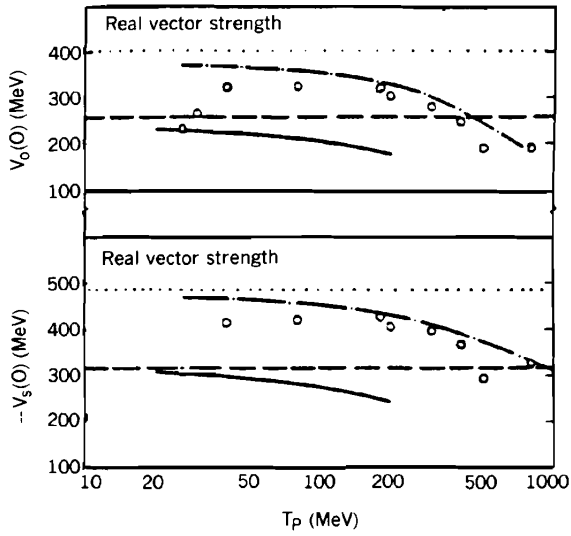

FIG. 2.33. Values of the real scalar V_s and V_0 potentials at $r = 0$ determined from the 12-parameter analysis of p–^{40}Ca data, The upper dotted lines are the values from the relativistic mean field calculation of Arnold, Clark, Mercer, and Schwandt (81). The dashed lines are from Boguta (81); the curved lines are from the relativistic Brueckner Hartree–Fock calculations of Shakin (83); the dashed–dotted curves are from Arnold et al. (82). [From Clark, Hama, and Mercer (83).]

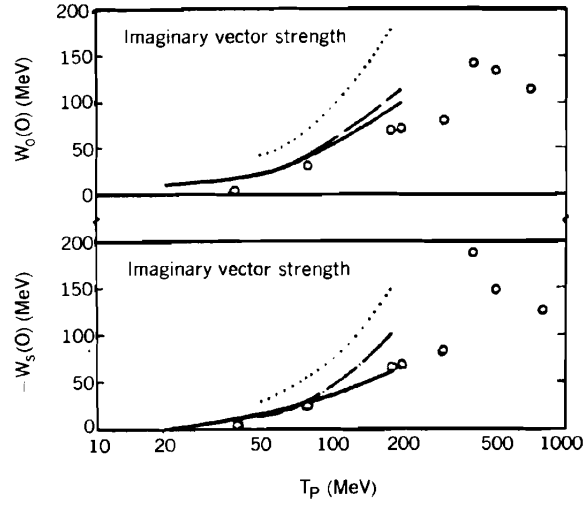

FIG. 2.34. Values of the imaginary scalar W_s and vector W_0 potentials at $r = 0$ determined from the 12-parameter analysis of p–^{40}Ca data described in the text. The dotted lines are the calculations of Jaminon (83); the dashed lines of Horowitz (82), the smooth curves, of Shakin (83). [From Clark, Hama, and Mercer (83).]

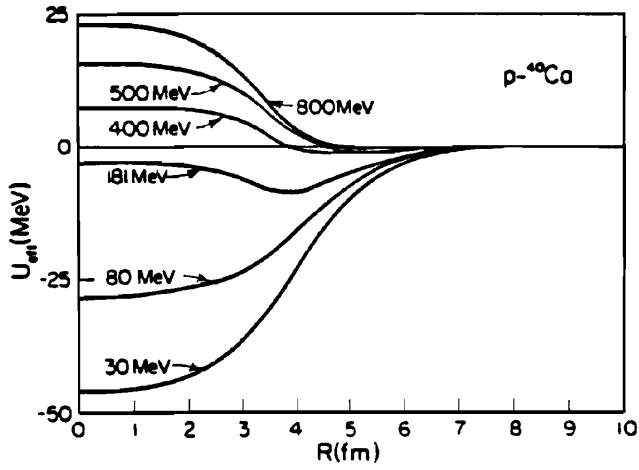

FIG. 2.35. Real part of the Schrödinger equivalent central potential U_{eff}, determined from the Dirac equation based analysis of $\mathbf{p}$–^{40}Ca elastic scattering experiments. The Darwin term is omitted. [From Arnold et al. (82).]

where f_0, f_s, g_0, and g_s are in the Woods–Saxon form:

$$\frac{1}{1+e^{(r-R)/a}}$$

The geometrical parameters for f_0 and f_s are obtained by comparison with the results of the Walecka relativistic model (74) obtained by Horowitz and Serot (81). For the case of 181-MeV protons incident on ^{40}Ca, the parameters are as follows:

$$R_0 = 3.474\,\text{fm}$$

$$R_s = 3.453\,\text{fm}$$

$$a_0 = 0.668\,\text{fm}$$

$$a_s = 0.692\,\text{fm}$$

The methods used to obtain these results are described in Arnold, Clark, Mercer, and Schwandt (81). In that paper the geometrical parameters for the imaginary components of U_0 and U_s were chosen identical with those of Re U_s. These, together with the depths $V_{0,s}$ and $W_{0,s}$, were varied in order to obtain a fit of the experimental data, making a six-parameter fit in all. The standard model uses 12 parameters. The fits to the 181-MeV proton data are shown in Fig. 2.32.

The values of the parameters to be combined with those given above are Re $U_0 = 334$ MeV, Re $U_s = -437$ MeV, Im $U_0 = -107$ MeV, and Im $U_s =$

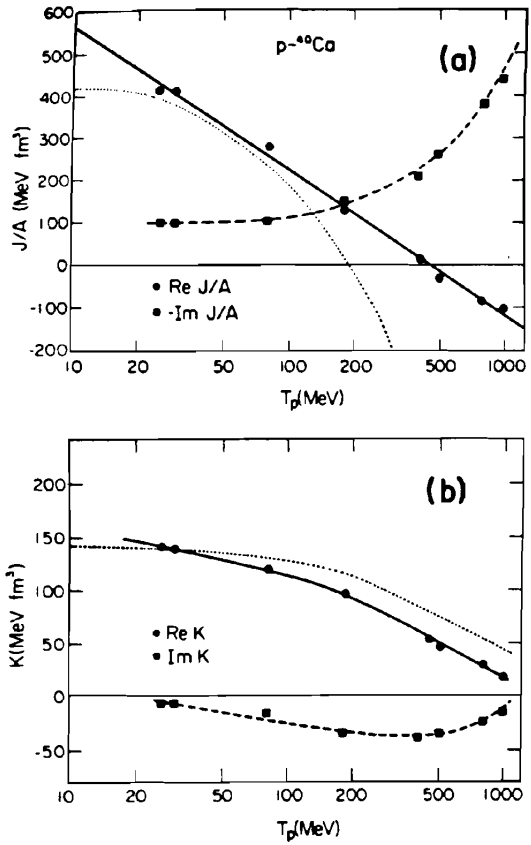

FIG. 2.36. (*a*) Values of the volume integrals of the real and imaginary parts of the Schrödinger equivalent central potential for ^{40}Ca. The smooth line is a linear fit. The dashed line is to guide the eye. The dotted line gives the Dirac–Hartree values. (*b*) Values of the volume integrals of the real and imaginary parts of the Schrödinger equivalent spin-orbit potential for ^{40}Ca. The smooth and dashed lines are to guide the eye. The dotted line gives the Dirac–Hartree values. [From Arnold et al. (82).]

109 MeV, where the geometrical parameters for Im U_0 are $R = 3.487$ fm and $a = 0.716$ fm. The energy dependence of the potential depths is shown in Figs 2.33 and 2.34.

The real part of the effective potential, (2.98), is shown in Fig. 2.35. The characteristic intermediate wine bottle shape is seen at 181 MeV. The potential is mainly repulsive at 400 MeV and above, with a small attractive tail that diminishes in amplitude as the energy increases. The radial dependence of the effective spin-orbit potential is shown in Fig. 2.36. The excellent agreement at 181 MeV and 400 MeV is repeated at 497 MeV. A new feature at this energy is the measurement of the spin rotation function $Q(\theta)$ shown in Fig. 2.37. The

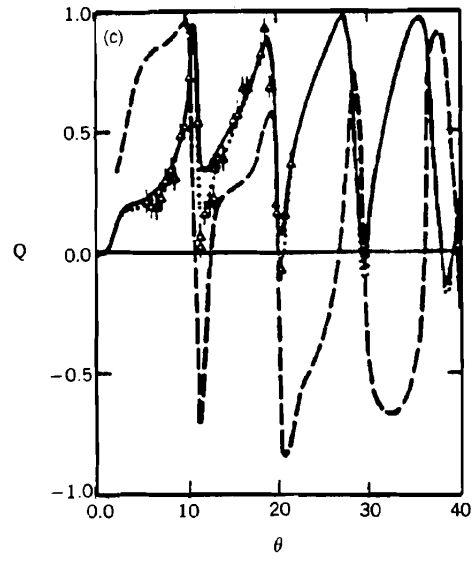

FIG. 2.37. Spin rotation function Q. (From Schwandt (83).]

relativistic model agrees very well indeed, whereas the standard model result given by the dashed line is in strong disagreement with experiment.

The excellent agreement obtained with the relativistic theory over a wide range of energies is a strong incentive for further study, especially those involving reactions, which will serve as tests of the theory. The one-boson exchange picture used by Walecka (74) and Shakin (83) involving a scalar (σ) and a vector boson (ρ) is not easily made consistent with the quark picture of a nucleon with a root-mean-square radius of 0.8 fm. Thus at the time this is being written, much remains to be done.

3. CHARGE EXCHANGE REACTIONS: OPTICAL MODEL DESCRIPTION‡

Because of the near identity of the neutron and proton, the charge exchange reactions (p,n) or (n,p) should be closely related to the elastic (p,p) and (n,n) elastic scattering. However, these connections are not simple because of the presence of interactions, such as the the Coulomb interaction, which do not conserve isospin. To make this issue more concrete, consider the final state in a (p,n) reaction, in which the target nucleus (Z,N,A) is converted into the nucleus $(Z+1,N-1,A)$. The target nucleus is in the ground state. The energy-level spectra of the two nuclei, the target and residual are compared in Fig. 3.1. We see that the level in the nucleus $(Z+1,N-1)$, corresponding to the ground state in the target nucleus (Z,N), is not its ground state, but rather one lifted by an energy approximately equal to the Coulomb energy, which is

‡Satchler (69), Robson (69), Auerbach, Gal, Hüfner, and Kerman (72).

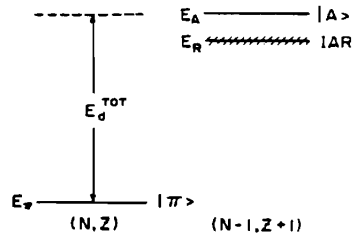

FIG. 3.1. Schematic representation of the relation of the displacement energy $E_d^{(\mathrm{tot})} = E_A - E_w$ and the observed energy of the isobaric analog resonance, E_R. [From Auerbach, Gal, Hüfner, and Kerman (72).]

the dominant isospin symmetry-breaking term. This state in the $(Z+1, N-1)$ nucleus is referred to as the *analog* of the ground state of the (Z, N) nucleus. To the extent that T, the isospin, is a good quantum number, it is the ground state (i.e., the lowest state) of the $T = (N-Z)/2$ states in the $(Z+1, N-1)$ nucleus. The value of T_Z for the ground state of the (Z, N) nucleus is $-T$, while for the analog, $T_Z = -T+1$. It is clear that the channel which should be considered along with the proton, plus the ground state of the (Z, N) nucleus channel, in discussing elastic scattering is the neutron plus analog state of the $(Z+1, N-1)$ nucleus. In other words, we consider elastic scattering in the $T = (N-Z)/2$ channel, which, because of the Coulomb shift, should better be referred to as *quasi-elastic scattering*.

One should question the use of isospin quantum numbers for the target and residual nuclei in the presence of a symmetry-breaking Coulomb force, which, particularly for heavy nuclei, must be regarded as strong. The saving grace is that this force is long range, that is, varies slowly over the nuclear volume. Thus its nondiagonal matrix elements between nuclear states are relatively small. As a consequence, the principal effect of this long-range symmetry-breaking force will be to shift the position of the energy levels but not to change substantially the wave functions inside the nuclear volume. In this respect, it therefore makes good sense to continue the use of isospin concepts and nomenclature even for the heavier nuclei, although it should be kept in mind that the states under consideration are not pure. This argument breaks down at sufficiently high excitation energies, for then the smallness of the nondiagonal matrix elements will be compensated by the high density of states with differing isospins that couple to a state with a specific isospin via the isospin symmetry-breaking interaction. Isospin impurity will therefore grow with increasing excitation energy.

We turn now to a consideration of the isospin extension of the optical model. First, we collect some simple results regarding the states involved. The state of the target nucleus will be designated by $|\pi\rangle$ for "parent" and the state of the proton plus target by $|p\pi\rangle$. The analog state, $|A\rangle$, is obtained by converting a neutron in the target to a proton[‡]

$$|A\rangle \equiv \alpha T_+ |\pi\rangle \tag{3.1}$$

[‡]Recall that in these volumes $\tau_+|p\rangle = 0, \tau_+|n\rangle = |p\rangle, \tau_-|p\rangle = |n\rangle, \tau_-|n\rangle = 0, \mathbf{t} = \boldsymbol{\tau}/2$.

where α is a normalization factor. We determine α by calculating $\langle A|A\rangle$ and choosing α so that $\langle A|A\rangle$ is unity:

$$\langle A|A\rangle = \alpha^2\langle \pi|T_- T_+|\pi\rangle = \alpha^2[T(T+1) - T_Z^2 - T_Z]$$

where it has been assumed that $|\pi\rangle$ is a state with a well-defined isospin T with the projection

$$T_Z|\pi\rangle = -\tfrac{1}{2}(N-Z)|\pi\rangle$$

With $T = (N-Z)/2$ we find that

$$\frac{1}{\alpha} = (N-Z)^{1/2} = (2T)^{1/2}$$

so that

$$|A\rangle = \frac{1}{\sqrt{N-Z}} T_+|\pi\rangle = \frac{1}{\sqrt{2T}} T_+|\pi\rangle \tag{3.2a}$$

Note that

$$T_-|\pi\rangle = 0 \tag{3.2b}$$

Note. The corrections to (3.2) because of the isospin impurity are discussed by Auerbach, Gal, Hüfner, and Kerman (72).

The states $|p\pi\rangle$ and $|nA\rangle$ can be written as linear combinations of states with isospin $T_>(= T + \frac{1}{2})$ and $T_<(= T - \frac{1}{2})$ using Clebsch–Gordan coefficients:

$$|p\pi\rangle \equiv |\tfrac{1}{2}\tfrac{1}{2}; TT_Z\rangle = \langle T+\tfrac{1}{2}, T_Z+\tfrac{1}{2}|\tfrac{1}{2}\tfrac{1}{2}; TT_Z\rangle|T_>, T_Z+\tfrac{1}{2}\rangle + \langle T-\tfrac{1}{2}, T_Z+\tfrac{1}{2}|\tfrac{1}{2}\tfrac{1}{2}; TT_Z\rangle|T_<, T_Z+\tfrac{1}{2}\rangle$$

Taking $T_Z = -T$, we obtain [see deShalit and Feshbach (74, p. 927)]

$$|p\pi\rangle \equiv |\tfrac{1}{2}\tfrac{1}{2}, T, -T\rangle = \frac{1}{\sqrt{2T+1}}[|T_>\rangle + \sqrt{2T}|T_<\rangle] \tag{3.3a}$$

Similarly,

$$|nA\rangle = |\tfrac{1}{2}, -\tfrac{1}{2}, T, -T+1\rangle = \frac{1}{\sqrt{2T+1}}[\sqrt{2T}|T_>\rangle - |T_<\rangle] \tag{3.3b}$$

Inverting yields

$$|T_>\rangle = \frac{1}{\sqrt{2T+1}}[|p\pi\rangle + \sqrt{2T}|nA\rangle] \tag{3.4a}$$

$$|T_<\rangle = \frac{1}{\sqrt{2T+1}}[\sqrt{2T}|p\pi\rangle - |nA\rangle] \tag{3.4b}$$

The isospin operators that will enter into our discussion include t_3 ($\equiv \frac{1}{2}\tau_3$) operating on the nucleon projectile and $\mathbf{t}\cdot\mathbf{T}(\mathbf{t} \equiv \frac{1}{2}\boldsymbol{\tau})$, where $\mathbf{t}$ operates on the nucleon and $\mathbf{T}$ on the nuclear (π or A) coordinates. The matrix elements of t_3 in the two representations (3.3) and (3.4) are

$$\begin{aligned} &\langle p\pi|t_3|p\pi\rangle = \tfrac{1}{2} \qquad \langle p\pi|t_3|nA\rangle = 0 = \langle nA|t_3|p\pi\rangle \\ &\langle nA|t_3|nA\rangle = -\tfrac{1}{2} \\ &\langle T_>|t_3|T_>\rangle = -\frac{1}{2}\frac{2T-1}{2T+1} = -\langle T_<|t_3|T_<\rangle \end{aligned} \tag{3.5}$$

$$\langle T_>|t_3|T_<\rangle = \langle T_<|t_3|T_>\rangle = \frac{\sqrt{2T}}{2T+1} \tag{3.6}$$

The matrix elements of $\mathbf{t}\cdot\mathbf{T}$ operator are most easily obtained in the representation given by (3.4) since

$$\mathbf{T}\cdot\mathbf{t} = \frac{(\mathbf{T}+\mathbf{t})^2 - T^2 - t^2}{2}$$

One obtains

$$\begin{aligned} &\langle T_>|\mathbf{T}\cdot\mathbf{t}|T_>\rangle = \tfrac{1}{2}T \\ &\langle T_<|\mathbf{T}\cdot\mathbf{t}|T_<\rangle = -\tfrac{1}{2}(T+1) \\ &\langle T_>|\mathbf{T}\cdot\mathbf{t}|T_<\rangle = 0 = \langle T_<|\mathbf{T}\cdot\mathbf{t}|T_>\rangle \end{aligned} \tag{3.7}$$

In representation (3.3),

$$\begin{aligned} &\langle p\pi|\mathbf{T}\cdot\mathbf{t}|p\pi\rangle = -\frac{T}{2} \\ &\langle nA|\mathbf{T}\cdot\mathbf{t}|nA\rangle = \tfrac{1}{2}(T-1) \\ &\langle nA|\mathbf{T}\cdot\mathbf{t}|p\pi\rangle = \langle p\pi|\mathbf{T}\cdot\mathbf{t}|nA\rangle = \tfrac{1}{2}\sqrt{2T} \end{aligned} \tag{3.8}$$

Note that the operator $\mathbf{T}\cdot\mathbf{t}$ induces the charge exchange reaction $p\pi \leftrightarrow nA$.

With these results in hand it will be possible to discuss the extension to the optical model in isospin space proposed by Lane (62), namely,

$$V = V_0 + 4V_1\frac{\mathbf{t}\cdot\mathbf{T}}{A} \tag{3.9}$$

These are the only invariants on isospin spin space since the isospin operator for the projectile $\mathbf{t}$ can at most appear linearly. If we were dealing with other projectiles (e.g., heavy ions, pions) whose isospin is greater than unity, other

invariants are possible [Satchler (69)]. In the original Lane model, V_0 and V_1 were assumed to be central potentials, but obviously this can be extended to include spin–orbit terms or other spin-dependent terms, so that generally V_0 and V_1 can have the general form given in (2.38). The spin-dependent term can have a profound effect. For the present we shall assume that V_0 and V_1 depend only on the radial coordinate.

The potential equation (3.9) is not complete since, for example, it does not include the symmetry-breaking interaction between the incident proton and the target nucleus. The principal component of this interaction is the Coulomb force, which in (2.38) is taken to be the interaction of the proton with a spherical distribution of charge of radius R_c and charge Ze. This is an approximation to the sum of Coulomb interactions between the incident protons and the protons in the nucleus. There are additional electromagnetic terms, including magnetic terms, describing the interaction of the magnetic moment and orbital current of the proton with the currents and magnetic moments of the nucleons inside the target nucleus. It should be noted that the Coulomb interaction is modified by vacuum polarization. These effects, which should be added on to Coulomb potential, are discussed in considerable detail by Auerbach, Gal, Hüfner, and Kerman (72). They will not be included in the empirical analysis discussed below.

In the $|nA\rangle$ channel the electromagnetic symmetry-breaking interaction of the neutron with the nucleus A is a consequence of the interaction of its magnetic moment with the currents and fields inside the nucleus. These are similar to those discussed in the preceding paragraph and will be neglected in the empirical analysis.‡

The optical model Hamiltonian is thus

$$H = H_0 + T_0 + V_0 + 4V_1 \frac{\mathbf{t}\cdot\mathbf{T}}{A} + V_C(\tfrac{1}{2} + t_3) \tag{3.10}$$

The last term is present only in the $|p\pi\rangle$ channel vanishing in the $|nA\rangle$ channel. The operator H_0 is the Hamiltonian for the target nuclear system of A nucleons; T_0 is the kinetic energy of the nucleon relative to the nucleus. The state vector $|\pi\rangle$ is an eigenstate of H_0 with the energy scale chosen so that the eigenvalue is zero.

With this Hamiltonian, the Schrödinger equation

$$H\Psi = E\Psi$$

can be reduced to a pair of coupled-channel equations by using either

‡However, the small-angle scattering induced by the interaction of the neutron moment with the electric field of the nucleus can be used to produce polarized neutrons, as pointed out by Schwinger and referred to as *Schwinger polarization scattering* [Schwinger (48)].

representation

$$\Psi = \psi_p(\mathbf{r})|p\pi\rangle + \psi_n(\mathbf{r})|nA\rangle \tag{3.11a}$$

or

$$\Psi = \psi_>(\mathbf{r})|T_>\rangle + \psi_<(\mathbf{r})|T_<\rangle \tag{3.11b}$$

Inserting (3.11*a*) into the Schrödinger equation and using (3.5)–(3.7), one obtains

$$\left[E - T_0 - V_0 + \frac{2TV_1}{A} - V_C\right]\psi_p = 2\sqrt{2T}\frac{V_1}{A}\psi_n \tag{3.12a}$$

$$\left[E - T_0 - \Delta_C - V_0 - \frac{2(T-1)V_1}{A}\right]\psi_n = 2\sqrt{2T}\frac{V_1}{A}\psi_n \tag{3.12b}$$

with the asymptotic boundary condition that ψ_p approach the incident plane wave plus outgoing scattered wave, while ψ_n yield only an outgoing wave if the total energy in the neutron channel is positive; if negative, an exponentially decaying wave would be required. From (3.12*b*) one sees that the energy in the neutron channel is $E - \Delta_C$ with

$$\Delta_C = \langle A|H_0|A\rangle - \langle \pi|H_0|\pi\rangle \tag{3.13}$$

If isospin were conserved, Δ_C would be zero. But in virtue of the isospin symmetry-breaking potential, the Coulomb potential, Δ_C, is not zero but rather gives the additional Coulomb energy possessed by the analog nucleus because of the replacement of a neutron in the parent nucleus by a proton. To demonstrate this more closely, we introduce (3.1) expressing $|A\rangle$ in terms of $|\pi\rangle$. One obtains

$$\Delta_C = \frac{1}{2T}\langle \pi|T_-[H_0, T_+]|\pi\rangle \simeq \frac{1}{2T}\langle \pi|[T_-, [H_0, T_+]]|\pi\rangle \tag{3.14}$$

Only if H_0 contains a term that does not conserve isospin and therefore leads to a nonzero value of the commutator $|H_0, T_+]$ will Δ_C differ from zero.

Problem. Assume that the only isospin symmetry-breaking term in H_0 is the Coulomb energy [see (II.6.6) in deShalit and Feshbach (74)]. Express it in terms of isospin spin operators and A ($\equiv N + Z$) and evaluate the double commutator in (3.14).

The value of Δ_C using the Fermi-gas model turns out to be

$$\Delta_C \simeq \frac{3}{5}\frac{e^2}{R}[(2Z+1) - 1.02Z^{1/3}] \tag{3.15}$$

[see Spencer and Kerman (72)], where R is the nuclear radius. For ^{88}Sr, Δ_C is about 11.5 MeV.

For a sufficiently low E, the available energy for the neutron analog channel, (3.12*b*), is negative, so that the wave function decays exponentially. Moreover, the homogeneous form of (3.12*b*) obtained by placing the right-hand side equal to zero will admit bound-state solutions. As we know from the example introducing Chapter III, this has the consequence that the proton channel will exhibit a resonance at an energy close to the energies of these bound states. These are the elastic isobar analog resonances.

Before discussing these, one more feature must be added to (3.12*a*). The imaginary component of the potential, V_0, is not necessarily the same for the proton and neutron channel since the coupling of these channels to other channels and to more complex excitations differ. In other words, additional isospin dependence needs to be added. The issues involved are clearer if we make use of the $T_>$ ($= T + \frac{1}{2}$) and $T_<$ ($= T - \frac{1}{2}$) representations Inserting (3.11*b*) into the Schrödinger equation yields

$$\left[E - T_0 - V_0 - \frac{2TV_1}{A} - \Delta_C + \frac{1}{2T+1}(\Delta_C - V_C)\right]\psi_> = -\frac{1}{2T+1}\sqrt{2T}(\Delta_C - V_C)\psi_< \tag{3.16a}$$

$$\left[E - T_0 - V_0 + \frac{2(T+1)}{A}V_1 - V_C - \frac{1}{2T+1}(\Delta_C - V_C)\right]\psi_< = -\frac{1}{2T+1}\sqrt{2T}(\Delta_C - V_C)\psi_> \tag{3.16b}$$

As is clear from (3.4), the major component of $\psi_>$ is the neutron channel. As originally emphasized by Robson (65), we also note that the coupling between the $T_>$ and $T_<$ channel occurs "outside" the nucleus. In the nuclear interior Δ_C and V_C will cancel approximately. Thus the mixing between the two states is referred to as *external.*

It is anticipated that the coupling of the $T_>$ channel to channels and states that have not been included in (3.16) will be small since the density of $T_>$ states is relatively small, whereas the density of $T_<$ states will be normal. We therefore add an imaginary term to (3.16*b*) only, that is, replace V_0 by $V_0 + iW_0$ in that equation. In isospin language this is described by

$$V_0 \to V_0 + iW_0\frac{(T+\frac{1}{2})(T+\frac{3}{2}) - (\mathbf{T}+\mathbf{t})^2}{2T+1} \tag{3.17}$$

Equations (3.12) are modified as a consequence. They now become

$$\left[E - T_0 - V_0 + \frac{2TV_1}{A} - V_C - \frac{2T}{2T+1} iW_0\right]\psi_p = \left(\frac{2V_1}{A} - \frac{iW_0}{2T+1}\right)\sqrt{2T}\psi_n \tag{3.18a}$$

$$\left[E - \Delta_C - T_0 - V_0 - \frac{2(T-1)V_1}{A} - \frac{iW_0}{2T+1}\right]\psi_n = \left(\frac{2V_1}{A} - \frac{iW_0}{2T+1}\right)\sqrt{2T}\psi_p \tag{3.18b}$$

These equations can now be used to study the isobar analog resonances using the optical model forms of Perey and Buck (62) or Rosen, Beery, Goldhaber, and Auerbach (65), taking V_1 to have the same form as W_0. An example of a fit to the observed resonances in the reaction ($p + {}^{88}$Sr) is shown in Fig. 3.2. Note that the proton energy employed is always considerably less than the value of Δ_C, which is taken to be 11.45 MeV. Writing

$$V_1 = v_1 f_W(x)$$

where $f_W(x)$ is given by (2.28), $4v_1/A$ has the value of 2.2 MeV and v_1 the value 48.4 MeV.

When the target nucleus has a spin, as, for example, ^{89}Y with a spin of $\frac{1}{2}$, the analog resonance can have two spin values ($j \pm \frac{1}{2}, j \neq 0$) according to the value of the spin of the neutron in the neutron channel [see (3.18*b*)]. To obtain a fit, it is necessary to add a spin-dependent term to the optical model Hamiltonian of the form $\boldsymbol{\sigma}\cdot\mathbf{I}$, a possibility mentioned earlier in this chapter [see

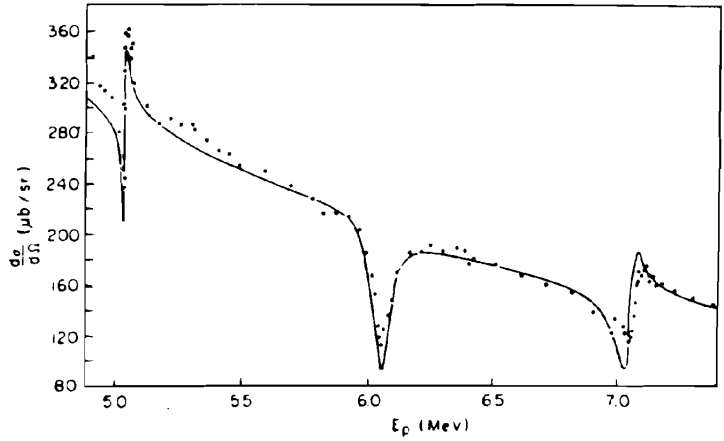

FIG. 3.2. Calculated differential cross sections at 90° for $p + {}^{88}$Sr. [From Auerbach and Dover (66).]

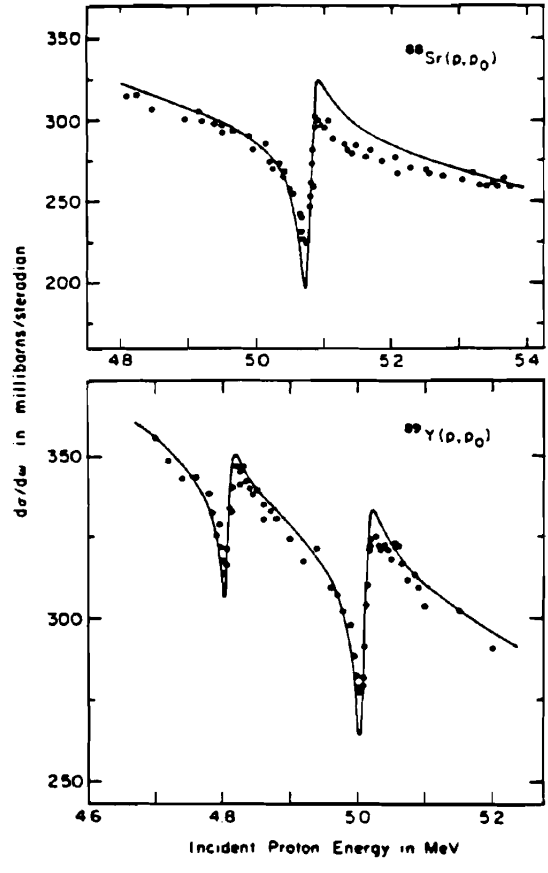

FIG. 3.3. Comparison of the calculated energy dependence of the cross-sections at 90° for ^{88}Sr and ^{89}Y with experiment. [From Spencer and Kerman (72).]

(2.41)]. Taking this additional term as

$$\frac{V_2}{A} f_W(x)$$

Spencer and Kerman (72) find V_2/A to equal to 0.7 MeV. Their results are shown in Fig. 3.3.

We now turn to a discussion of the global analysis of the (p,p), (n,n), and (p,n) reaction, where the last goes to the isobar analog state, developed by Patterson, Doering, and Galonsky (76). These authors use (3.12), employing the DWA for the (p,n) reaction. In this application of the DWA, the homogeneous

forms of (3.12) are used to describe the proton and neutron scattering:

$$\left[E - T_0 - V_0 + \frac{2TV_1}{A} - V_C\right]\psi_p \simeq 0 \tag{3.19a}$$

$$\left[E - \Delta_C - T_0 - V_0 - \frac{2(T-1)V_1}{A}\right]\psi_n \simeq 0 \tag{3.19b}$$

while the (p, n) transition amplitude is given approximately by

$$\mathscr{T}_{pn}^{\mathrm{IAS}} \simeq \left\langle \psi_n^{(-)} \middle| 2\sqrt{2T}\frac{V_1}{A} \middle| \psi_p^{(+)} \right\rangle \tag{3.20}$$

The potential (3.9) is written

$$V = -\mathscr{V}_0(r, E) + \mathscr{V}_{so}(r) + 4\mathscr{V}_1(r, E)\frac{\mathbf{t}\cdot\mathbf{T}}{A} \tag{3.21}$$

where

$$\mathscr{V}_k(r, E) = (V_{kC} + EV_{kE})f(r, R_R, a_R) + i(W_{kC} + EW_{kE})f(r, R_I, a_I)$$
$$- ia_I(WS_{kC} + EWS_{kC})\frac{d}{dr}f(r, R_I, a_I) \qquad k = 0, 1 \tag{3.22}$$

and where

$$f(r, R, a) = \left[1 + \exp\left(\frac{r - R}{a}\right)\right]^{-1} \qquad R_p = r_p A^{1/3} \tag{3.23}$$

The spin-orbit potential is

$$\mathscr{V}_{so}(r) = V_{so}\left(\frac{\hbar}{m_\pi c}\right)^2 \boldsymbol{\sigma}\cdot\mathbf{l}\frac{1}{r}\frac{d}{dr}f(r, R_{so}, a_{so}) \tag{3.24}$$

They also take V_C in the form given by (2.27) with

$$R_C = 1.149A^{1/3} + 1.788A^{-1/3} - \frac{1.163}{A}$$

Patterson, Doering, and Galonsky (76) find (for details, see their paper)

$$\mathrm{Re}\left(-\mathscr{V}_0 \pm \frac{2T\mathscr{V}_1}{A}\right) = \left(55.8 - 0.32\mathrm{E} \pm 17.7\frac{N-Z}{A}\,\mathrm{MeV}\right)f(r, R_R, a_R)$$
$$r_R = 1.17\,\mathrm{fm} \qquad a_R = 0.75\,\mathrm{fm} \tag{3.25}$$

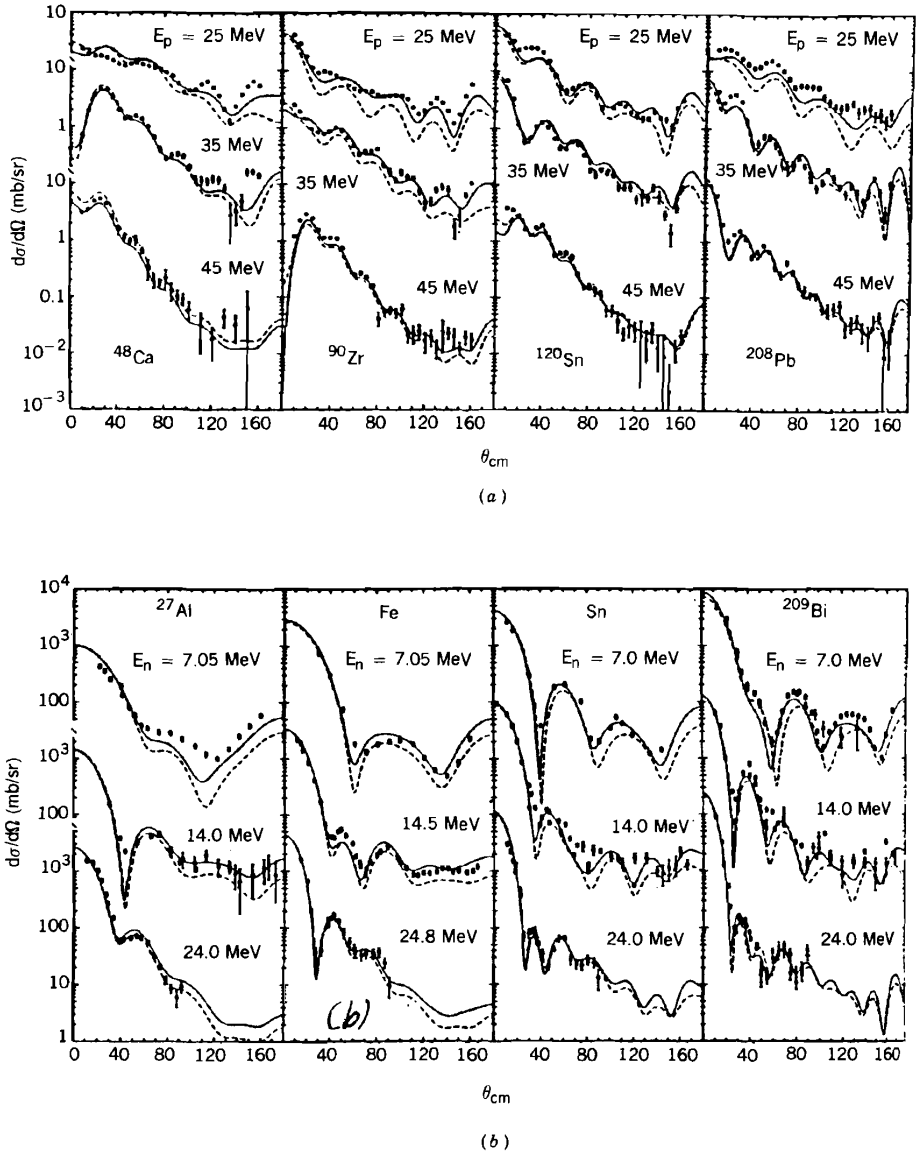

FIG. 3.4. (*a*) Comparison of DWA calculations with (p,n) isobar analog differential cross-section data; (*b*) comparison of optical model calculations with (n,n) elastic differential cross-section data. [From Patterson, Doering, and Galonsky (76).]

$$\mathrm{Im}\left(-\mathscr{V}_0 \pm \frac{2TV_1}{A}\right) = (-1.4 + 0.22\mathrm{E})\,\mathrm{MeV}\, f(r, R_I, a_I)$$

$$- a_I\left(9.6 - 0.22\mathrm{E} \pm (18.1 - 0.31\mathrm{E})\frac{N-Z}{A}\right)\frac{d}{dr} f(r, R_i, a_i)$$

$$r_I = 1.32\,\mathrm{fm} \qquad a_I = 0.51 + 0.7\frac{N-Z}{A} \tag{3.26}$$

The spin–orbit strength

$$V_{so} = 6.2\,\mathrm{MeV} \tag{3.27}$$

with

$$r_{so} = 1.01\,\mathrm{fm} \qquad a_{so} = 0.75\,\mathrm{fm}$$

The plus sign in the results above refers to the proton channel, the negative to the neutron channel. In (3.19), $T-1$ has been replaced by T. The coupling term in (3.20) is

$$-\frac{2\sqrt{N-Z}}{A}[17.7\,\mathrm{MeV}\, f(r, R_R, a_R) + i(18.1 - 0.31\mathrm{E}) f(r, R_I, a_I)] \tag{3.28}$$

Comparisons with the fit to (p,p) elastic scattering data ($E_p = 25, 35, 45$ MeV) by Becchetti and Greenlees (69), with (p,n) cross sections for the same energies and the same target nuclei, ^{48}Ca, ^{90}Zr, ^{120}Sn, and ^{208}Pb, are made. Predictions of neutron elastic scattering at E_n of about 7, 14, and 24 MeV for target nuclei ^{27}Al, Fe, Sn, and ^{209}Bi are compared with experiment. The results are satisfactory. A representative sample is shown in Fig. 3.4.

4. INELASTIC SCATTERING

In this section we consider the inelastic scattering reaction, in which an incident projectile excites the target nucleus:

$$a + A \rightarrow A^* + a' \tag{4.1}$$

We assume that the process is a prompt one; that is, it is the result of a direct interaction. As a consequence, we expect the angular distribution of nucleon a' in the center-of-mass system to be asymmetric, peaked in the forward cone. The energy variation of the cross section will be relatively slow, while the angular distribution will exhibit characteristic diffraction oscillations, a consequence of the relatively well-defined nuclear radius.

At low and intermediate energies, the surface region of the target plays the important dynamic role. A qualitative discussion of surface reactions is given

in Chapter I. We repeat some of the arguments here. Let the incident and final momentum of the projectile be $\mathbf{p}_i$ and $\mathbf{p}_f$, respectively. Since we are dealing with a surface reaction, the incident and final orbital angular momenta are $\mathbf{p}_i R$, and $\mathbf{p}_f R$, respectively, where R is the nuclear radius. The net resulting change in angular momentum $\hbar \Delta J$ is thus

$$\hbar \Delta J = |\mathbf{p}_i - \mathbf{p}_f| R \equiv \hbar q R \tag{4.2}$$

implying a maximum in the angular distribution at an angle θ_M given by

$$\sin^2 \frac{\theta_M}{2} = \frac{1}{4 p_i p_f} \left[\left(\frac{\hbar \Delta J}{R} \right)^2 - (p_i - p_f)^2 \right] \tag{4.3}$$

When $p_i \approx p_f$, as often occurs,

$$\theta_M \simeq \frac{\hbar \Delta J}{p_i R} \tag{4.4}$$

We note that θ_M increases with increasing ΔJ. It also follows from (4.3) that the cross section will vanish for $\theta < \theta_M$ since in this region, $\hbar \Delta J < |\mathbf{p}_i - \mathbf{p}_f| R$. This is a classical result, of course. Quantum mechanically, the cross section will diminish rapidly as θ decreases from θ_M, so that θ_M is the first maximum in the angular distribution. In Chapter I this simple result is compared with the measured angular distributions for inelastic α-scattering by ^{58}Ni and is shown to give good results, especially when a Coulomb correction is made. The oscillations in the cross section have an angular separation $\Delta\theta$ predictd by the uncertainty principle to be

$$\Delta\theta \simeq \frac{1}{\Delta J} = \frac{1}{qR}$$

Some further insight into the inelastic scattering process can be obtained if one makes use of the high-energy approximation to the optical model wave function in (1.14):

$$\mathcal{T}_{fi}^{(\mathrm{dir})} = \langle \chi_f^{(-)} | H_{fi}^{(\mathrm{opt})} \psi_i^{(+)} \rangle \tag{4.5}$$

We assume that $\psi_i^{(+)}$ and $\chi_f^{(-)}$ can be written as a product of the projectile wave function and the target nuclear wave function Ψ_i and Ψ_f for the ground and excited states, respectively. Thus

$$\psi_i^{(+)} = \phi_i^{(+)} \Psi_i$$

and

$$\chi_f^{(-)} = \phi_f^{(-)} \Psi_f \tag{4.6}$$

For didactic simplicity we have neglected the antisymmetrization that is required when the projectile consists of one or more nucleons (the effect of antisymmetrization is discussed on p. 195). The transition Hamiltonian $H_{fi}^{(\mathrm{opt})}$ is taken to be a sum of two particle interactions between the incident nucleon and the nucleons of the target, and, again for simplicity, we assume these residual interactions to be central and complex:

$$H_{fi}^{\mathrm{opt}} = \sum_i v(\mathbf{r}_0, \mathbf{r}_i) \tag{4.7}$$

where $\mathbf{r}_i$ is the coordinate of the target nucleus and $\mathbf{r}_0$ that of the incident projectile. With these assumptions, (4.5) becomes

$$\mathscr{T}_{fi}^{(\mathrm{dir})} = \langle \phi_f^{(-)}(\mathbf{r}_0) | \mathscr{V}_{fi}(\mathbf{r}_0) \phi_i^{(+)}(\mathbf{r}_0) \rangle \tag{4.8}$$

where

$$\mathscr{V}_{fi}(\mathbf{r}_0) \equiv \langle \Psi_f | \sum_j v(\mathbf{r}_0, \mathbf{r}_j) \Psi_i \rangle \tag{4.9}$$

The high-energy approximation[‡] assuming a spin-independent central optical potential to $\phi_i^{(+)}$ is [see (II.5.7)]

$$\phi_i^{(+)} \sim \exp\left\{ i \left[\mathbf{k}_i \cdot \mathbf{r}_0 - \frac{\mu}{\hbar^2 k_i} \int_{-\infty}^{z_0} V_{\mathrm{opt}}(\mathbf{b}_0, z)\, dz \right] \right\} \tag{4.10}$$

The z direction is given by $\mathbf{k}_i$, and $\mathbf{b}_0$ is the coordinate vector (x_0, y_0) perpendicular to $\mathbf{k}_i$. The magnitude, b_0, is the *impact parameter*. Similarly,

$$\phi_f^{(-)*} \sim \exp i \left\{ \left[-\mathbf{k}_f \cdot \mathbf{r}_0 + \frac{\mu}{\hbar^2 k_f} \int_{\infty}^{z_0'} V_{\mathrm{opt}}(\mathbf{b}_0', z) dz \right] \right\} \tag{4.11}$$

where z_0' is the direction of $\mathbf{k}_f$. In combining (4.10) and (4.11) we shall, for the second term in the exponential of (4.11), make the approximation $k_i \approx k_f$, valid when the excitation energy is small compared to the projectile energy, and the approximation that the directions of $z_0', \mathbf{b}_0'$ are the same[§] as that of z_0 and $\mathbf{b}_0$, implying small-angle scattering. Under these circumstances, the product $\phi_f^{(-)*}\phi_i^{(+)}$ is given by the simple expression

$$\phi_f^{(-)*}\phi_i^{(+)} \simeq \exp\{i[(\mathbf{k}_i - \mathbf{k}_f)\cdot\mathbf{r}_0]\} \exp\left[-i \frac{\mu}{\hbar^2 k_i} \int_{-\infty}^{\infty} V_{\mathrm{opt}}(\mathbf{b}_0, z)\, dz \right]$$

[‡]This is accurate at sufficiently high energy, $E > 100$ MeV [Bassichis, Feshbach, and Reading (71)], but the results obtained will be useful, as they are qualitatively correct below that energy.

[§]Some improvement in the last of these approximations can be made if the mutual directions of z_0 and z_0' is taken to that of $\frac{1}{2}(\mathbf{k}_i + \mathbf{k}_f)$.

The first exponential is that which appears in the Born approximation. The second is an approximation to the effect of the distortion caused by the optical potential. We note that it depends only on the impact parameter b_0; there is no z dependence. Since V_{opt} has a negative imaginary component ($\equiv -iW$), to take absorption into account, the magnitude of the second factor is less than 1 and is given by

$$\exp\left[-\frac{\mu}{\hbar^2 k_i}\int_{-\infty}^{\infty} W(\mathbf{b}_0, z)\,dz\right] \tag{4.12}$$

The integral is the total absorption along a path parallel to the z axis (i.e., in the incident direction) at a distance b_0 away from that axis. The maximum attenuation for the optical potentials commonly used will occur for a ray through the center of the nucleus. The attenuation will decrease as b_0 increases, since the path length is shorter and the absorption generally weaker. Once $b > R$, $W \to 0$ and the attenuation will go to zero. The factor, (4.12), therefore emphasizes the contribution of the nuclear surface to the direct reaction amplitude.

To complete the calculation, we need to evaluate $\mathscr{V}_{fi}(\mathbf{r}_0)$, defined by (4.9), and then perform the integral over $\mathbf{r}_0$ indicated by (4.8) to obtain $\mathscr{T}_{fi}^{(\text{dir})}$. The problem is simplified somewhat if we let v be a delta function of strength g, so that

$$\begin{aligned}
\mathscr{V}_{fi} &= g\langle \Psi_f | \sum_i \delta(\mathbf{r}_0 - \mathbf{r}_i)\Psi_i \rangle \\
&= Ag\langle \Psi_f | \delta(\mathbf{r}_0 - \mathbf{r}_1)\Psi_i \rangle \\
&= Ag\int \Psi_f^*(\mathbf{r}_0, \mathbf{r}_2, \ldots)\Psi_i(\mathbf{r}_0, \mathbf{r}_2, \ldots)\,d\mathbf{r}_2 \cdots \qquad (4.13) \\
&= Ag\rho_{fi}(\mathbf{r}_0) \qquad (4.14)
\end{aligned}$$

where ρ_{fi} is the density matrix measuring the overlap of the initial and final nuclear wave functions. The density matrix can be expanded in spherical harmonics (in the absence of spin),

$$\rho_{fi}(\mathbf{r}_0) = \sum \rho_{fi,lm}(r_0)\,Y_{lm}(\Omega_0) \tag{4.15}$$

where

$$|J_i - J_f| \leqslant l \leqslant (J_i + J_f) \tag{4.16}$$

The quantity, l is then the transferred angular momentum.

With these approximations, (4.8) for $\mathscr{T}_{fi}^{(\text{dir})}$ has the form

$$\mathscr{T}_{fi}^{(\text{dir})}(lm) \sim \int d\mathbf{r}_0 e^{i\mathbf{q}\cdot\mathbf{r}_0} e^{i\chi(\mathbf{b}_0)} \rho_{fi,lm}(r_0)\,Y_{lm}(\Omega_0) \tag{4.17}$$

where various constants of proportionality have been omitted and one of the Y_{lm}'s has been selected. The function $\chi(\mathbf{b}_0)$ is

$$\chi(\mathbf{b}_0) = -\frac{\mu}{\hbar^2 k_i}\int_{-\infty}^{\infty} V_{\text{opt}}(\mathbf{b}_0, z)\,dz \tag{4.18}$$

The vector $\mathbf{q} \equiv (\mathbf{k}_i - \mathbf{k}_f)$ has the components

$$q_z = k_i - k_f\cos\theta \qquad q_x = -k_f\sin\theta \qquad q_y = 0$$

so that

$$\mathbf{q}\cdot\mathbf{r}_0 = (k_i - k_f\cos\theta)z_0 - k_f b_0 \sin\theta\cos\varphi_0$$

The angle θ is the scattering angle, the angle between $\mathbf{k}_f$ and $\mathbf{k}_i$.

It is natural to use cyclindrical coordinates, (z_0, b_0, φ_0) in evaluating integral equation (4.17). Recalling that $Y_{lm}(\Omega) \sim e^{im\varphi_0}P_{lm}(\cos\theta_0)$, the φ_0 integral can be performed immediately to yield $2\pi\cdot i^m J_m(k_f b_0 \sin\theta)$. The z_0 integration requires the calculation of a Fourier transform of the z_0 dependence of $\rho_{fi,lm}(r_0)P_{lm}(\cos\theta)$. To obtain a rough value, we assume that the longitudinal momentum transfer $(k_i - k_f\cos\theta)R$ is small and that the overlap, $\rho_{fi,lm}(r_0)$, has its maximum at the nuclear radius. The first of these assumptions holds if the scattering angle is small and if the energy loss is small compared to the incident energy. The second specifies the interaction to favor a surface reaction. Combined with the attenuation originating in $\chi(\mathbf{b}_0)$, these assumptions lead to the result that the contribution to the z_0 integral comes primarily from the $z_0 = 0$ region. Thus the active region in the target nucleus for inelastic scattering in the forward direction and with small energy loss is the neighborhood of the perimeter of the great circle (for a spherical nucleus) perpendicular to the incident direction. With $z_0 = 0$ one may replace $P_{lm}(\cos\theta)$ by $P_{lm}(0)$ (i.e., $\theta_0 = \pi/2$). This function differs from zero only when $l + m$ is even.

Returning to k_0, (4.17), one finds that

$$\mathscr{T}_{fi}^{(\text{dir})}(lm) \sim P_{lm}(0)\int db_0 b_0 e^{i\chi(b_0)}J_m(k_f b_0\sin\theta)\int \rho_{fi,lm}e^{i(k_i - k_f\cos\theta)z_0}dz_0 \tag{4.19}$$

The angular dependence originating in the z_0 integral is relatively weak by assumption. In the strong absorption model the magnitude of $e^{i\chi_0}$ is zero for small b_0 and rises sharply to unity at the nuclear radius R. The l, m component density matrix $\rho_{fi,lm}$, on the other hand, drop off rapidly beyond this value of b_0, so that the b_0 integrand peaks at R and one can approximate $\mathscr{T}_{fi}^{(\text{dir})}(lm)$ by

$$\mathscr{T}_{fi}^{(\text{dir})}(lm) \sim P_{lm}(0)J_m(k_f R\sin\theta) \tag{4.20}$$

Thus, for a given angular momentum transfer l, $\mathscr{T}_{fi}^{(\text{dir})}(l)$ will be a linear combination of $J_0, J_2, \ldots, J_l$ if l is even and $J_1, J_3, \ldots, J_l$ if l is odd. For large

values of $k_f R \sin\theta$,

$$J_m(k_f R \sin\theta) \to \sqrt{\frac{2}{\pi k_f R \sin\theta}} \cos\left(k_f R \sin\theta - \frac{\pi}{4} - \frac{m\pi}{2}\right)$$

$$\to \sqrt{\frac{2}{\pi k_f R \sin\theta}} (-)^{m/2} \cos\left(k_f R \sin\theta - \frac{\pi}{4}\right) \qquad m \text{ even}$$

$$\to \sqrt{\frac{2}{\pi k_f R \sin\theta}} (-)^{(m-1)/2} \sin\left(k_f R \sin\theta - \frac{\pi}{4}\right) \qquad m \text{ odd}$$

Hence, away from the forward direction, the even l angular momentum transfer reaction angular distribution will be 180° out of phase with the angular distribution for the odd-l case. In the same approximation [see (II.5.25a) the elastic scattering angular distribution is proportional to $J_1(kR\sin\theta)/\sin\theta$, in phase with the l-odd inelastic angular distribution. This set of phase relations are known as *Blair's phase rule.* The agreement of this with appropriate experiments is excellent, as can be seen from Fig. 4.1. However, as one can also see, the theoretical curves fall much less sharply than experiment.

The result is sensitive to the sharp-cutoff, strong absorption model leading to (4.20), as can be seen if we use a specific model for $\rho_{fi,lm}$. Let

$$\rho_{fi,lm} \sim r^{2\bar{l}} e^{-\mu r^2}$$

where

$$\bar{l} = \tfrac{1}{2}(l_f + l_i)$$

Moreover,‡ let $e^{i\chi}$ be

$$e^{i\chi} = 1 - e^{-\gamma b_0^2} \tag{4.21}$$

Inserting these forms into (4.19), taking $m = 0$, and considering only the b_0 integration yields the following integral for consideration:

$$I_0 = \int_0^\infty db_0\, b_0^{2\bar{l}+1} (1 - e^{-\gamma b_0^2}) e^{-\mu b_0^2} J_0(k_f b_0 \sin\theta)$$

This integral can be evaluated in closed form when $\bar{l}$ is an integer:

$$I_0 = \frac{1}{2}\Gamma(\bar{l}+1)\left[\frac{e^{-k_f^2 \sin^2\theta/4\mu}}{\mu^{\bar{l}+1}} P_{\bar{l}+1}\left(\frac{k_f^2 \sin^2\theta}{4\mu}\right) - \frac{e^{-k_f^2 \sin^2\theta/4(\mu+\gamma)}}{(\mu+\gamma)^{\bar{l}+1}} P_{\bar{l}+1}\left(\frac{k_f^2 \sin^2\theta}{4(\mu+\gamma)}\right)\right] \tag{4.22}$$

‡This is a simplified version of the form used by Lee and McManus (67).

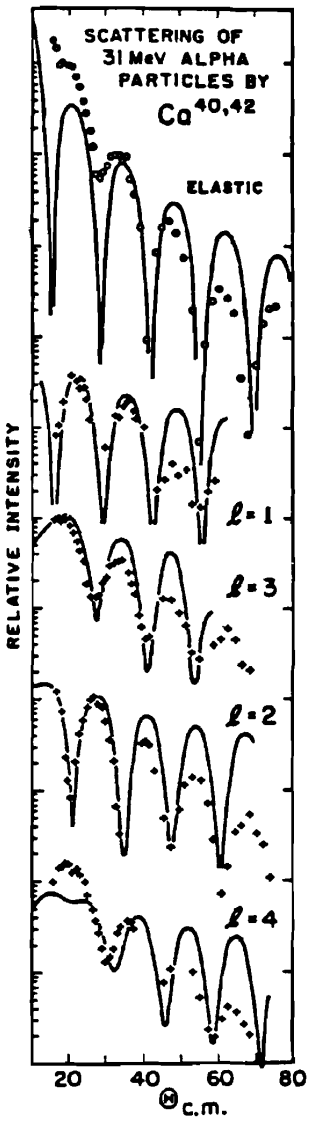

FIG. 4.1. Comparison of the Blair theory with experimental data for the elastic and inelastic scattering of 31-MeV α-particles by ^{40,42}Ca. The elastic and $l = 1$ data for ^{40}Ca, all others are for ^{42}Ca. [From Austern (70).]

where $p_{\bar{l}+1}$ is a polynomial of order $\bar{l}+1$ in the variable indicated. Compared to (4.20), the new feature is the exponential decrease $[\times (k_f^2 \sin\theta/4\mu)^{\bar{l}+1}]$ with increasing scattering angle, as required by the experimental data. Comparison with the data indicates that the experimental situation lies between assumption (4.21) and that leading to (4.20).

At sufficiently small angles,

$$\mathcal{T}_{fi}^{(\mathrm{dir})}(lm) \sim \sin^{|m|}\theta \tag{4.23}$$

so that for even l, the dominant term is the J_0 one, whereas for odd l, it is J_1. Thus the angular momentum transferred is approximately perpendicular to the scattering plane.

A. Diffraction

The oscillating angular distributions are very similar to those that prevail in the diffractive scattering of short-wavelength sound and electromagnetic waves by absorbing obstacles. In these classical cases, it can be shown [see Morse and Feshbach (53, p. 1552)] that the scattering in the forward direction is given by the radiation from the shadowed surface of the obstacle. The illumination on that side is taken to be zero, $\psi = 0$, so that the scattered wave $\psi_s = \psi - \psi_i$ on the surface is just equal and opposite to the incident wave, ψ_i, evaluated in the surface. This classical case is developed for elastic scattering. In the discussion that follows we extend the diffractive analysis to quantum-mechanical inelastic scattering.

This development focuses on the projectile wave functions. The dependence on the target nuclear coordinates is carried along. The final expression is then an operator whose matrix element with respect to the initial Ψ_i and final Ψ_f, the target nuclear wave functions, yields the transition matrix for direct inelastic scattering. The full Hamiltonian is used:

$$(E - T_0 - H_N - V^{\text{opt}})\phi = 0 \tag{4.24}$$

where H_N is the Hamiltonian for the target nucleus, T_0 the projectile kinetic energy operator, and V^{opt} the full many-channel optical potential. The target nuclear variables in both H_N and V^{opt}, and therefore in ϕ, are temporarily to be regarded as constants. We shall replace H_N by E_i for $\phi = \phi_i$ and similarly for ϕ_f. This is known as the *adiabatic approximation*. The equation for $\mathcal{T}_{fi}^{(\text{dir})}$ can then be written as

$$\mathcal{T}_{fi}^{(\text{dir})} = \langle \Psi_f | \varphi_f^{(-)} V^{\text{opt}} \phi_i^{(+)} | \Psi_i \rangle \tag{4.25}$$

Substituting for $V^{\text{opt}}\phi_i^{(+)}$ from (4.24) leads to

$$\mathcal{T}_{fi}^{(\text{dir})} = \langle \Psi_f | \varphi_f^{(-)*} (E - E_i - T_0) \phi_i^{(+)} | \Psi_i \rangle$$

But $\varphi_f^{(-)}\Psi_f$ satisfies (4.24) in the absence of V^{opt}, so that

$$(E - T_0 - H_N)\varphi_f^{(-)} = (E - T_0 - E_f)\varphi_f^{(-)} = 0$$

that is, $\phi_f^{(-)}$ is a plane wave. Replacing E, then, by $T_0 + E_f$ yields

$$\mathcal{T}_{fi}^{(\text{dir})} = \langle \Psi_f | (T_0 \varphi_f^*)\phi_i^{(+)} - \varphi_f^* (T_0 \phi_i^{(+)}) + (E_f - E_i)\varphi_f^* \phi_i^{(+)} | \Psi_i \rangle$$

The last term vanishes because of orthogonality, so that

$$\mathcal{T}_{fi}^{(\mathrm{dir})} = \langle \Psi_f | M | \Psi_i \rangle \tag{4.26}$$

where

$$M \equiv -\frac{\hbar^2}{2\mu} \int d\mathbf{r}_0 [\varphi_f^* \nabla_0^2 \phi_i^{(+)} - (\nabla_0^2 \varphi_f^*) \phi_i^{(+)}] \tag{4.27}$$

M is an operator in target nuclear space because of the dependence of ϕ_i on target nuclear variables such as the radius. Assuming that ρ_{fi} falls off sharply beyond the "nuclear radius", R, the integral in (4.27) should be evaluated within the nuclear volume. Writing first

$$\phi_i^{(+)} = e^{i\mathbf{k}_i \cdot \mathbf{r}} + \phi_{\mathrm{scatt}}$$

so that for $k_f \approx k_i$

$$M = -\frac{\hbar^2}{2\mu} \int d\mathbf{r}_0 [\varphi_f^* \nabla_0^2 \phi_{\mathrm{scatt}} - (\nabla_0^2 \varphi_f^*) \phi_{\mathrm{scatt}}]$$

and using Green's theorem yields

$$M = -\frac{\hbar^2}{2\mu} \int dS \mathbf{n}_0 \cdot [\varphi_f^* \nabla_0 \phi_{\mathrm{scatt}} - (\nabla_0 \varphi_f^*) \phi_{\mathrm{scatt}}]$$

where $\mathbf{n}_0$ is the outward-pointing normal to the surface. We can break up this surface integral into two parts; the front half of the nuclear volume in the shadow and the back illuminated portion. The front half leads to the diffraction scattering. On that front surface, ϕ_{scatt} scattering equals $-e^{i\mathbf{k}_i \cdot \mathbf{r}}$, so that the total ϕ is zero. Hence

$$M_{\mathrm{diff}} = -\frac{\hbar^2}{2\mu} \int_{\mathrm{front}} dS_0 \mathbf{n}_0 \cdot [e^{-i\mathbf{k}_f \cdot \mathbf{r}_0} \nabla_0 e^{i\mathbf{k}_i \cdot \mathbf{r}_0} - \nabla_0 (e^{-i\mathbf{k}_f \cdot \mathbf{r}_0}) e^{i\mathbf{k}_i \cdot \mathbf{r}_0}]$$

It can be shown‡ [Morse and Feshbach (53, p. 1552)] that the surface integral can be reduced to a line integral on the edge of the shadowed surface. (If the scatterer is spherical, this argument is not necessary, as the surface integration over the spherical surface can be readily performed.) As a consequence, any

‡The transformation is known as the Maggi transformation (Copson). A Simple proof [Morse and Feshbach (53, p. 1552)] notes that the quantity in brackets is divergenceless if $k_f \approx k_i$, already assumed. It may then be written as the curl of a vector and by Stokes' theorem reduced to a line integral.

surface will do. We shall use a disk bounded by the surface edge, assuming that the edge is a circle perpendicular to the incident projectile direction. In that event

$$M_{\text{diff}} = -i(k_i + k_f \cos\theta)\frac{\hbar^2}{2\mu}\int_0^{2\pi} d\phi \int_0^B b\, db\, e^{-ik_f b \sin\theta\cos\phi}$$

$$= -\frac{ik\hbar^2}{\mu}\int_0^{\pi} d\phi \int_0^B b\, db\, e^{-ik_f b\sin\theta\cos\phi} \tag{4.28}$$

Note. It is possible to improve on this result by using the high-energy approximation for ϕ_{sc}. From (4.11),

$$\phi_{\text{sc}}^* = e^{-i\mathbf{k}_f\cdot\mathbf{r}_0}\left[e^{-i(\mu/\hbar^2 k_f)\int_{z_0}^{\infty} V_{\text{opt}}(\mathbf{b}_0,z)dz} - 1\right]$$

to be evaluated on the shadowed surface, that is, at $z_0 = (R^2 - b^2)^{1/2}$. For strong absorption the first term is negligible.

To illustrate the use of this formula, consider the case for which the disk radius B is given by

$$B = R + \sum \xi_{lm} Y_{lm}^*\left(\frac{\pi}{2}, \phi\right) \tag{4.29}$$

where ξ_{lm} are operators in the target nuclear space. Such an expansion is employed in the Bohr–Mottelson picture when the target is a spherical vibrator [see Chapter VI) in deShalit and Feshbach (74)]. The disk of integration is circular, passing through the center of the nucleus. Hence θ in Y_{lm} is $\pi/2$. Then to first order in ξ_{lm},

$$M_{\text{diff}} = \frac{-ik\hbar^2}{\mu}\int_0^{2\pi} d\phi \left\{\int_0^R e^{-ik_f b\sin\theta\cos\phi} b\, db + R\sum \xi_{lm}(-)^m\left[\frac{2l+1}{4\pi}\frac{(l-|m|)!}{l+|m|!}\right]^{1/2}\right.$$

$$\left.\times P_{lm}(0)e^{im\phi}e^{-ik_f R\sin\theta\cos\phi}\right\}$$

$$= -\frac{2\pi ik\hbar^2}{\mu}\left[\int_0^R J_0(k_f b\sin\theta) b\, db + R\sum_{lm}\xi_{lm}\left[\frac{2l+1}{4\pi}\frac{(l-|m|)!}{(l+|m|)!}\right]^{1/2}\right.$$

$$\left.\times P_{lm}(0)(-)^{1/2(l-m)} J_m(k_f R\sin\theta)\right] \tag{4.30}$$

Matrix elements of M_{diff} must now be taken between initial and final nuclear states. The first term in (4.30), under the assumption that the target nuclear density is constant over the nuclear volume, yields the elastic scattering

amplitude

$$M_{\text{diff}}^{(\text{el})} = -\frac{2\pi i\hbar^2 R}{\mu \sin\theta} J_1(k_f R \sin\theta)$$

and the differential elastic cross section quoted earlier,

$$\left(\frac{d\sigma}{d\Omega}\right)_{\text{diff}}^{(\text{el})} = R^2 \frac{|J_1(k_f R \sin\theta)|^2}{\sin^2\theta} \tag{4.31}$$

The inelastic cross section is given by

$$\left(\frac{d\sigma}{d\Omega}\right)_{\text{diff}}^{(\text{inel})} = (k^2R^2)\sum_{lm} |\langle \Psi_f | \xi_{lm} | \Psi_i \rangle|^2 \left[\frac{2l+1}{4\pi}\frac{(l-|m|)!}{(l+|m|)!}(P_{lm}(0))^2\right] |J_m(k_f R \sin\theta)|^2 \tag{4.32}$$

One can verify that the Blair phase rule is a consequence of (4.32) since $P_{lm}(0)$ differs from zero only for $l+m$ even.

To finish the calculation we need to specify the properties of the target nucleus as described by Ψ_f and Ψ_i and the quantities ξ_{lm} that follows from the dynamics upon which (4.29) is based. The nuclear model that can readily be inserted into this theory is the model of Bohr and Mottelson (62). We consider two situations:

Vibrational Nuclei [see deShalit and Feshbach (74, p. 471 et seq.)]. In this case the target nucleus is a vibrator with sets of equally spaced levels. The spacing of each is given by $\hbar w_l$, where w_l can be expressed in terms of a mass parameter B_l and a force constant C_l:

$$w_l = \sqrt{\frac{C_l}{B_l}}$$

The excited states can conveniently be thought of as consisting of the ground state plus a number of phonons. Each of the phonons carries an energy $\hbar w_l$, and angular momentum l_1 with a z component of m. In terms of this model [see deShalit and Feshbach (74, p. 473)]

$$\xi_{lm} = \left(\frac{\hbar}{2B_l w_l}\right)^{1/2} b_{lm}^{\dagger} \tag{4.33}$$

where $b_{lm}^{\dagger}$ is a boson creation operator, creating a phonon of the lm type. If the final state involves a one-phonon excitation,

$$\Psi_f = b_{lm}^{\dagger} \Psi_i$$

so that

$$|\langle \Psi_f | \xi_{lm} | \Psi_i \rangle|^2 = \frac{\hbar}{2B_l w_l} = \frac{\hbar w_l}{2C_l} \tag{4.34}$$

independent of m. Therefore,

$$\left(\frac{d\sigma}{d\Omega}\right)_{\text{diff}}^{(\text{inel})} = k^2 R^2 \sum_l \frac{\hbar w_l}{2C_l} \cdot \frac{2l+1}{4\pi} \left\{ \sum_m \frac{(l-|m|)!}{(l+|m|)!} [P_{lm}(0)]^2 |J_m(k_f R \sin\theta)|^2 \right\} \tag{4.35}$$

From its derivation it is clear that $\hbar w_l / 2C_l$ is a measure of the amplitude of oscillation away from the spherical equilibrium shape.

The analysis above can readily be extended to multiphonon states by including higher-order terms in the evaluation of M_{diff} of (4.30). The Blair phase rule in its simplest form will not be valid if both single phonon and multiphonon excitation are equally important. Note that the effects of the Coulomb interaction, which can be of great importance, have been omitted in this discussion.

Deformed Nuclei. We begin with the more complex expression for the deformation given on page 471 of deShalit and Feshbach (74), which we rewrite as

$$\delta R = \sum_{lm'} \alpha_{lm'} Y^*_{lm'}(\theta' \phi') \tag{4.36}$$

The volume-conserving term has been omitted in (4.36), as it will not play a role in the excitations discussed below. The angles, (θ', ϕ'), are in the body-fixed system, so that the expression in (4.36) needs to be transformed to the scattering frame [see (A.2.26) in the Appendix of deShalit and Feshbach (74)] as follows:

$$\delta R = \sum \alpha_{lm'} D^{(l)*}_{mm'}(\theta_k) Y^*_{lm}(\theta, \phi) \tag{4.37}$$

where θ_k are the collective coordinates. Therefore,

$$\xi_{lm} = \sum_{m'} \alpha_{lm'} D^{(l)}_{mm'}(\theta_k)$$

The matrix element in (4.32) becomes

$$\langle \Psi_f | \xi_{lm} | \Psi_i \rangle = \sum_{m'} \langle \Psi_f | D^{(l)*}_{mm'}(\theta_k) \alpha_{lm'} | \Psi_i \rangle$$

where the nuclear wave functions are given by (VI.4.9) in deShalit and Feshbach (74). The value of this matrix element is given by (VI.6.9) in deShalit and Feshbach (74):

$$\langle I_f K_f M_f | \alpha_{lm'} D^{(l)*}_{m'm} | I_i K_i M_i \rangle$$
$$= (-)^{M-K} \sqrt{(2I_i+1)(2I_f+1)} \begin{pmatrix} I_f & l & I_i \\ -M_f & m & M_i \end{pmatrix}$$
$$\times \left[\begin{pmatrix} I_f & l & I_i \\ -K_f & m' & K_i \end{pmatrix} \langle K_f | \alpha_{lm'} | K_i \rangle + (-)^{I_i} \right.$$
$$\left. \times \begin{pmatrix} I_f & l & I_i \\ -K_f & m' & -K_i \end{pmatrix} \langle K_f | \alpha_{lm'} | -K_i \rangle \right] \tag{4.38}$$

where the quantum numbers I_i, K_i and M_i specify the initial rotational state of the target nucleus, I_f, and so on, specify the final state. The matrix elements of α_{lm} are taken with respect to the intrinsic wave functions describing the rotational nucleus.

To obtain the cross section we must take the square of the magnitude of $\langle \Psi_f | \xi_{lm} | \Psi_i \rangle$, sum over M_f, and average over M_i. We need consider only the factors outside the brackets in (4.38), since they contain the entire m dependence. We recall that

$$\frac{1}{2I_i+1} \sum_{M_i, M_f} (2I_i+1)(2I_f+1) \begin{pmatrix} I_f & l & I_i \\ -M_f & m & M_i \end{pmatrix}^2 = \frac{2I_f+1}{2l+1} \tag{4.39}$$

Note the important result that any dependence on M disappears upon summing over final states and averaging over initial states. As a consequence, in (4.32) one can remove the matrix element of ξ_{lm} from the sum on m:

$$\left(\frac{d\sigma}{d\Omega} \right)^{(\text{inel})}_{\text{diff}} = k^2 R^2 \sum_l \frac{2l+1}{4\pi} |\langle \Psi_f \| \xi_l \| \Psi_i \rangle|^2 \left\{ \sum_m \frac{(l-|m|)!}{(l+|m|)!} |P_{lm}(0)|^2 |J_m(k_f R \sin\theta|^2 \right\} \tag{4.40}$$

We see that the excitation of rotational level leads to same angular distribution as the excitation of a vibrational level for each multiple given by the expression within the braces in (4.40) and (4.35). The weighting of each multipole will differ. For the rotational case [see (VI.7.1) in deShalit and Feshbach (74)],

$$|\langle \Psi_f \| \xi_l \| \Psi_i \rangle| \approx \beta_l R$$

A more detailed microscopic theory would need the more detailed statement for (4.38).

B. Adiabatic Approximation and Elastic Scattering

The calculations described in Section 4.A are examples of the use of the adiabatic approximation in which the scattering of the projectile is determined in terms

of properties of the target nucleus that are considered to remain fixed during the encounter. This is a reasonable description if the passage time for the projectile is small compared to the periods of the characteristic modes of motion of the nucleus. The passage time τ_p is approximately given by

$$\tau_p \sim \frac{R}{v} \sim \frac{r_0 A^{1/3}}{c}\left[\frac{mc^2}{2(V+E)}\right]^{1/2}$$

where V is a measure of the interaction energy given by the real part of the depth of the central components of the optical potential. It can readily be shown that the characteristic times associated with rotation and vibration are much longer than the passage time. However, τ_p is much shorter than the characteristic times associated with single-particle motion only if the energy E is sufficiently high.

When the adiabatic approximation is valid, one can consider the projectile scattering to occur in the presence of a fixed configuration of nucleons of the nucleus. The resulting projectile transition matrix, $\mathscr{T}_p$, is then a function of the target nucleon coordinates. Its matrix element with respect to the initial and final nuclear states gives an approximation for the transition matrix for the process.

To be more specific, the many-body Schrödinger equation describing the projectile–target interaction is

$$(E - H_t - V_{tp} - T_p)\Phi = 0 \tag{4.41}$$

where H_t is the target nuclear Hamiltonian, V_{tp} the interaction of the projectile with the target nucleons, and T_p the projectile kinetic energy. Centre-of-mass frame variables are assumed. If we now consider the target nucleons to be fixed, (4.41) becomes a single-channel equation whose transition matrix is $\mathscr{T}_p(\mathbf{r}_1, \mathbf{r}_2, \ldots; \mathbf{k}_f, \mathbf{k}_i)$, where $\mathbf{r}_i$ are the coordinates of the target nucleons and $\mathbf{k}_f$ and $\mathbf{k}_i$ are the final and initial momenta, respectively. Only when the scattering is elastic will $k_f = k_i$. The transition matrix for the nuclear transition $\Psi_i \to \Psi_f$ in this approximation is given by

$$\mathscr{T}_{fi} = \langle \Psi_f | \mathscr{T}_p(\mathbf{r}_1, \mathbf{r}_2, \ldots)\Psi_i \rangle \tag{4.42}$$

This adiabatic approximation is an essential part of the multiple scattering formalism of Chapter II. We now wish to discuss its use when collective coordinates are the primary nuclear dynamical variables involved in the collision. In that case we go to the energy averaged optical model as described in Chapter III, with the consequence that (4.41) is replaced by

$$(E - T_p - V_{\text{opt}})\chi = 0 \tag{4.43}$$

where the collective coordinates such as the nuclear radius appear as a parameter

in V_{opt}. The transition matrix corresponding to (4.43) will then be a function of the collective coordinates, which we shall symbolize by R, so that

$$\mathcal{T}_p = \mathcal{T}_p(R; \mathbf{k}_f, \mathbf{k}_i)$$

The transition matrix element for the transition is given by

$$\mathcal{T}_{fi} = \langle \Psi_f | \mathcal{T}_p(R; \mathbf{k}_f, \mathbf{k}_i) \Psi_i \rangle \tag{4.44}$$

The Austern–Blair result [Austern (70, pp. 278–280)] is a perturbation result in which R is assumed to be close to a fixed value R_0. When the perturbation involves the projectile coordinates, it is convenient to write $\mathcal{T}_p$ as follows:

$$\mathcal{T}_p(R; \mathbf{k}_f, \mathbf{k}_i) = \iint e^{-i\mathbf{k}_f \cdot \mathbf{r}} \mathcal{T}_p(R; \mathbf{r}, \mathbf{r}_0) e^{i\mathbf{k}_i \cdot \mathbf{r}_0} d\mathbf{r}\, d\mathbf{r}_0 \tag{4.45}$$

Perturbatively, R is given by

$$R = R_0 + \delta R$$

so that

$$\mathcal{T}_p(R; \mathbf{k}_f, \mathbf{k}_i) = \mathcal{T}_p(R_0; \mathbf{k}_f, \mathbf{k}_i) + \delta \mathcal{T}_p$$

where

$$\begin{aligned} \delta \mathcal{T}_p &= \frac{\partial}{\partial R_0} \iint e^{-i\mathbf{k}_f \cdot \mathbf{r}} \mathcal{T}_p(R_0, \mathbf{r}, \mathbf{r}_0) \delta R e^{i\mathbf{k}_i \cdot \mathbf{r}_0} d\mathbf{r}\, d\mathbf{r}_0 \\ &= \frac{\partial}{\partial R_0} \int e^{-i\mathbf{k}_f \cdot \mathbf{r}} \delta R V(\mathbf{r}, R_0) \psi_i^{(+)}(\mathbf{k}_i, \mathbf{r}; R_0)\, d\mathbf{r} \end{aligned} \tag{4.46}$$

Austern and Blair proceed by expanding $\psi_i^{(+)}$ in a partial wave series and evaluating the integrals term by term. This is left as a problem for the reader.

In the case that we are dealing with, surface reactions, it is possible to develop expression (4.46) further without resorting to a partial wave expansion. Let us then assume that

$$\delta R = \delta R(\xi; r, \theta, \phi)$$

where, as before, ξ represents a set of operators operating on the nuclear wave functions $\Psi_{f,i}$. Then (4.46) becomes

$$\delta \mathcal{T}_p = \frac{\partial}{\partial R_0} \int d\mathbf{r} e^{-i\mathbf{k}_f \cdot \mathbf{r}} \delta R(\xi; r, \theta, \phi) V(r, R_0) \psi_i^{(+)}$$

We now make use of the fact that δR can be written as a function of $\cos\theta$ and

$e^{\pm i\phi}$ and these can be expressed as differential operators as follows:

$$\cos\theta e^{-i\mathbf{k}_f\cdot\mathbf{r}} = i\frac{\mathbf{k}_i}{k_i r}\cdot\nabla_{k_f} e^{-i\mathbf{k}_f\cdot\mathbf{r}}$$

where the z direction has been chosen along $\mathbf{k}_i$. (It is, of course, possible to make a choice that will result in a more symmetric final expression.) Second,

$$e^{i\phi}e^{-i\mathbf{k}_f\cdot\mathbf{r}} = \frac{i}{r}\left(\frac{\partial}{\partial k_{f_x}} + i\frac{\partial}{\partial k_{f_y}}\right)e^{-i\mathbf{k}_f\cdot\mathbf{r}}$$

Hence

$$\delta\mathcal{T}_p = \frac{\partial}{\partial R_0}\left\{\delta R\left[\xi; R_0, \frac{i\mathbf{k}_i\cdot\nabla_{k_f}}{k_i R_0}, \frac{i}{R_0}\left(\frac{\partial}{\partial k_{f_x}} + i\frac{\partial}{\partial k_{f_y}}\right)\right]\mathcal{T}_p(R_0; \mathbf{k}_f, \mathbf{k}_i)\right\} \quad (4.47)$$

where r has been replaced by R_0 because of the surface reaction assumptions and $\delta R[\cdot]$ is defined by

$$\delta R[\xi; \cos\theta, e^{i\phi}] \equiv \delta R(\xi; \theta, \phi)$$

The net transition matrix given by (4.44) is obtained from (4.47). The quantity $\mathcal{T}_p(R_0; \mathbf{k}_f, \mathbf{k}_i)$ is not the elastic scattering amplitude since $k_f \neq k_i$. At sufficiently small angles (where in any event the DWA is most reliable) and for sufficiently small energy losses, E_f and E_i, and therefore k_f and k_i, can be replaced by some average value. Another approximation suggested by Hahne (67, 68) [see also Austern (70, p. 280)] is appropriate when the Austern–Blair partial wave analysis is used. For the formulation above we have only the Schwarz inequality result,

$$|\mathcal{T}_p(R_0; \mathbf{k}_f, \mathbf{k}_i)| \leqslant |\mathcal{T}_p(R_0, \mathbf{k}_f, \mathbf{k}_f)\mathcal{T}_p(R_0, \mathbf{k}_i, \mathbf{k}_i)|^{1/2} \quad (4.48)$$

This implies that the geometric mean may be adequate but useful at best only for a low order of differentiation in (4.47).

C. Formal DWA

The numerical evaluation of the direct transition matrix element given by (4.8) and (4.9) for a given model of the nuclear structure has been studied extensively, and a number of computer codes for this purpose have been developed and widely used. In this section we carry out the kinematic reductions to the point where numerical methods must be invoked. To illustrate the methods involved, we consider the somewhat simplified case for which the optical potential defining the distorted wave functions $\phi_{f,i}$ is spin and isospin independent, as is appropriate when the exciting projectile is an α-particle.

Consider the form factor $\mathcal{V}_{fi}(\mathbf{r}_0)$ defined by (4.9). Because of the antisymmetry of the wave functions $\Psi_{f,i}$, (4.9) can be rewritten as

$$\mathcal{V}_{fi}(\mathbf{r}_0) = A\langle J_f M_f | v(\mathbf{r}_0, \mathbf{r}_1) | J_i M_i \rangle \tag{4.49}$$

where A is the mass number of the target nucleus and $J_{f,i}$ and $M_{f,i}$ are the angular momentum quantum numbers for the nuclear states involved. Recall that $\mathbf{r}_0$ is the projectile coordinate. The interaction can be expanded in a *multipole series*:

$$v(\mathbf{r}_0, \mathbf{r}_1) = \sum_{l,\mu} v_l(r_0, r_1)(-)^l T^{(l)}_{-\mu}(0) T^{(l)}_{\mu}(1)$$

where $T^{(l)}$ is a spherical tensor that depends on spherical angular coordinates and spin.‡ Taking the matrix element in (4.49) and using the Wigner–Eckart theorem, one obtains

$$\mathcal{V}_{fi} = A\sum_{l\mu}(-)^{J_f - M_f}\begin{pmatrix} J_f & l & J_i \\ -M_f & \mu & M_i \end{pmatrix}(J_f \| v_l(r_0, r_1) T^{(l)}(1) \| J_i)(-)^l T^{(l)}_{\mu} \tag{4.50}$$

where the reduced matrix element involves an integration over $\mathbf{r}_1$.

From the properties of the $3-j$ symbol it follows that the angular momentum transferred equals l:

$$\mathbf{J}_f = \mathbf{J}_i + \mathbf{l}$$

If v is spin independent, so that $T^{(l)}_{\mu} \sim Y_{l\mu}$, the transferred parity is $(-)^l$. If $J_i = 0^+$, a spin independent v_l will excite only states of *natural parity*, that is, states with spin l and parity $(-)^l$, such as 0^+, 1^-, 2^+, and so on. When spin dependence is included, $T^{(l)}_{\mu}$ can include as well

$$[i^k Y_k \otimes \boldsymbol{\sigma}]^{(l)}_m = \sum_{\kappa_1 \kappa_2} (k\kappa_1, 1\kappa_2 | lm)(i^k Y_{k\kappa_1})\sigma_{\kappa_2} \tag{4.51}$$

To indicate the composite character of such a term, the notation $T^{(k\sigma)l}_m$ is often used. We shall for the most part not use this more detailed notation in this section. The presence of such terms as well as spin-dependent terms will permit transitions in which for $J_i = 0^+$, states of unnatural purity can be excited.

The reduced matrix element in (4.50) is directly dependent on the nondigonal

‡If there is no spin dependence,

$$v(\mathbf{r}_0, \mathbf{r}_1) = \sum_{l,m} v_l(r_0, r_1)\frac{4\pi}{2l+1}(i^l Y_{lm}(\hat{\mathbf{r}}_0))^*(i^l Y_{lm}(\hat{\mathbf{r}}_1))$$

density matrix, ρ_{fi}. The matrix element can be determined from

$$\begin{aligned}
&\begin{pmatrix} J_f & l & J_i \\ -J_f & m & J_i \end{pmatrix}(J_f \| v_l(r_0, r_1) T^{(l)} \| J_i) \\
&= \int \Psi_f^*(J_f, M_f = J_f; \mathbf{r}_1, \mathbf{r}_2, \ldots) v_l(r_0, r_1) T_m^{(l)}(\hat{\mathbf{r}}_1) \Psi_i(J_i, M_i = J_i; \mathbf{r}_1 \mathbf{r}_2 \cdots) \, d\mathbf{r}_1 \, d\mathbf{r}_2 \cdots \\
&= \int \rho_{fi}(\mathbf{r}_1) v_l(r_0, r_1) T_m^{(l)}(\hat{\mathbf{r}}_1) \, d\mathbf{r}_1
\end{aligned} \tag{4.52}$$

where

$$\rho_{fi} \equiv \int \Psi_f^*(J_f, M_f = J_f; \mathbf{r}_1, \mathbf{r}_2, \ldots) \Psi_i(J_i, M_i = J_i; \mathbf{r}_1, \mathbf{r}_2, \ldots) \, d\mathbf{r}_2 \cdots$$

As a probe of nuclear structure, inelastic scattering thus provides information on ρ_{fi}. Other probes (e.g., inelastic electron and pion scattering) act similarly, however weighting ρ_{fi} in different ways, depending on the excitation interaction responsible. That is, the operator, $v_l(r_0, r_1)$ in (4.26) depends on the probe involved, but ρ_{fi} does not change. By using a variety of probes it is possible to determine the space-symmetry structure of both ρ_{fi} and the interactions involved. It should be emphasized that this conclusion relies on the validity of the DWA.

We now insert multipole series (4.50) into the expression for the transition matrix $\mathcal{T}_{fi}$:

$$\mathcal{T}_{fi} = \langle \phi_f^{(-)} | \mathcal{V}_{fi} | \phi_i^{(+)} \rangle \tag{4.53}$$

where $\phi_i^{(+,-)}$ are solutions of the optical model Schrödinger equation with indicated outgoing and incoming boundary conditions. Expanding these in a partial wave series (the assumption of spin independence for reason of simplicity is made at this point) yields

$$\begin{aligned}
\phi_i^{(+)} &= \sum (2l_i + 1) i^{l_i} P_{l_i}(\hat{\mathbf{k}}_i \cdot \hat{\mathbf{r}}) e^{i\delta_{l_i}} \frac{u_{l_i}(r)}{k_i r} \\
&= \sum \sqrt{4\pi(2l_i + 1)} \mathscr{Y}_{l_i 0}(\hat{\mathbf{k}}_i \cdot \hat{\mathbf{r}}) e^{i\delta_{l_i}} \frac{u_{l_i}(r)}{k_i r}
\end{aligned} \tag{4.54}$$

The complex conjugate $\phi_f^{(-)*}$ is

$$\phi_f^{(-)*} = \sum (2l_f + 1) i^{l_f} P_{l_f}(-\hat{\mathbf{k}}_f \cdot \hat{\mathbf{r}}) e^{i\delta_{l_f}} \frac{u_{l_f}(r)}{k_f r}$$

Using the properties of P_{l_f}, such as the addition theorem, we obtain

$$\phi_f^{(-)*} = 4\pi \sum \mathcal{Y}^*_{l_f,m_f}(\hat{\mathbf{k}}_i \cdot \hat{\mathbf{r}}) Y_{l_f,m_f}(\hat{\mathbf{k}}_i \cdot \hat{\mathbf{k}}_f) e^{i\delta_{l_f}} \frac{u_{l_f}(r)}{k_f r} \tag{4.55}$$

Combining these results with (4.50) it is an easy matter to obtain $\mathcal{T}_{fi}$:

$$\mathcal{T}_{fi} = (4\pi)^{3/2} \sum (-)^{J_f - M_f + m + l_f - m_f} \begin{pmatrix} J_f & l & J_i \\ -M_f & m & M_i \end{pmatrix} \begin{pmatrix} l_f & l & l_i \\ -m_f & -m & 0 \end{pmatrix} \sqrt{2l_i + 1}$$
$$\times I^{(l)}(l_f J_f; l_i J_i) e^{i(\delta_{l_i} + \delta_{l_f})} Y_{l_f,m_f}(\hat{\mathbf{k}}_i \cdot \hat{\mathbf{k}}_f) \tag{4.56}$$

where $I^{(l)}$ is given by

$$I^{(l)}(l_f J_f; l_i J_i) = \frac{4\pi A}{k_f k_i} (J_f l_f \| T^{(l)}(0) v_l(r_0, r_1) T^{(l)}(1) \| J_i l_i) \tag{4.57}$$

We now must average the square magnitude of $\mathcal{T}_{fi}$ over M_i and sum over M_f. One obtains, using the $3-j$ normalization [(A.2.70) in the Appendix of deShalit and Feshbach (74)],

$$\frac{1}{2J_i + 1} \sum_{M_i, M_f} |\mathcal{T}_{fi}|^2 = (4\pi)^3 \sum \frac{\sqrt{(2l_i + 1)(2l_i' + 1)}}{(2l + 1)(2J_i + 1)} (-)^{l_f + l_f' - m_f - m_f'}$$
$$\times \begin{pmatrix} l_f & l & l_i \\ -m_f & -m & 0 \end{pmatrix} \begin{pmatrix} l_f' & l & l_i' \\ -m_f' & -m & 0 \end{pmatrix} Y_{l_f m_f} Y^*_{l_f' m_f'}$$
$$\times e^{i(\delta_{l_i} + \delta_{l_f} - \delta^*_{l_i'} - \delta^*_{l_f'})} I^{(l)}(l_f J_f; l_i J_i) I^{(l)*}(l_f' J_f; l_i' J_i) \tag{4.58}$$

This can be written as a sum over multipole order as follows:

$$\frac{1}{2J_i + 1} \sum_{M_i, M_f} |\mathcal{T}_{fi}|^2 = (4\pi)^3 \sum_{l,m} \frac{1}{(2l + 1)(2J_i + 1)} \left| \sum_{l_f, l_i, m_f} (-)^{l_f - m_f} \sqrt{(2l_i + 1)} \right.$$
$$\left. \times \begin{pmatrix} l_f & l & l_i \\ -m_f & -m & 0 \end{pmatrix} Y_{l_f m_f} I^{(l)}(l_f J_f; l_i J_i) e^{i(\delta_{l_i} + \delta_{l_f})} \right|^2 \tag{4.59}$$

a result that is often the most convenient one to use. However, it is possible to carry (4.58) further by expanding the product of the Y's in (A.2.35) of deShalit and Feshbach (74):

$$Y^*_{l_f' m_f'} Y_{l_f, m_f} = (-)^{m_f'} \sum_{\lambda \mu} \sqrt{\frac{(2l_f' + 1)(2l_f + 1)(2\lambda + 1)}{4\pi}}$$
$$\times \begin{pmatrix} l_f' & l_f & \lambda \\ 0 & 0 & 0 \end{pmatrix} \begin{pmatrix} l_f' & l_f & \lambda \\ -m_f' & m_f & \mu \end{pmatrix} Y_{\lambda \mu}$$

The resultant product of $3-j$ symbols can be summed to a $6-j$ symbol using (A.2.93) of deShalit and Feshbach (74). Finally, relating the result to the reduced matrix element of Y_λ gives

$$\frac{1}{2J_i+1}\sum|\mathscr{T}_{fi}|^2=\sum\frac{(-)^{l_f}(2\lambda+1)}{(2J_i+1)(2l+1)}\begin{pmatrix}l'_f & l_f & \lambda\\ 0 & 0 & 0\end{pmatrix}(l_i l l_f\|\sqrt{4\pi}Y_\lambda\|l'_i l l'_f)$$
$$\times e^{i(\delta_{l_f}+\delta_{l_i}-\delta^*_{l'_f}-\delta^*_{l'_i})}I^{(l)}(l_fJ_f;l_iJ_i)I^{(l)*}(l'_fJ_f;l'_iJ_i)P_\lambda(\hat{\mathbf{k}}_f\cdot\hat{\mathbf{k}}_i) \tag{4.60}$$

The cross section is obtained by multiplying this result by $(\mu/2\pi\hbar^2)^2(k_f/k_i)$. The total inelastic cross section $\sigma_T^{(\text{inel})}$ is given by

$$\sigma_T^{(\text{inel})}=\left(\frac{\mu}{2\pi\hbar^2}\right)^2\frac{k_f}{k_i}\sum\frac{1}{(2J_i+1)(2l+1)}|I^{(l)}(l_fJ_f;l_iJ_i)|^2e^{-2Im(\delta_{l_f}+\delta_{l_i})} \tag{4.61}$$

The properties of the reduced matrix element of Y_λ in (4.60) provide most of the kinematic properties of the reaction. It vanishes unless

$$\mathbf{l}_i+\mathbf{l}=\mathbf{l}_f$$
$$\mathbf{l}'_i+\mathbf{l}=\mathbf{l}'_f \tag{4.62a}$$
$$\mathbf{l}_i+\boldsymbol{\lambda}=\mathbf{l}'_i$$
$$\mathbf{l}_f+\boldsymbol{\lambda}=\mathbf{l}'_f \tag{4.62b}$$
$$l'_i+l_i+\lambda=\text{even number}$$
$$l'_f+l'_f+\lambda=\text{even number} \tag{4.62c}$$

where the last equation is a property of the $3-j$ symbol multiplying the reduced matrix element of Y_L. Relations (4.62*a*) show that l is the angular momentum transfer. Equation (4.62*b*) yields the C.N. Yang result on the complexity of the angular distribution, namely that $\lambda<\min(2l_i,2l_f)$. Other properties are present in the $I^{(l)}$ factors that contain the reduced matrix elements of $T^{(l)}$. These will be proportional to [see (A.2.48) in deShalit and Feshbach (74)]

$$(a)\ \begin{pmatrix}J_f & l & J_i\\ 0 & 0 & 0\end{pmatrix}\quad\text{and}\quad(b)\ \begin{pmatrix}l_f & l & l_i\\ 0 & 0 & 0\end{pmatrix} \tag{4.63}$$

The first of these combined with the results (4.59*a*) yields conservation of angular momentum for the reaction

$$\mathbf{J}_i+\mathbf{l}=\mathbf{J}_f$$
$$\mathbf{l}_i+\mathbf{l}=l_f$$

while the evenness of $J_f + l + J_i$ and $l_f + l + l_i$ yields conservation of parity. The dynamics of the reaction is contained in the $I^{(l)}$ factors, as these involve integrations over $v_l(r_0, r_1)$. Note also the exponential factors in (4.60) and (4.61), which explicitly demonstrate the effects of absorption in both the initial and final optical model channels.

Some further insight into the kinematic factors can be obtained for strong absorption in the limit $l_{i,f} \gg 1$. In the case of strong absorption, the contribution to (4.60) comes from a narrow range of l_i and of l_f, so that $l_i \approx l_i'$ and $l_f \approx l_f'$. It therefore becomes a good approximation for the expression appearing in (4.60):

$$\begin{pmatrix} l_f & l_f' & \lambda \\ 0 & 0 & 0 \end{pmatrix} (l_i l l_f \| \sqrt{4\pi} Y_\lambda \| l' l l_f')$$
$$= (-)^{l+\lambda+l_f} \sqrt{(2l_i+1)(2l_i'+1)(2l_f+1)(2l_f'+1)(2\lambda+1)}$$
$$\times \begin{pmatrix} l_f & l_f' & \lambda \\ 0 & 0 & 0 \end{pmatrix} \begin{pmatrix} l_i & l_i' & \lambda \\ 0 & 0 & 0 \end{pmatrix} \begin{Bmatrix} l_i & l_f & l \\ l_f' & l_i' & \lambda \end{Bmatrix} \tag{4.64}$$

to replace l_i and l_i' by an average value, $\bar{l}_i$, and similarly, l_f and l_f' by $\bar{l}_f$. Then, using the result valid for large $\bar{l}_{i,f}$ [Brusaard and Tolhoek (57); Biedenharn (53); Racah (51)], we have

$$\begin{Bmatrix} \bar{l}_i & \bar{l}_f & l \\ \bar{l}_f & \bar{l}_i & \lambda \end{Bmatrix} \simeq \frac{(-)^{l+\bar{l}_i+\bar{l}_f}}{\sqrt{2\bar{l}_i+1)(2\bar{l}_f+1)}} P_\lambda(\cos l(\bar{\mathbf{l}}_i \cdot \bar{\mathbf{l}}_f))$$
$$\cos(l(\bar{\mathbf{l}}_i \cdot \bar{\mathbf{l}}_f)) \equiv \frac{l(l+1) - \bar{l}_i(\bar{l}_i+1) - \bar{l}_f(\bar{l}_f+1)}{2\bar{l}_i\bar{l}_f}$$

so that

$$\begin{pmatrix} l_f & l_f' & \lambda \\ 0 & 0 & 0 \end{pmatrix} (l_i l l_f \| \sqrt{4\pi} Y_\lambda \| l_i' l l_f') \simeq (-)^{\bar{l}_i} \sqrt{(2\bar{l}_i+1)(2\bar{l}_f+1)(2\lambda+1)}$$
$$\times \begin{pmatrix} l_f & l_f' & \lambda \\ 0 & 0 & 0 \end{pmatrix} \begin{pmatrix} l_i & l_i' & \lambda \\ 0 & 0 & 0 \end{pmatrix} P_\lambda(\cos l(\bar{\mathbf{l}}_i \cdot \bar{\mathbf{l}}_f)) \tag{4.65}$$

From the expression for $\cos(\bar{\mathbf{l}}_i \cdot \bar{\mathbf{l}}_f)$, we see that $|P_\lambda|$ achieves a maximum value close to unity when $l = \bar{l}_i \pm \bar{l}_f$, for then the cosine is close to ± 1. The two vectors, the incident angular momentum $\mathbf{l}_i$ and the final $\mathbf{l}_f$, tend to line up, to be parallel or antiparallel, the net sum being equal to the multipole order l. If the multipole order is large (e.g., $J_f \gg 1, J_f \gg J_i$), then either $\bar{l}_f$ or $\bar{l}_i$ or both are large. As we shall see, the matching condition that maximizes the integrals $I^{(l)}$ when the energy of the incident beam is much larger than the excitation energy

yields $l_i \approx l_f$. Under these conditions $l_i \approx l_f \approx l/2$, so that the maximum value of λ will be l, the multipole order. At sufficiently high energy and large multipole order, the angular distribution (4.60) will reflect the multipole order quite directly. This consequence has clearly been verified by inelastic proton scattering experiments for energies in the range above 100 MeV. Here it has been possible to determine, as we shall discuss, the nature of the coupling potential $v(\mathbf{r}_0, \mathbf{r}_1)$.

To go further it is necessary to examine the integrals $I^{(l)}$. We take the simple case, the excitation of a single nucleon creating a residual nucleus in a particle-hole state. Consider the excitation of a nucleon in an orbital (j_i, Λ_i, m_i), to another orbital (j_f, Λ_f, m_f), where j is the total nuclear spin, m its z projection, and Λ the orbital angular momentum. The corresponding wave function is

$$|jm\Lambda s\rangle = \sum_{m_\Lambda} \langle jm|\Lambda m_\Lambda \tfrac{1}{2} m_s\rangle \mathscr{Y}_{\Lambda, m_\Lambda} \chi_{s, m_s} \frac{R_\Lambda}{r_0}$$

Additionally, to keep the discussion as simple as possible, let the interaction $v(\mathbf{r}_0, \mathbf{r}_1)$ be spin independent, so that

$$T_m^{(l)} \to \mathscr{Y}_{lm}$$

It immediately follows that

$$I^{(l)}(l_f j_f; l_i j_i) = \frac{4\pi}{k_f k_i} (l_f \| \mathscr{Y}_l \| l_i)(j_f \Lambda_f \tfrac{1}{2} \| \mathscr{Y}_l \| j_i \Lambda_i \tfrac{1}{2}) \mathscr{I}^{(l)}(l_f j_f; l_i j_i) \tag{4.66}$$

where

$$\mathscr{I}^{(l)}(l_f j_f; l_i j_i) = \iint u_{l_f}(r_0) R^*_{\Lambda_f}(r_1) v_l(r_0, r_1) u_{l_i}(r_0) R_\Lambda(r_0)\, dr_0\, dr_1 \tag{4.67}$$

The reduced matrix elements are given in (A.2.48) and (A.2.49) of deShalit and Feshbach (74):

$$(l_f \| \sqrt{4\pi} \mathscr{Y}_l \| l_i) = i^{l_f + l + l_i} (2l_f + 1)^{1/2} (2l_i + 1)^{1/2} (2l + 1)^{1/2} \begin{pmatrix} l & l_i & l_f \\ 0 & 0 & 0 \end{pmatrix}$$

$$(j_f \Lambda_f \tfrac{1}{2} \| \sqrt{4\pi} \mathscr{Y}_l \| j_i \Lambda_i \tfrac{1}{2}) = (i)^{2j_f + l - 1} \tfrac{1}{2} [1 + (-)^{\Lambda_f + l + \Lambda_i}] \begin{pmatrix} j_f & l & j_i \\ -\frac{1}{2} & 0 & \frac{1}{2} \end{pmatrix} (2j_f + 1)^{1/2}$$

$$\times (2j_i + 1)^{1/2} (2l + 1)^{1/2}$$

We note parity conditions

$$l + l_i + l_f = \text{even number}$$

$$\Lambda_f + \Lambda_i + l = \text{even number}$$

so that the parity change in the projectile wave function is compensated by the parity change in the nuclear transition.

The double radial integral depends on the transition densities, $\rho_{fi}^{(N)} \equiv R_{\Lambda f}^{*} R_{\Lambda i}$ and $\rho_{fi}^{(P)} \equiv u_{l_f} u_{l_i}$. The Coulomb repulsion plays an important role. Obviously, a strong repulsion will reduce the value of $\rho_{fi}^{(P)}$. The density $\rho_{fi}^{(P)}$ will also be reduced in the nuclear interior if the effective absorption in the projectile channels is large. Under these circumstances, Coulomb repulsion and/or strong absorption, surface reactions will be favored. The cross section will be greatest, then, for nuclear densities $\rho_{fi}^{(N)}$ which peak at the surface, an effect that is strengthened if $v_l(r_0, r_1)$ is largest on the surface or short ranged. Maximum overlap at the surface occurs for l_f^0 and l_i^0 such that

$$\frac{l_f^0}{k_f} \approx \frac{l_i^0}{k_1} \approx R$$

For l_i and l_f greater than l_i^0 and l_f^0, respectively, the angular momentum barrier will further reduce the amplitude of u_{l_f} and u_{l_i}, so that $\mathscr{I}^{(l)}$ will be small for these values of $l_{i,f}$. Thus the major contributions to the angular distribution comes from a narrow range in l_i and l_f, a result that has been employed above and in agreement with results obtained using the WKB approach leading to (4.20).

D. Exchange Effects

The effect of antisymmetry with respect to the incident nucleon has not been explicitly considered. In the "naive" approach the incident-state (and similarly for the final-state) wave function used above is antisymmetrized:

$$\phi_i^{+}(0)\psi_i(1,2,\ldots) \to \mathscr{A}[\phi_i^{(+)}(0)\psi_i(1,2,\ldots)] = \left(1 - \sum_{\mu} P_{0\mu}\right)\phi_i^{(+)}\psi_i(1,2,\ldots) \quad (4.68)$$

where $P_{0\mu}$ is the permutation operator, for example,

$$P_{01}\phi_i^{(+)}(0)\psi_i(1,2,\ldots) = \phi_i^{(+)}(1)\psi_i(0,2,\ldots)$$

However, this procedure is incorrect since the resulting initial- and final-state wave functions are not orthogonal. In fact (see Section III.5),

$$\frac{1}{A+1}\langle \mathscr{A}\phi_f^{(-)}(0)\psi_f(1,2,\ldots)|\mathscr{A}\phi_i^{(+)}(0)\psi_i(1,2,\ldots)\rangle = \langle \phi_f^{(-)}|\delta_{fi} - K_{fi}|\phi_i^{(+)}\rangle$$

where

$$K_{fi}(\mathbf{r}, \mathbf{r}_0) = A\langle \psi_f(\mathbf{r}, \mathbf{r}_2, \ldots|\psi_i(\mathbf{r}_0, \mathbf{r}_2, \ldots\rangle \quad (4.69)$$

The resolution of this problem is indicated by the discussion of the impact of the Pauli principle upon the theory of reactions in Section III.5. We recall [Eq. (III.5.33)] that

$$EU_\nu = \sum_{\nu'} \langle \psi_\nu | H_{\text{eff}} \mathscr{A} \psi_{\nu'} u_{\nu'} \rangle \tag{4.70}$$

$$= \sum_{\nu'} \left\langle \psi_\nu | H_{\text{eff}} A \psi_{\nu'} \left(\frac{1}{1-K'} \right)_{\nu'\nu''} U_{\nu''} \right\rangle \tag{4.71}$$

which are simply the coupled channel Schrödinger equations in which the target wave functions range through a finite set $\{\psi_\nu\}$, $\nu = 1, \ldots, n$. U_ν is the projection of the Schrödinger wave function on ψ_ν:

$$U_\nu(0) = \langle \psi_\nu(1,2,\ldots) | \Psi \rangle \tag{4.72}$$

The function u_ν is given by [see (III.5.15)]

$$U_\nu = u_\nu - \sum K'_{\nu\nu'} u_{\nu'} = (1-K')_{\nu\nu'} u_{\nu'} \tag{4.73}$$

where all eigenstates $\omega_\alpha^{(1)}$ of $K_{\nu\nu'}$ with eigenvalues 1 have been removed, as indicated by the prime on K. These are the superfluous solutions of Section III.5 satisfying the condition (III.5.9)

$$\mathscr{A} \sum_\nu \omega_{\alpha\nu}^{(1)} \psi_\nu = 0 \tag{4.74}$$

Hence

$$K'_{\nu\nu'} = K_{\nu\nu'} - \sum_\alpha \omega_{\alpha\nu}^{(1)} \rangle \langle \omega_{\alpha\nu'}^{(1)} \tag{4.75}$$

From (4.71) the DWA amplitude with Pauli principle included is

$$\mathscr{T}_{fi}^{(\text{dir})} = \left\langle U_f^{(-)} \psi_f \left| \sum_i v(\mathbf{r}_0, \mathbf{r}_i) \right| \mathscr{A} \sum_{\nu'} \psi_{\nu'} u_{\nu'}^{(+)} \right\rangle \tag{4.76}$$

$$u_{\nu'} = \sum \left(\frac{1}{1-K'} \right)_{\nu'\nu''} U_{\nu''} = \left(\frac{1}{1-K'} \right)_{\nu' i} U_i$$

where the last of these equations is a consequence of the initial condition on $U_{\nu''}$. Equation (4.75) implies orthogonality of $U_f \psi_f$ with $\mathscr{A} \sum \psi_{\nu'} u_{\nu'}$. Orthogonality does indeed follow:

$$\langle U_f\psi_f|\mathscr{A}\psi_{\nu'}u_{\nu'}\rangle = \sum_{\nu'}\langle U_f^{(-)}|(1-K')_{f\nu'}|u_{\nu'}^{(+)}\rangle$$

$$= \sum_{\nu'}\langle U_f^{(-)}|(1-K')_{f\nu'}\left(\frac{1}{1-K'}\right)_{\nu' i}|U_i^{(+)}\rangle$$

$$= \langle U_f^{(-)}|\delta_{fi}|U_i^{(+)}\rangle = 0$$

since $i \neq f$.

Evaluation of (4.76) requires the determination not only of U_f and U_i but also of the eigenvalues and eigenfunctions of K, those for which the eigenvalues are neither 1 or zero. The problem of determining K for the shell model description has been solved by Friedman (67) Some of his results are given in Section III.5 (see (III.6.51) and (III.6.52)]. In the case where the eigenvalues of K are 0 and 1, u_i equals U_i. This simplest case occurs if the wave functions ψ_ν are Slater determinants made up of mutually orthogonal single-particle wave functions.

Returning to (4.76), one obtains

$$\mathscr{T}_{fi}^{(\mathrm{dir})} = \left\langle U_f^{(-)}(\mathbf{r}_0)\psi_f(\mathbf{r}_1,\mathbf{r}_2,\ldots)\middle|\sum_j v(\mathbf{r}_0,\mathbf{r}_j)\middle|\sum\psi_\nu(\mathbf{r}_1,\mathbf{r}_2,\ldots)u_\nu^{(+)}(\mathbf{r}_0)\right\rangle$$

$$- A\left\langle U_f^{(-)}(\mathbf{r}_0)\psi_f(\mathbf{r}_1,\mathbf{r}_2,\ldots)\middle|\sum_j v(\mathbf{r}_0,\mathbf{r}_j)\middle|\sum\psi_\nu(\mathbf{r}_0,\mathbf{r}_2,\ldots)u_\nu^{(+)}(\mathbf{r}_1)\right\rangle$$

or

$$\mathscr{T}_{fi}^{(\mathrm{dir})} = A\left\langle U_f^{(-)}(\mathbf{r}_0)\psi_f(\mathbf{r}_1,\mathbf{r}_0,\ldots)|v(\mathbf{r}_0,\mathbf{r}_1)(1-P_{01})|\sum\psi_\nu(\mathbf{r}_1,\mathbf{r}_2,\ldots)u_\nu^{(+)}(\mathbf{r}_0)\right\rangle$$

$$- A\left\langle U_f^{(-)}(\mathbf{r}_0)\psi_f(\mathbf{r}_1,\mathbf{r}_2,\ldots)\middle|\sum_2^A v(\mathbf{r}_0,\mathbf{r}_j)\middle|\sum_\nu\psi_\nu(\mathbf{r}_0,\mathbf{r}_2,\ldots)u_\nu^{(+)}(\mathbf{r}_1)\right\rangle \quad (4.77)$$

Thus $\mathscr{T}_{fi}^{(\mathrm{dir})}$ consists of a direct term [the first term in (4.77)], an exchange term referred to as the *knock-on term* [the second term in (4.77)], and finally, the *heavy-particle stripping term* [the third and last term in (4.77)]. The knock-on term is just what would be expected if one is dealing with a two-body interaction in which the rest of the target (the core) does not participate in the reaction, that is, acts as spectator. In the heavy-particle stripping term the particle labeled $\mathbf{r}_0$ becomes unbound while the particle labeled $\mathbf{r}_1$ becomes bound, under the influence of interactions, $v_{02}+v_{03}\cdots$. This is most unlikely, being proportional to the "amount" of $u_\nu^{(+)}(\mathbf{r}_1)$ present in $\psi_f(\mathbf{r}\cdots)$, going to zero if $u_i^{(+)}$ and ψ_f are orthogonal. This, indeed, would be the case if ψ_f is a Slater determinant of bound orthogonal orbitals and $u_i^{(+)}$ is a continuum wave function that is orthogonal to all bound single-particle wave functions. It is the virtue of anti-

symmetrization and the elimination of the superfluous states that one is not required to include, in the sum over v in (4.26) and (4.77), terms in which any of the target nucleons are in continuum orbitals. It appears, therefore, to be a good approximation to drop the last term in (4.77), that is, to use models in which the u_v are orthogonal to ψ_f.

Finally, one makes the approximation of dropping all but ψ_i in the sum over v in the leading terms of (4.77), so that

$$\mathcal{T}_{fi}^{(\mathrm{dir})} \simeq A\langle U_f^{(-)}(\mathbf{r}_0)\psi_f(\mathbf{r}_1, \mathbf{r}_2, \ldots)|v(\mathbf{r}_0, \mathbf{r}_1)(1 - P_{01})|\psi_i(\mathbf{r}_1, \mathbf{r}_2, \ldots)u_i^{(+)}(\mathbf{r}_0)\rangle \quad (4.78)$$

This result is also obtained in the high-energy limit where first-order multipole scattering theory applies. The impulse approximation, in which the incident projectile interacts only with one of the nucleons in the nucleus, is applicable and only the two-body Pauli principle, as in (4.78), is involved. Comparing (4.78) with (4.76), we see that this approximation is valid only when the eigenvalues of the K matrix are either 1 (the Slater determinant case) or zero. When this is not the case [Friedman (67) provides important examples; see Chapter III], the orthogonality between the initial and final states is destroyed in this approximation and one must keep the sum over v in (4.77).

The importance of the errors induced by the approximations is not clear. The initial wave functions and the interactions v_{01} used in (4.78) are determined empirically, for example, from elastic scattering. Then some of the required attributes of the wave functions used in (4.78) may be implicitly contained. However, that these sufficiently reduce the error remains, at the present time, a speculation.

The operator P_{01} equals the product of the space exchange P_{01}^x, spin exchange P_{01}^σ, and the isospin exchange operators P_{01}^τ:

$$P_{01} = P_{01}^x P_{01}^\sigma P_{01}^\tau$$

Introducing the projection operators P^{ST} of (2.84), where S and T are the spin and isospin quantum numbers of the two nucleon system, respectively, one obtains

$$\begin{aligned} P_{01} &= P_{01}^x(P_{01}^{11} - P_{01}^{01} - P_{01}^{10} + P_{01}^{00}) \\ &= P_{01}^x \sum(-)^{S+T} P_{01}^{(ST)} \end{aligned}$$

Therefore, using (2.89) yields

$$\begin{aligned} v_{01}(1 - P_{01}) &= \sum_{ST} v_{01}^{(ST)} P_{01}^{(ST)}(1 - P_{01}) \\ &= \sum_{ST} v_{01}^{(ST)} P_{01}^{(ST)}[1 - (-)^{S+T} P_{01}^x] \end{aligned} \quad (4.79)$$

When $S + T$ is odd (i.e., in states in which the relative wave function is even),

the direct and exchange terms add, whereas when $S+T$ is even, they have opposite signs.

Inserting (4.79) into the expression for the transition matrix (4.78) yields

$$\mathcal{T}_{fi} = A \sum_{ST} \langle U_f^{(-)}(\mathbf{r}_0)\psi_f(\mathbf{r}_1, s^f, t^f)|v_{01}^{(ST)}P_{01}^{(ST)}(1-(-)^{S+T}P_{01}^{x})|\psi_i(\mathbf{r}_1, s^i, t^i, \ldots)u_i^{(+)}(\mathbf{r}_0)\rangle$$

where the spin and isospin coordinates are explicitly given. Then

$$\mathcal{T}_{fi} = A \sum_{ST} [\langle U_f^{(-)}(\mathbf{r}_0, s_0^f, t_0^f)|\rho_{fi}^{(ST)}(\mathbf{r}_1, \boldsymbol{\sigma}_0, \mathbf{t}_0)v_{01}^{ST}u_i^{(+)}(\mathbf{r}_0, s_0, t_0)\rangle$$

$$-(-)^{S+T}\langle U_f^{(-)}(\mathbf{r}_0 s_0^f t_0^f)|K_{fi}^{(ST)}(\mathbf{r}_1; \mathbf{r}_0\boldsymbol{\sigma}_0\boldsymbol{\tau}_0)v_{01}^{ST}u_i^{(+)}(\mathbf{r}_1, s_0^i, t_0^i)\rangle] \quad (4.80)$$

where

$$\rho_{fi}^{(ST)}(\mathbf{r}_1, \boldsymbol{\sigma}_0\boldsymbol{\tau}_0) = \langle \psi_f(\mathbf{r}_1 \cdots)|P_{01}^{(ST)}|\psi_i(\mathbf{r}_1 \cdots)\rangle \quad (4.81)$$

and

$$K_{fi}^{(ST)}(\mathbf{r}_1; \mathbf{r}_0, \boldsymbol{\sigma}_0\boldsymbol{\tau}) = \langle \psi_f(\mathbf{r}_1, s_1, t_1; \ldots|P_{01}^{(ST)}|\psi_i(\mathbf{r}_0, s_1, t_1; \ldots)\rangle \quad (4.82)$$

The transition densities $\rho_{fi}^{(ST)}$ are a generalization of the one-body densities discussed earlier [see the note following (2.82)]. They occur in the Born approximation (distorted or plane wave) treatment of the inelastic scattering from ψ_i to ψ_f produced by a collision with a nucleon, pion, electron, and so on. Generally, then, these densities can be deduced by considering the data obtained with all of these projectiles. The data obtained with electrons play a central role since in that case the interaction is best known, although exchange current effects do introduce some uncertainties.

The mixed density $K_{fi}^{(ST)}(\mathbf{r}_1, \mathbf{r}_0)$ is present only for the nucleon projectile case because it is only then that the Pauli principle acts. It does, however, occur when second-order (multi-step) processes are considered and then is intimately related to the correlation function [see Feshbach (81)].

$$C_{fi}(\mathbf{r}_1, \mathbf{r}_2) = \rho_{fi}(\mathbf{r}_1, \mathbf{r}_2) - \rho_{fi}(\mathbf{r}_1)\rho_{ii}(\mathbf{r}_2) - \rho_{ff}(\mathbf{r}_1)\rho_{fi}(\mathbf{r}_2)$$

However, up to now it has proven difficult to extract this quantity from experiment.

In a complete DWA theory one will need to diagonalize $K_{fi}^{(ST)}(\mathbf{r}_1, \mathbf{r}_0)$ to most readily obtain orthogonality as discussed earlier in this section, and that diagonalization can be used in this context as well. We write (dropping the superscripts S and T for notational simplicity)

$$K_{fi}(\mathbf{r}_1, \mathbf{r}_0) = \sum w_a^{(f)}(\mathbf{r}_1)\rangle\langle w_a^{(i)}(\mathbf{r}_0)$$

where w_a are the eigenfunctions of K and $w_a^{(f)}$ is its component in the final state channel in (see the discussion in Section III.5). These are single-particle wave

functions. They are finite in number and permit a relatively simple evaluation of the exchange term in (4.80), which involves the matrix elements

$$\sum_a \langle U_f^{(-)}(\mathbf{r}_0) w_a^{(f)}(\mathbf{r}_1) | v_{01} | w_a^{(i)}(\mathbf{r}_0) u_i^{(+)}(\mathbf{r}_1) \rangle$$

The local approximation is generally used in evaluating the exchange term in (4.80). The technique is identical with that used in the discussion following (2.9). Consider (suppressing spin variables)

$$V_{\text{exch}}(\mathbf{r}_0) u_i^{(+)}(\mathbf{r}_0) = \int K_{fi}(\mathbf{r}_1, \mathbf{r}_0) v(\mathbf{r}_1 - \mathbf{r}_0) u_i^{(+)}(\mathbf{r}_1)\, d\mathbf{r}_1 \tag{4.83}$$

Introducing $\boldsymbol{\rho} = \mathbf{r}_1 - \mathbf{r}_0$, we obtain

$$\begin{aligned} V_{\text{exch}}(\mathbf{r}_0) u_i^{(+)}(\mathbf{r}_0) &= \int K_{fi}(\boldsymbol{\rho} + \mathbf{r}_0, \mathbf{r}_0) v(\boldsymbol{\rho}) u_i^{(+)}(\mathbf{r}_0 + \boldsymbol{\rho})\, d\boldsymbol{\rho} \\ &= \int v(\boldsymbol{\rho}) K_{fi}(\boldsymbol{\rho} + \mathbf{r}_0, \mathbf{r}_0) e^{i[(\boldsymbol{\rho}\cdot\hat{\mathbf{p}})/\hbar]} d\boldsymbol{\rho} u_i^{(+)}(\mathbf{r}_0) \end{aligned} \tag{4.83'}$$

where the operator $i\hat{\mathbf{p}}/\hbar = \nabla$ operates only the $\mathbf{r}_0$ variable, so that

$$V_{\text{exch}}(\mathbf{r}_0) = \int v(\boldsymbol{\rho}) K_{fi}(\boldsymbol{\rho} + \mathbf{r}_0, \mathbf{r}_0) e^{i[(\boldsymbol{\rho}\cdot\hat{\mathbf{p}})/\hbar]} d\boldsymbol{\rho} \tag{4.84}$$

The Perey–Saxon approximation consists in replacing operator $\hat{\mathbf{p}}/\hbar$ by the incident momentum $\mathbf{p}_i/\hbar = \mathbf{k}_i$. A somewhat more elaborate approximation takes the variation of the index of refraction inside the interaction region into account:

$$\frac{\hat{\mathbf{p}}}{\hbar} \to \left[\frac{2\mu}{\hbar^2} (E - V_{\text{opt}}(r_0)) \right]^{1/2} \tag{4.85}$$

With this replacement of $\hat{\mathbf{p}}$, $V_{\text{exch}}(\mathbf{r}_0)$ becomes a local operator. A further approximation is made by Petrovich, McManus et al. (69, 79) and Love (79a). When $\mathbf{k}_i$ is very large, that is, for sufficiently large energies, the value of $V_{\text{exch}}(\mathbf{r}_0)$ comes mostly from small values of $\boldsymbol{\rho}$, so that in that limit

$$\begin{aligned} V_{\text{exch}}(\mathbf{r})_0 &\to \rho_{fi}(\mathbf{r}_0) \int e^{i\mathbf{k}_i\cdot\boldsymbol{\rho}} v(\boldsymbol{\rho})\, d\boldsymbol{\rho} \\ &\to \rho_{fi}(\mathbf{r}_0) \tilde{v}(\mathbf{k}_i) \end{aligned} \tag{4.86}$$

where $\tilde{v}$ is the Fourier transform of v.

With the local approximation, (4.80) becomes

$$\mathcal{T}_{fi} = A \sum_{ST} \langle U_f^{(-)}(\mathbf{r}_0)[V_{\text{direct}}^{(ST)} - (-)^{S+T} V_{\text{exch}}^{(ST)}] u^{(+)}(\mathbf{r}_0) \rangle \tag{4.87}$$

where

$$V_{\text{direct}}^{(ST)} = \int d\mathbf{r}_1 \rho_{fi}^{(ST)}(\mathbf{r}_1) v^{ST}(01) \tag{4.88}$$

We note that in this approximation only the single-particle transition density $\rho_{fi}^{(ST)}$ enters in both (4.86) and (4.88). This represents a great reduction in the complexity of the calculation, and as noted earlier, permits the use of empirical information on $\rho_{fi}^{(ST)}(\mathbf{r})$ available for example from electron scattering.

The analysis leading to (4.87) requires modification for the spin-orbit and tensor interactions present for the spin triplet state of the projectile nucleon and target nucleon. For example, consider the case of the spin-orbit interaction, (2.90), appearing in components of $V^{(ST)}$, V^{10}, and V^{11}, in the form

$$v^{LS}(\boldsymbol{\rho}) \tfrac{1}{2}(\boldsymbol{\sigma}_0 + \boldsymbol{\sigma}_1) \cdot [(\mathbf{r}_1 - \mathbf{r}_0) \times (\mathbf{p}_1 - \mathbf{p}_0)] = v^{LS}(\boldsymbol{\rho})(\boldsymbol{\sigma}_0 + \boldsymbol{\sigma}_1) \cdot (\boldsymbol{\rho} \times \mathbf{p}_\rho) \tag{4.89}$$

In evaluating $V_{\text{exch}}^{(SL)}$, using the procedures described above, one needs explicitly to include the result that $V_{\text{exch}}^{(SL)}$ vanishes when K_{fi} is independent of $\mathbf{r}_1$, which we shall now demonstrate. Under this condition

$$V_{\text{exch}}^{(SL)} \sim \int v^{LS}(\rho)(\boldsymbol{\rho} \times \nabla_\rho) u(\mathbf{r}_1)\, d\boldsymbol{\rho}$$

Integrating by parts gives

$$V_{\text{exch}}^{(SL)} \sim \int [(\boldsymbol{\rho}) \times \nabla_\rho v^{LS}(\rho)] u(\mathbf{r}_1)\, d\boldsymbol{\rho} = 0 \qquad K_{fi} \quad \text{constant}$$

In the analysis that follows we take this result into account by replacing $K_{fi}(\mathbf{r}_1, \mathbf{r}_0)$ by ΔK_{fi}:

$$\Delta K_{fi} = K_{fi}(\mathbf{r}_0 + \boldsymbol{\rho}, \mathbf{r}_0) - K_{fi}(\mathbf{r}_0, \mathbf{r}_0)$$

The $\boldsymbol{\sigma}_0$ term will be considered in detail. Because $\boldsymbol{\sigma}_0 + \boldsymbol{\sigma}_1$ automatically selects triplet ($S = 1$) states, one can drop the operator P^{ST} in (4.79). Inserting (4.89) into (4.84) yields

$$\begin{aligned} V_{\text{exch}}^{(LS)}(\mathbf{r}_0) &\equiv \boldsymbol{\sigma}_0 \cdot \int d\boldsymbol{\rho} \Delta K_{fi}(\mathbf{r}_0 + \boldsymbol{\rho}, \mathbf{r}_0) v^{LS}(\boldsymbol{\rho})[\boldsymbol{\rho} \times \mathbf{p}_\rho] e^{i[(\boldsymbol{\rho} \cdot \mathbf{p}_0)/\hbar]} \\ &= \boldsymbol{\sigma}_0 \cdot \int d\boldsymbol{\rho} \Delta K_{fi}(\mathbf{r}_0 + \boldsymbol{\rho}, \mathbf{r}_0) v^{LS}(\boldsymbol{\rho})[\boldsymbol{\rho} \times \mathbf{p}_0] e^{i[(\boldsymbol{\rho} \cdot \mathbf{p}_0)/\hbar]} \\ &= \boldsymbol{\sigma}_0 \cdot \int d\boldsymbol{\rho} \Delta K_{fi}(\mathbf{r}_0 + \boldsymbol{\rho}, \mathbf{r}_0) v^{LS}(\boldsymbol{\rho})[\hbar i \nabla_{p_0} \times \mathbf{p}_0] e^{i[(\boldsymbol{\rho} \cdot \mathbf{p}_0)/\hbar]} \end{aligned} \tag{4.90}$$

or using $\hbar i\nabla_{p_0} = \mathbf{r}_0$, and making the Perey–Saxon approximation $\mathbf{p}_0 \to \hbar\mathbf{k}_i$ in the exponent, one finally has

$$V_{\text{exch}}^{(LS)}(\mathbf{r}_0) = \int d\boldsymbol{\rho} \Delta K_{fi}(\mathbf{r}_0 + \boldsymbol{\rho}, \mathbf{r}_0) v^{LS}(\boldsymbol{\rho}) e^{i\mathbf{k}_i \cdot \boldsymbol{\rho}} \boldsymbol{\sigma}_0 \cdot \mathbf{L}_0$$

$$\mathbf{L}_0 = \mathbf{r}_0 \times \mathbf{p}_0 \tag{4.91}$$

Problem. Verify (4.90) using Fourier transforms to momentum space of $u(\mathbf{r}_1)$, and so on.

In the high momentum limit,

$$V_{\text{exch}}^{LS}(\mathbf{r}_0) = \frac{1}{ik_i} \mathbf{k}_i \cdot \nabla_1 K_{fi}(\mathbf{r}_1, \mathbf{r}_0)_{1\to 0} \frac{\partial \tilde{v}^{LS}(k_i)}{\partial k_i} \boldsymbol{\sigma}_0 \cdot \mathbf{L}_0 \tag{4.92}$$

where

$$\nabla_1 K_{fi}(\mathbf{r}_1, \mathbf{r}_0)_{1\to 0} = \lim_{\mathbf{r}_1 \to \mathbf{r}_0} \nabla_{r_1} K_{fi}(\mathbf{r}_1, \mathbf{r}_0)$$

A local approximation can also be derived for the $\boldsymbol{\sigma}_1$ term in (4.89). However, $K_{fi}(\mathbf{r}_1, \mathbf{r}_0)$ must be replaced by a vector $\mathbf{K}_{fi}^{\sigma}$ in spin space:

$$\mathbf{K}_{fi}^{\sigma}(\mathbf{r}_1; \mathbf{r}_0) = \langle \psi_f(\mathbf{r}_1 s_1 t_1, \ldots) | \boldsymbol{\sigma}_1 | \psi_1(\mathbf{r}_0, s_1, t_1; \ldots) \rangle \tag{4.93}$$

a term that is important if the transition involves a spin-flip of a target nucleon.

5. THE INTERACTION POTENTIALS

In this section we discuss the interaction potentials, v_{0i}, to be inserted into the expression for the direct process inelastic $\mathcal{T}$ matrix. For the present, our attention will be focused on their derivation from the nucleon–nucleon force. Comparison with experiment is deferred to Section 6. Prediction of experimental results depends on both v_{0i} and the properties of the incident and final wave functions as contained in the transition density matrix.

Bertsch, Borysowicz, McManus, and Love (77) [see also Love, Scott, et al. (78) and earlier work of Slanina and McManus (68)] proceed by fitting the potentials v_{0i} so as to have the same matrix elements, in an oscillator basis, as the elements of the G matrix determined, for example, from the application of the G-matrix method to semiempirical nucleon–nucleon forces. The central and spin-orbit potentials are taken to be the sum of three terms, each of the Yukawa form, with the ranges 1.4, 0.7 and 0.4 fm. The first of these is the range of the one-pion exchange potential; the other two are phenemenological, corresponding to intermediate and short-range potentials. The final recommended interaction ($M3Y$) is based primarily on the Reid nucleon–nucleon potential [Reid

(68)]. This interaction potential is real and independent of density. It is applicable for the energy range $E \lesssim 60$ MeV. The resulting potentials are given in Fig. 5.1.

Petrovich, Stanley, and Bevelacqua (77) point out that the $M3Y$ interaction does not lead to saturation. They add a density-dependent term proportional to the density to achieve saturation. On the other hand, Geramb, Brieva, and Rook (79) use the more recently developed "Paris" nucleon–nucleon potential [Lacombe, Loiseau, et al. (80)]. The local density approximation [see Vol. deShalit and Feshbach (74)] is used, employing plane wave matrix elements. These are matched for each value of the density and energy by the plane wave

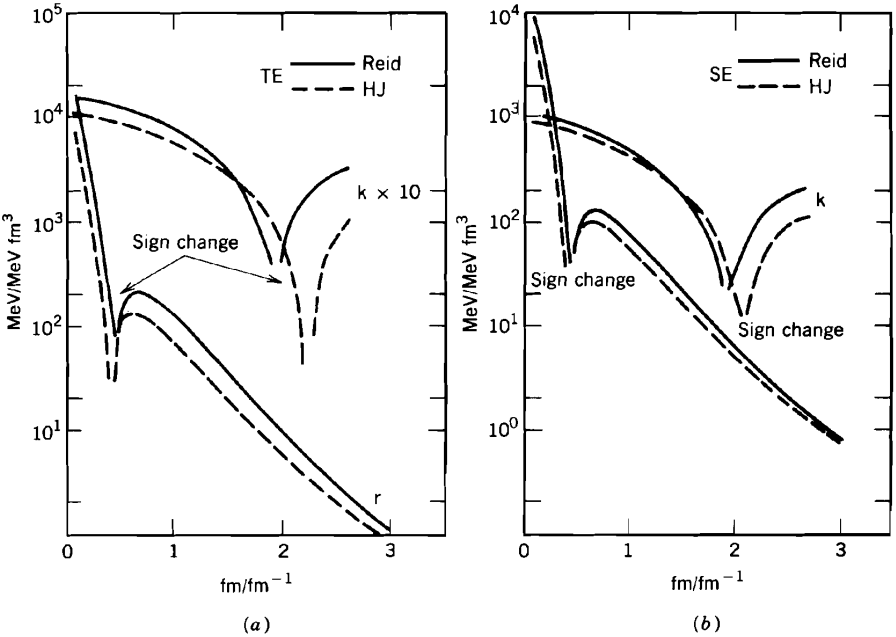

FIG. 5.1. (*a*) TE component of the interaction as fitted to three Yukawas is shown in configuration space (V in MeV versus r in fm and labeled by r) and in momentum space (V in MeV·fm^3 versus k in fm^{-1} and labeled by k). The change in sign of the interaction near the origin is shown in the figure. TE = Central triplet ($S = 1$) even ($T = 0$) [see (2.86).] (*b*) SE component of the interaction same convention as (a)]. SE = singlet ($S = 0$) even ($T = 0$) [see (2.86)]. (*c*) TNE component of the interaction. The solid and dashed curves correspond to r^2 Yukawa-type fits. The solid circles correspond to ROPEP fit (same convention (*a*)]. TNE = tensor even ($T = 0$). (*d*) TNO component of the interaction [same convention as (*a*)]. TNO = tensor odd ($T = 1$). (*e*) LSE and LSO components of the interaction [conventions as in (*a*) *except* $\bar{V}$ is in MeV·fm^5]. LSE = spin orbit, $T = 0$, LS0 = spinorbit $T = 1$. (*f*) SO and TO components of the interaction from Elliott matrix elements (same convention as in (*a*)]. SO = singlet central, $T = 1$. TO = triplet central, $T = 1$. [From Bertsch, Borysowicz, McManus, and Love (77).]

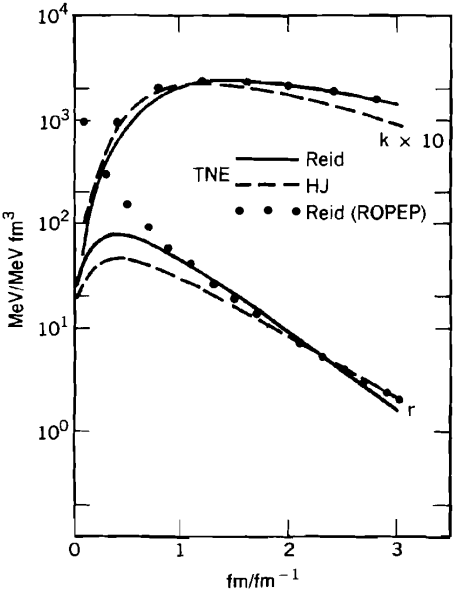

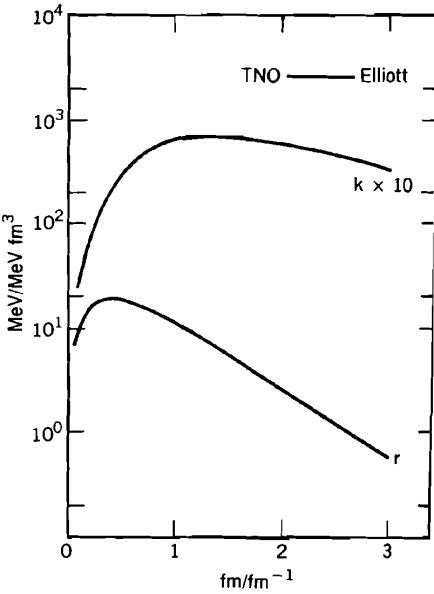

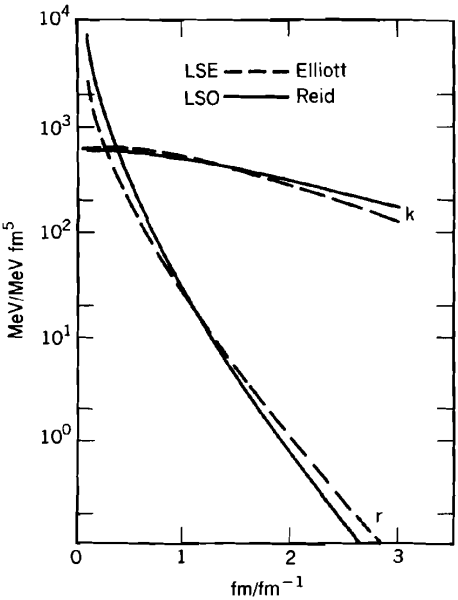

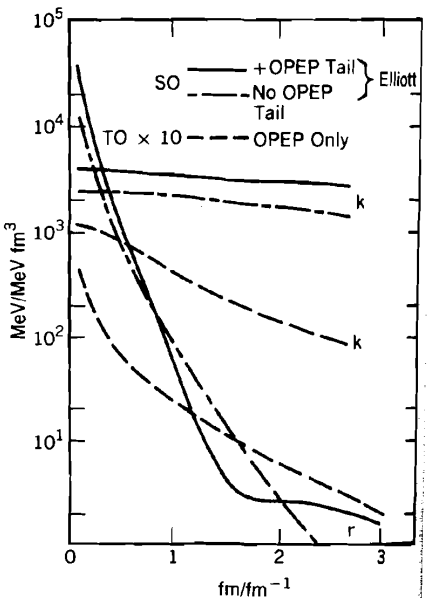

FIG. 5.1. (*Continued*)

matrix elements of a sum of four Yukawa potentials. Several averages are performed (over the Fermi sphere for the target nucleons, over angular momenta) to finally obtain a local potential. The details are given in the original paper [see also Geramb (83)]. The resulting interactions are complex and are density and energy dependent. They do not appear, however, to include the effective mass correction of Equation (2.21). Neither do Petrovich and Love (81) and Love and Franey (81), who advocate the use of the $M3Y$ at low energies (< 100 MeV) and the free-space nucleon–nucleon transition matrix as derived as the first term of the multiple scattering approximation (see Chapter II) for higher energies. The plane wave matrix elements are matched by the matrix elements of a sum of Yukawa potentials. The resulting interactions are complex and energy dependent. They are not density dependent.

Typical results following from the Brieva, Rook, and Geramb approach are shown in Fig. 5.2, in which the real and imaginary parts of $\tilde{v}^C_{00}$, the isoscalar central, are shown as a function of q, the momentum transfer, where

$$\tilde{v}^C_{00}(\mathbf{q}) \equiv \int e^{i\mathbf{q}\cdot\mathbf{r}} v^C_{00}(r)\, d\mathbf{r}$$

and of the density, which is related to the parameter k_F by

$$k_F = (\tfrac{3}{2}\pi^2\rho)^{1/3}$$

Recall that $k_F \sim 1.36\,\text{fm}^{-1}$ corresponds to normal nuclear density. Note the change in sign of $\text{Re}\,\tilde{v}^C_{00}$ and $\text{Im}\,\tilde{v}^C_{00}$. These provide the input required to construct the local density approximation to $v^C_{00}(|\mathbf{r}_0 - \mathbf{r}_i|)$, the density employed, and therefore the choice of the various curves shown in Fig. 5.2, being evaluated at the average position of the two points $\mathbf{r}_0$ and $\mathbf{r}_1$ [i.e., at $\frac{1}{2}(\mathbf{r}_0 + \mathbf{r}_1)$].

Figure 5.2 also contains the results obtained by Love and collaborators [Love and Franey (81)]. It is clear that at this energy (140 MeV) there is a substantial difference, so that the effect of the nuclear medium is significant and cannot be disregarded. Nevertheless, *qualitatively* the Brieva et al. curves are similar to the Love–Franey free-space results, so that within an overall reduction factor, one can obtain qualitatively useful results using the Love–Franey interaction. However, it cannot be expected to be quantitatively valid.

It is therefore appropriate to examine the results obtained by Love and Franey (81) given in Fig. 5.3, in which the magnitudes of the effective interactions are plotted as a function of the momentum transfer, q, for energy ranging from 100 to 800 MeV. As the energy increases, these effective interactions should become increasingly accurate. At the lower energies, the omitted medium effects become significant. In discussing these results, note that the relevant components of v [for normal parity transition from spin-zero target ground states is $\Delta\pi = (-)^J$, where J is the spin of the excited state] are the central interactions, v_{00} and v_{01}, and the spin-orbit terms, v^{LS}, while the abnormal parity transitions [$\Delta\pi = (-)^{J+1}$] are dominated by the spin-orbit, tensor and spin-dependent

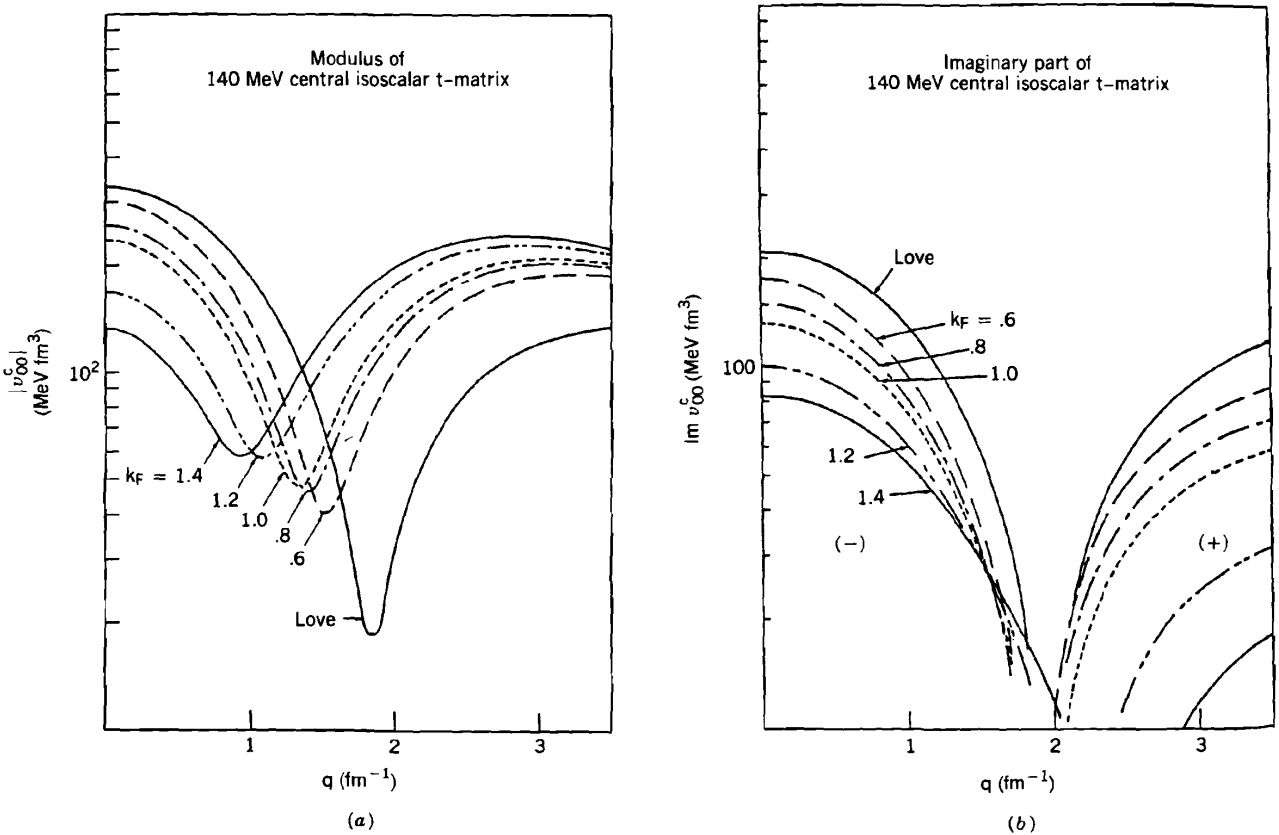

FIG. 5.2. Comparison of the isoscalar central potentials, (2.), computed from the calculation of von Geramb, Brieva, and Rook (79) for various values of k_F and those obtained by Love, Scott, et al. (78). q is the momentum transfer [From Kelly (81).]

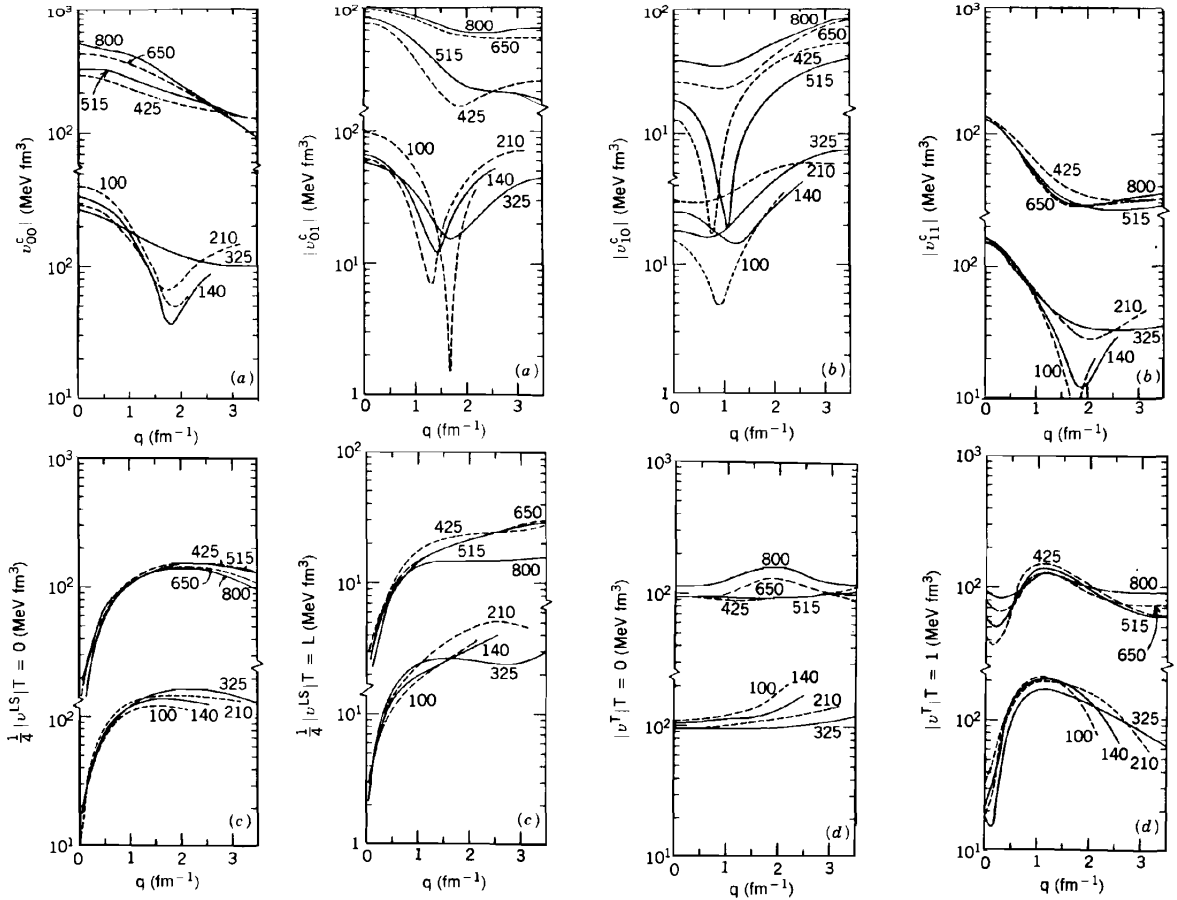

FIG. 5.3. Magnitudes of the effective nucleon–nucleon potential, (2.86), as a function of momentum transfer, q and bombarding energy (number on curve in MeV). [From Love and Franey (81).]

parts of the central terms, v_{10} and v_{11}. The parity change is accompanied by a spin flip of the target nucleon.

Problem. Prove this last statement.

We first discuss the normal parity transitions. In both v_{00} and v_{01}, note the strong minima in the range $100\ \text{MeV} < E < 210\ \text{MeV}$ for $q \sim 1.6\ \text{fm}^{-1}$. In this domain, the spin-orbit contributions, especially $v^{LS}(T=0)$, will dominate. At low q, the dominant contribution will come from scalar–isoscalar v_{00}. The latter is illustrated by Fig 5.4, which shows $v_{00} \gg v_{01}, v_{10}, v_{11}$.

Turning next to the unnatural parity excitations, the $T=1$ contribution is dominated at small q by v_{11}. At larger q and for the lower group of energies a minimum is present in v_{11}, and $v^{T}(T=1)$ should dominate. For $T=0$, the tensor term $v^{T}(T=0)$ is strongest at low q. At larger q, v_{10}, $v^{LS}(T=0)$ and $v^{T}(T=0)$ will all be important. Note that the last two are relatively constant for large q and slowly varying with energy.

We note the important result that the corresponding components of the density matrix will be measurable. For example, low-q normal parity transitions will be sensitive to the scalar density ρ^{00}. While for abnormal parity transition, the spin components ρ^{11} and ρ^{10} will be important. If, on the other hand, the nuclear structure is well known, the interactions can be extracted from experiment.

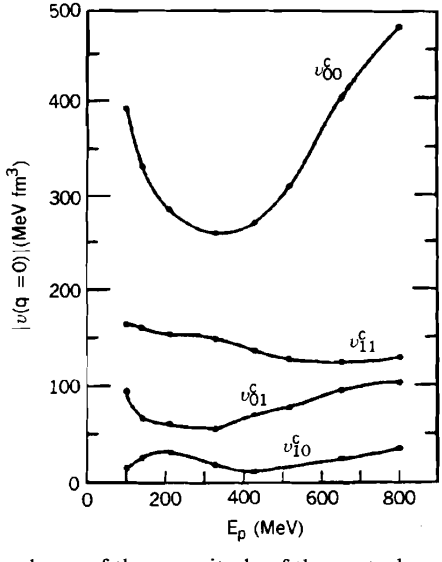

FIG. 5.4. Energy dependence of the magnitude of the central parts of the N–N t matrix as described in Fig. 5.3. [From Love and Franey (81).]

G-Matrix Method [Mahaux (79); Brieva and Rook (78)]. In this section we briefly outline and G-matrix method used in the lower-energy range to obtain the effective two-body interaction. The procedure used is called the Brueckner–Hartree–Fock method. [We refer the reader to deShalit and Feshbach (74), (VII.18.13) and (VII.18.14).] The first of these is the equation for the G matrix,

$$G(\varepsilon) = v + v\frac{Q_F}{\varepsilon - H_0}G(\varepsilon) \tag{5.1}$$

where v is the nucleon–nucleon potential, Q_F is the Pauli operator that projects on to unfilled states, and H_0 is the unperturbed Hamiltonian:

$$\begin{aligned} H_0 &= \sum h_i \\ h_i &= \frac{k^2}{2m} + U_i \end{aligned} \tag{5.2}$$

where U_i is a one-body potential chosen so as to minimize higher-order effects in the evaluation of the energy:

$$E = \sum_i \langle i|T|i\rangle + \tfrac{1}{2}\sum\langle ij|G(\varepsilon_i + \varepsilon_j)|ij\rangle \tag{5.3}$$

In the positive energy domain the Bethe–Goldstone equation (5.1) is replaced, using lower case g, by

$$g(E) = v + v\frac{Q_F}{E^{(+)} - H_0}g(E) \tag{5.4}$$

The resulting nucleon–nucleus interaction is then given by an extension of the second term of (5.3) as

$$V_{\text{eff}}(k, E) = \sum_{j<k_F} \langle k, j|g(E + e(j))|k, j\rangle \tag{5.5}$$

This is the Brueckner–Hartree–Fock approximation for V_{eff} for positive energies E. It contains the effects of particle–hole excitations but not, for example, excitations involving two or more holes. It is thus the first term in an expansion in the number of hole lines. Evidently, g is the effective two-nucleon interaction inside the nucleus.

There remains the problem of choosing U_i in (5.2). Jeukenne, Lejeune, and Mahaux (76) use a self-consistent procedure as follows. Take

$$U(k) = \text{Re}\, V_{\text{eff}}(k, E(k))$$

where

$$E(k) = \frac{k^2}{2m} + \text{Re}\, V_{\text{eff}}(k, E(k))$$

[Compare with (2.32).] Since H_0 depends on U, an iterative procedure is used, determining g, U, and V_{eff} simultaneously.

Jeukenne, Lejeune, and Mahaux (76) [see also Mahaux (78) and Brieva and Rook (77, 78)] have applied this method to the case of infinite nuclear matter, thereby deriving values of g and V_{eff} for various values of the density. Several differing approximations are made by each group which we will not parsue here. Using the local density approximation permits the approximate extension to finite nuclei. The results, as we have indicated earlier, are surprisingly good and as also shown by the comparison of the theoretical and empirical volume integrals of the potential shown in Fig. 5.5. One must bear in mind the omission,

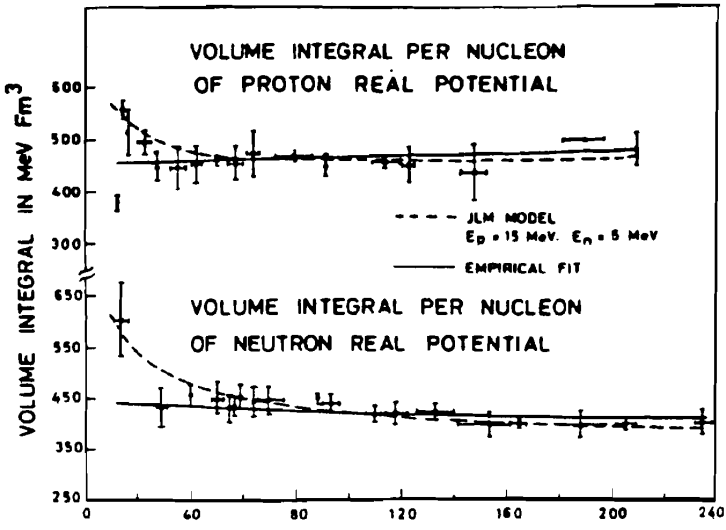

FIG. 5.5. (*a*) Compilation of empirical volume integrals per nucleon for $10 < E < 20$ MeV protons (upper part) and for $1 < E < 8$ MeV neutrons (lower part). The dashed curves are the theoretical values, computed for $E_p = 15$ MeV and $E_n = 5$ MeV [Jeukenne, Lejeune, and Mahaux.]

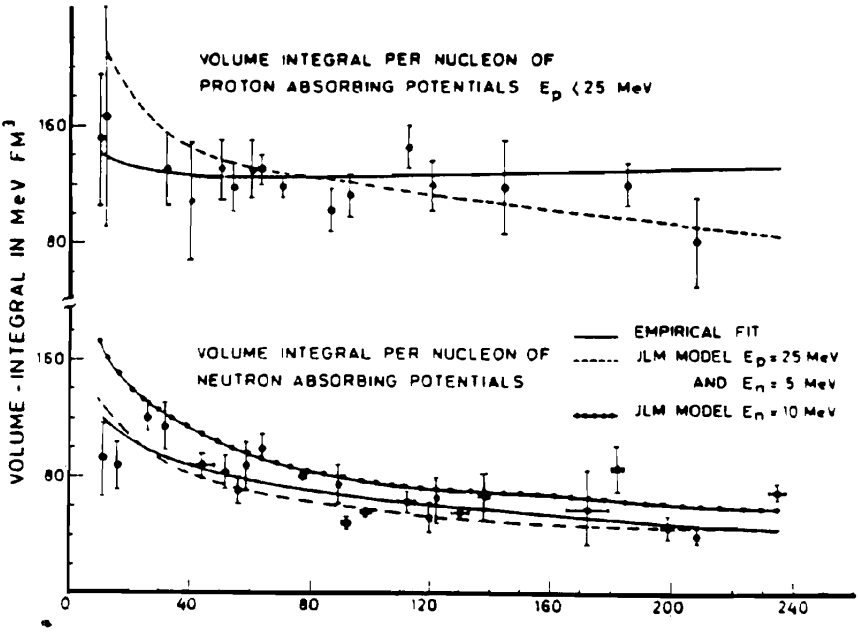

FIG. 5.5. (*b*) Dependence on A of the volume integral per nucleon of the imaginary part of the optical model potential. The dots are obtained from a compilation of empirical values for 17 ($\pm$ 8) MeV protons and for 5 ($\pm$ 3) MeV neutrons. The theoretical curves refer to $E_p = 25$ MeV and $E_n = 5$ MeV (short dashes) and $E_n = 10$ MeV (full curve with dots) [Jeukenne, Lejeune, and Mahaux (76)]. [From Mahaux (79).]

at least explicitly, of surface effects which in finite nuclei contribute importantly to the absorptive potential. Of equal, if not greater concern is the failure of the Brueckner–Hartree–Fock method [see Chapter VII in deShalit and Feshbach (74)], without some additional phenomenological devices, to predict the nuclear matter binding energy/nucleon as well as the properties of the bound states of finite nuclei.

6. COMPARISON WITH EXPERIMENT

We select a few examples from the immense literature on this subject. In comparing the direct interaction theory of inelastic scattering with experiment, one should bear in mind its major conceptual approximation. The assumption (see Sections 1 and 4) is made that the process can be described by a single step; that is, reaction paths in which the system passes through the intermediate states are not important. As we discuss in a later chapter, this is not the case for nucleon projectile energies in the range 25 to 65 MeV, where the multistep

contributions have been calculated [Bonetti, Colli-Milazzo Doda and P. E. Hodgson (82)]. At the endpoints of this interval the single-step direct process contributes 82% and 70%, falling to 50% in between, respectively, indicating that the multistep process becomes unimportant for energies somewhat below 25 MeV and above 65 MeV. These multistep contributions become more important as the scattering angle and/or the energy loss increases. Thus, at and below ~ 65 MeV, one can expect agreement of the DWA with experiment only at forward angles and small energy loss. In addition, because simple wave functions are used to describe the initial and final nuclear states, a normalization factor must be introduced to obtain the correct order of magnitude of the cross section. That factor is generally much smaller than unity, indicating that the model wave function used is a small component of the exact wave function. Above ~ 65 MeV, the nucleus is sufficiently transparent so that one-step processes dominate.

In addition to the coupling potentials of Section 4.D, to obtain a theoretical prediction to compare with experiment, one needs the distorted incident and outgoing nucleon wave function as well as the density matrices describing the nuclear transition [see (4.81)]. In principle, the distorted wave functions should be obtained as solutions of the Schrödinger equation using the folding optical potential obtained from the same "two-body" interactions used in deriving the interaction potentials for inelastic scattering. This procedure is not always used; rather, the empirical optical model, adjusted to fit the elastic scattering data, is used. This inconsistency is faced if the folding potential optical does not give a good fit to the elastic scattering. Generally, also, the orthogonality requirements on the initial and final wave functions [see the discussion following (4.68)] are not rigorously satisfied. With regard to derivations of the interaction potentials from the empirical nucleon–nucleon forces, it should be mentioned that the effects of effective nuclear mass [see (2.37)] are not taken into account.

Using the representation of the effective two-body potential given by (2.86), one sees that the density matrices that are needed include isoscalar and isovector components of ρ:

$$\rho_{fi}^{0} = \langle \psi_f | \sum \delta(\mathbf{r} - \mathbf{r}_i) | \psi_i \rangle$$

$$\boldsymbol{\rho}_{fi}^{\sigma} = \left\langle \psi_f(\mathbf{r}_1 \cdots) \middle| \sum_i \delta(\mathbf{r} - \mathbf{r}_0)\boldsymbol{\sigma}_i \middle| \psi_i \right\rangle$$

$$\rho_{fi}^{T} = \left\langle \psi_f(\mathbf{r}_1 \cdots) \middle| \sum_i \delta(\mathbf{r} - \mathbf{r}_0)\boldsymbol{\sigma}_i \mathbf{r}_i \middle| \psi_i \right\rangle$$

$$\boldsymbol{\rho}_{fi}^{L} = \left\langle \psi_f(\mathbf{r}_1 \cdots) \middle| \sum_i \delta(\mathbf{r} - \mathbf{r}_i)\mathbf{L}_i \middle| \psi_i \right\rangle$$

$$\rho_{fi}^{so} = \left\langle \psi_f(\mathbf{r}_1 \cdots) \middle| \sum_i \delta(\mathbf{r} - \mathbf{r}_i)\boldsymbol{\sigma}_i \cdot \mathbf{L}_i \middle| \psi_i \right\rangle$$

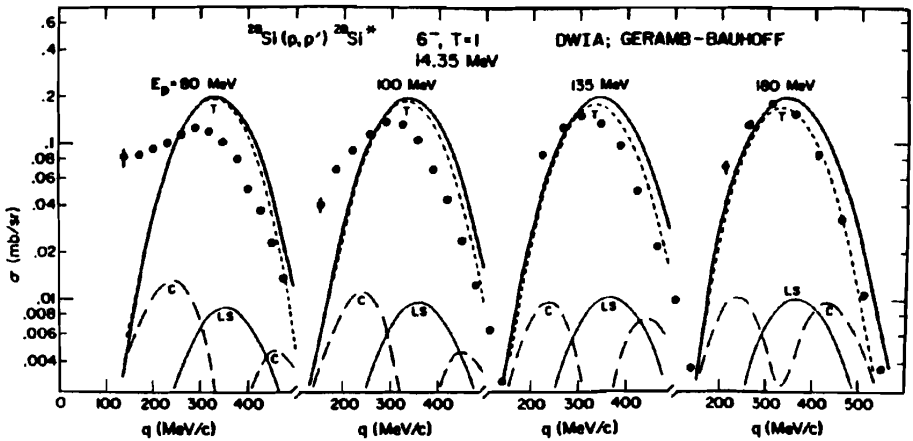

FIG. 6.1. Momentum transfer dependence of the cross sections for proton inelastic excitation of the 6^-, $T = 1$ state at 14.35 MeV in ^{28}Si. The curves are DWIA calculations (multiplied by 0.25) using the Geramb–Bauhoff effective interaction and optical potentials appropriate for the various incident energies. [From Olmer (83).]

Electron scattering from nuclei can provide information on these density matrices, but, of course, for a particular isovector and isoscalar combination, since the electron interacts primarily with the nuclear protons.[‡]

We shall give two examples of the applications of this analysis in the multi-hundred-MeV range. In the first, reported by Olmer (83), inelastic proton scattering from ^{28}Si to its 6^-, $T = 0$, $T = 1$ states[§] is compared to several theoretical interaction potentials, v_{ij}. We shall compare with the Geramb–Bauhoff interaction (80) based on the Paris potential Lecombe et al. (80). The ground state of ^{28}Si contains six $d_{5/2}$ orbital neutrons and six $d_{5/2}$ protons. The excitation lifts one of these to the $f_{7/2}$ forming the particle–hole configuration $(f_{7/2}d_{5/2}^{-1})$. These states are referred to as "stretched" since they correspond to the maximum possible spin for this configuration. Harmonic oscillation wave functions derived from inelastic electron scattering from the same nuclei are used for these orbitals. The "unnatural parity" of the resultant 6^- states requires the action of parity-changing parts of the interaction; that is, the spin–spin, spin–orbit, and tensor terms should be dominant.

The comparison between theory and experiment is shown in Fig. 6.1 for the excitation of the $T = 1$ state. As one can see, these transitions are dominated

[‡]The use of other probes, such as pions, kaons, and so on, can provide additional information. Elastic scattering by positive kaons would, in fact, be most effective in this regard.
[§]Olmer reports on excitations of the 5^+ state, as well.

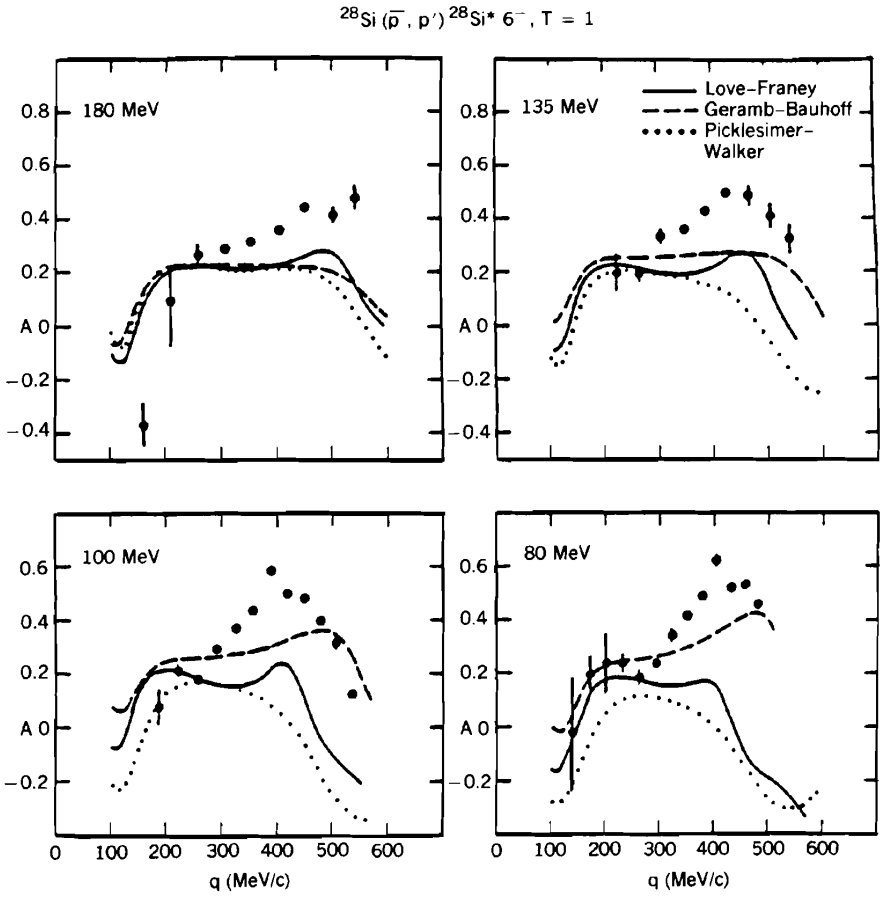

FIG. 6.2. Momentum transfer dependence of the analyzing powers for proton inelastic excitation of the 6^-, $T = 1$ state at 14.35 MeV in ^{28}Si. [From Olmer (83).]

by the tensor terms in qualitative agreement with the discussion presented in the preceding section. Agreement is not good for low momentum transfer, q, and lower E. Note that these are semilog plots of the cross section. Moreover, an overall reduction of the theoretical prediction by $\frac{1}{4}$ is required to obtain the correct magnitude. In Fig. 6.2 the analyzing powers, A, are shown. Although the magnitude of A is correctly predicted, the shapes, as a function of q, are not. The cross section for the excitation of the $T = 0, 6^-$ state is shown in Fig. 6.3. This time, the predicted magnitudes must be multiplied by a factor of 0.15. And again, there is a problem with the comparison at low q, and E. Note that the tensor and LS components dominate, in disagreement with the qualitative remarks of the preceding section. Obviously, much remains to be done!

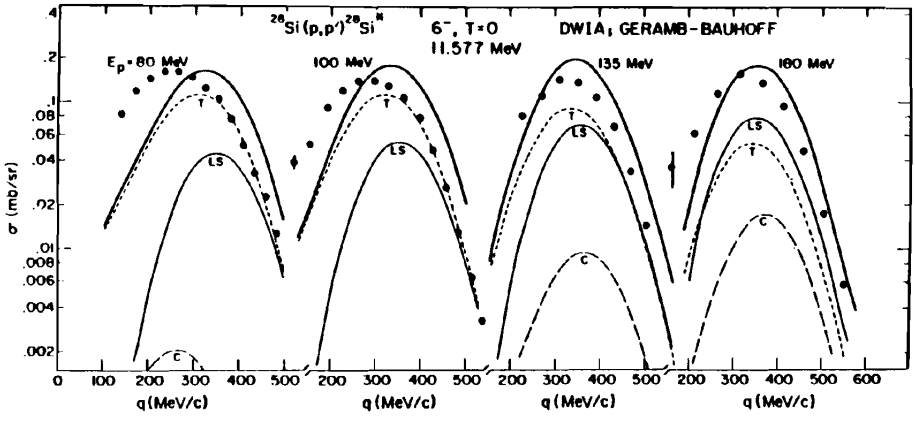

FIG. 6.3. Momentum transfer dependence of the cross sections (for proton inelastic excitation of the 6^-, $T = 0$ state at 11.58 MeV in ^{28}Si. The curves are DWIA calculations (multiplied by 0.15) using the Geramb–Bauhoff effective interaction and optical potentials appropriate for the various incident energies. [From Olmer (83).]

A more satisfactory picture is presented by Kelly (83) for the elastic scattering of 135-MeV protons by ^{16}O. The Paris potential is used, as developed by Brieva, Geramb, and Rook (78). Figure 6.4 compares the experimental elastic scattering and the analyzing power with the resultant theoretical predictions. The agreement is by no means perfect, but it must be remembered that there are no adjustable parameters! The inelastic scattering to the "normal" 1^- and 3^- state in ^{16}O is shown in Fig. 6.5. The agreement is very good, indeed. This indicates that the isoscalar spin-independent central component is given correctly by the microscopic theory of Brieva et al. Most important, the Love–Franey interactions, in which there are no medium corrections, fail to reproduce the inelastic cross section. We see from these data (the same can be inferred from Olmer's result) that the effective two-nucleon interaction is density dependent.

A few examples of comparisons at lower energies employing the *M3Y* interaction in the folding model will now be discussed. The paper of Bertsch, Barysowicz, McManus, and Love (77) in which this interaction was introduced contains a number of comparisons. As is generally the case in this energy range, an empirical optical model is used to describe the projectile wave functions. Figure 6.6 presents a comparison between experimental and theory for the excitation of states of normal parity 3^-, 5^- in ^{208}Pb by inelastic proton scattering.

The theory does provide reasonable agreement with the shapes of these angular distributions. The dominant role of the central component of the interaction is evident. On the other hand, the prediction of the cross section for the excitation of unnatural parity levels in ^{40}Ca is less successful (see Fig. 6.7). The central part of the interaction alone is inadequate, as expected,

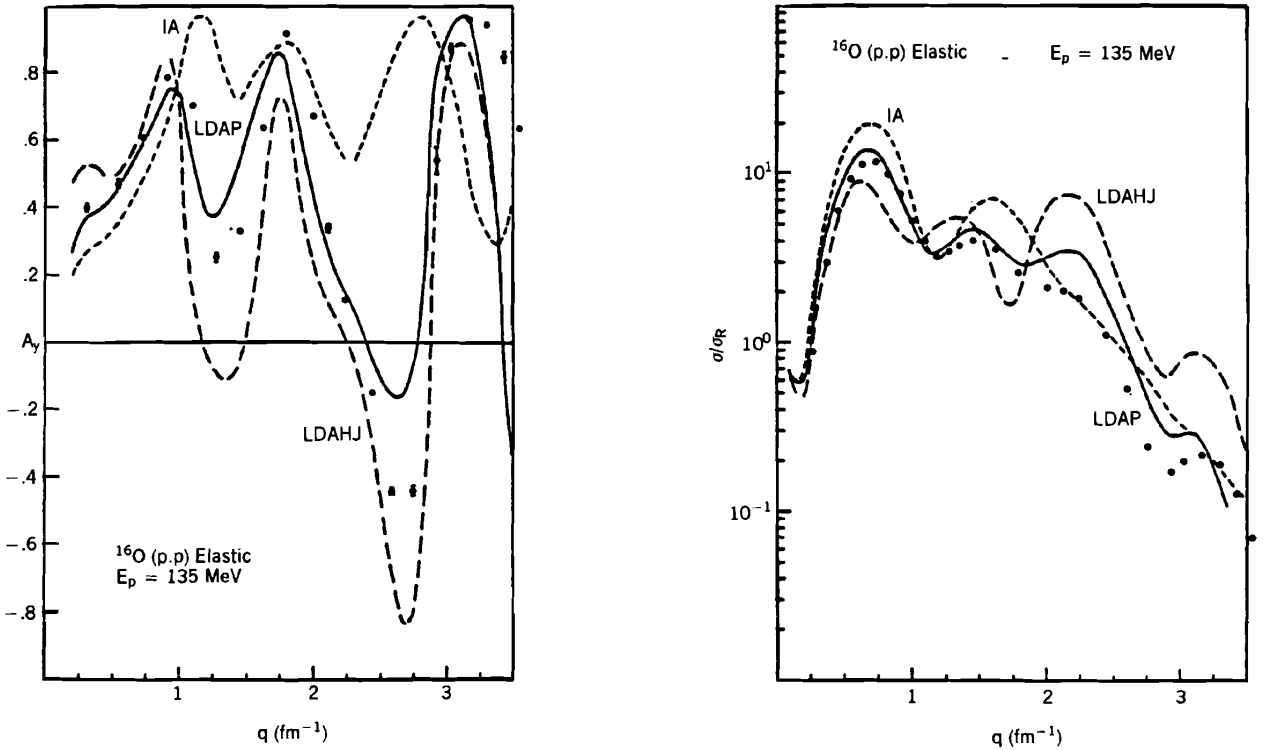

FIG. 6.4. Elastic Scattering of 135-MeV protons by ^{16}O. LDAP = local density approximation using the Paris potential; LDAHJ = local density approximation using the Hamada–Johnston potential. [From Kelly (83).]

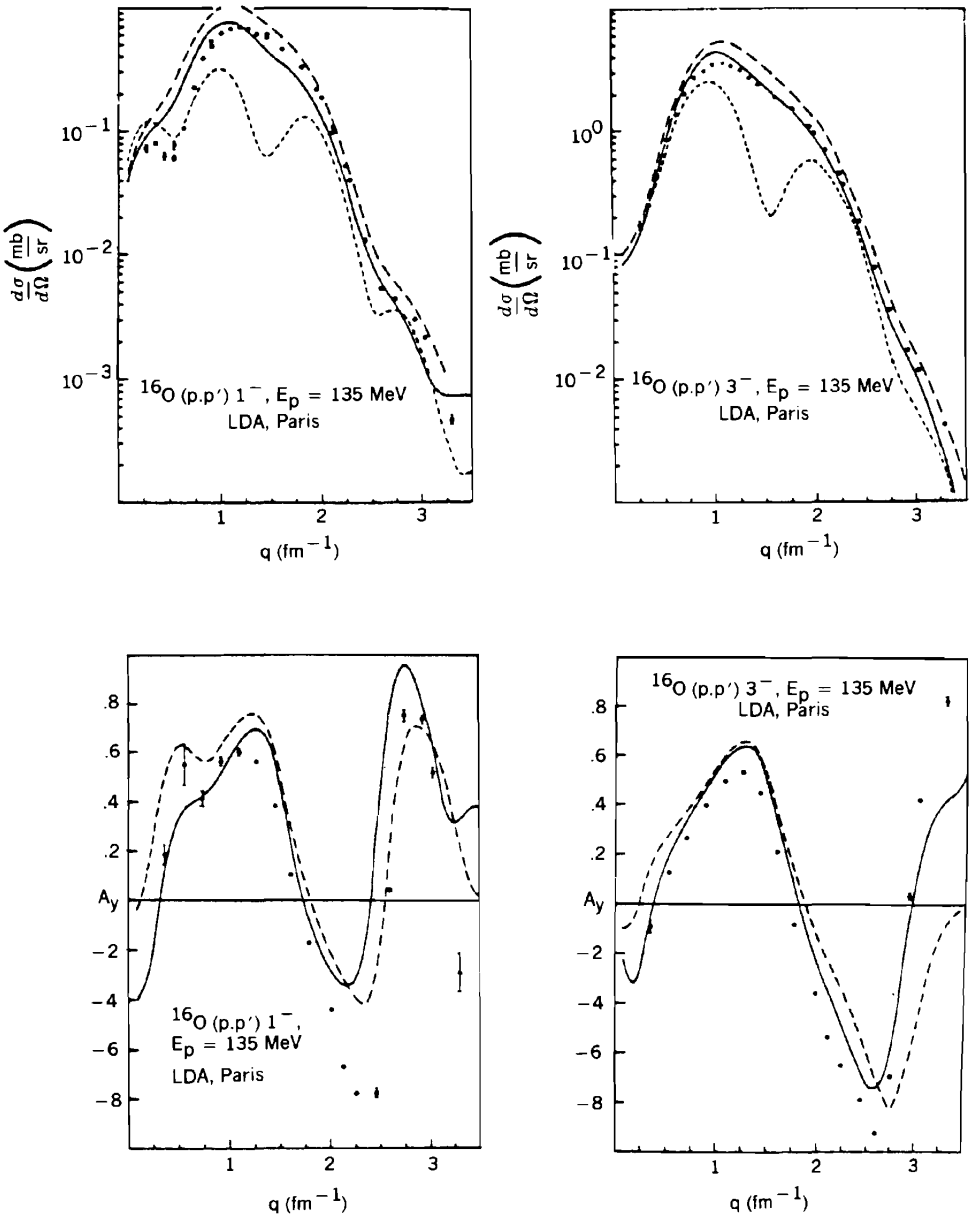

FIG. 6.5. Differential cross section and asymmetry for the inelastic scattering of protons by ^{16}O to the 1^- and 3^- levels compared with the LDA using the Paris potential. [From Kelly (83).]

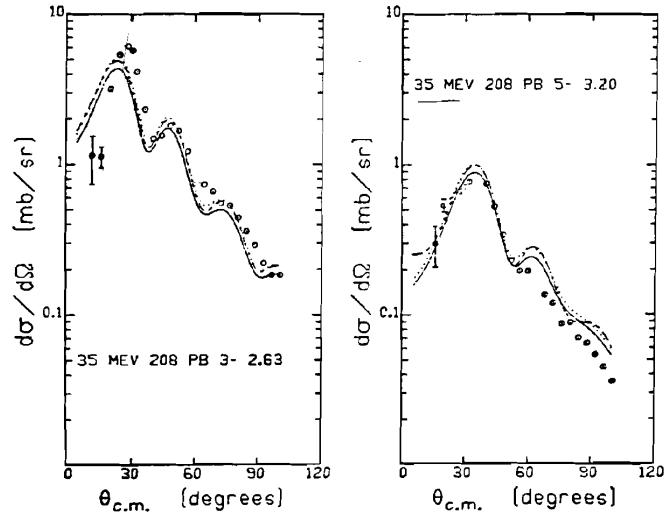

FIG. 6.6. Excitation of lowest 3^- and 5^- states in ^{206}Pb by 35-MeV protons. The solid lines are theory the dotted line is with the central odd interaction removed, and the dashed line is with the central even interaction only. [From Bertsch, Borysowicz, McManus, and Love (77).]

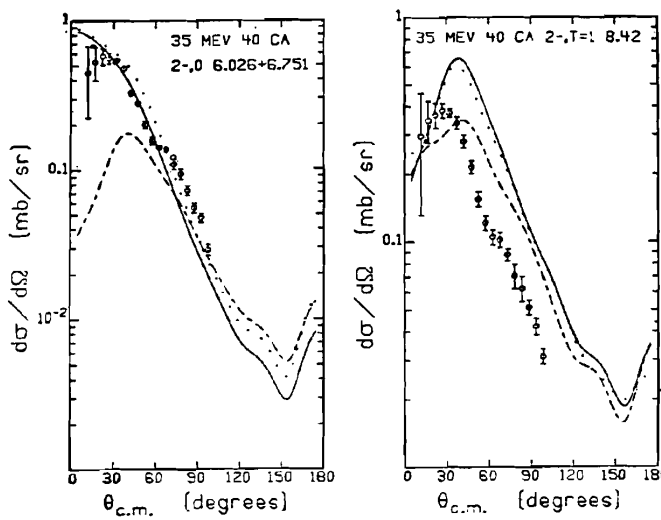

FIG. 6.7. Excitation of 2^-, $T = 0$ and 1 states in ^{40}Ca by 35-MeV protons. Conventions are as in Fig. 6.6. [From Bertsch, Borysowicz, McManus, and Love (77).]

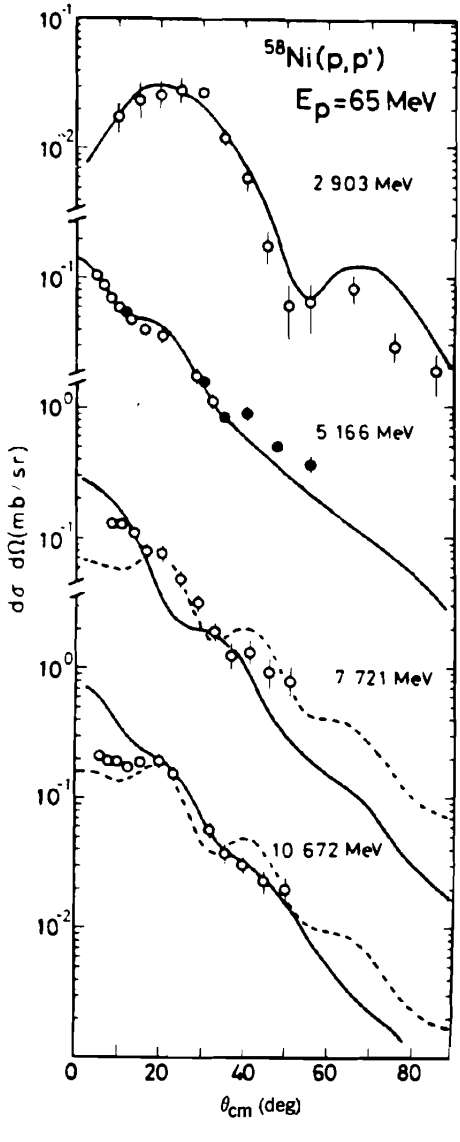

FIG. 6.8. Differential cross sections for the peaks corresponding to the 2.903$^-$, 5.166$^-$, 7.721$^-$, and 10.672 MeV states in ^{58}Ni. The solid curves are the microscopic DWA predictions calculated with the M3Y interaction [Bertsch, Borysowicz, McManus, and Love (77).] The results of the collective $L = 2$ DWA calculations are shown for comparison by the dashed curves. [From Fujiwara, Fujita, et al. (83).]

indicating the importance of spin-dependent terms. The disagreement becomes more severe when the excitation energy increases, as Bertsch et al. demonstrate for the 4^- ($T = 0$ and $T = 1$) levels in ^{40}Ca.

In a more recent comparison, Fujiwara et al. (83) study the excitation of the 1^+ levels in ^{58}Ni by 65-MeV protons. Their results are shown in Fig. 6.8. We

observe the excellent agreement for the excitation of the 2.903- and 5.166-MeV levels, aside for normalization factors of 0.31 and 0.24, respectively. The different shapes are in large part a reflection of the differing structure of the final states. The quality of the agreement decreases and the normalization factors become rather small with increasing excitation energy. The magnitude of the apparent disagreement in the forward direction is sensitive to the optical model parameters, as the authors points out.